A PARAMETRIC STUDY OF

RIGID BODY-VISCOUS FLOW INTERACTION

by

SHASHI MOORTY

B.Tech., Indian Institute of Technology, Kanpur, 1985

A THESIS SUBMITTED IN PARTIAL FULFILLMENT OF

THE REQUIREMENTS FOR THE DEGREE OF

MASTER OF APPLIED SCIENCE

in

THE FACULTY OF GRADUATE STUDIES

Department of Civil Engineering

We accept this thesis as conforming
to the required standard

THE UNIVERSITY OF BRITISH COLUMBIA

May 1987

© Shashi Moorty 1987

In presenting this thesis in partial fulfilment of the requirements for an advanced degree at the University of British Columbia, I agree that the Library shall make it freely available for reference and study. I further agree that permission for extensive copying of this thesis for scholarly purposes may be granted by the head of my department or by his or her representatives. It is understood that copying or publication of this thesis for financial gain shall not be allowed without my written permission.

Department of CIVIL ENGG

The University of British Columbia
1956 Main Mall
Vancouver, Canada
V6T 1Y3

Date MAY 4th 1987

Abstract

This thesis presents the numerical solution for two-dimensional incompressible viscous flow over a rigid bluff body which is elastically supported or alternately undergoing a specified harmonic oscillations. Solutions for the related associate flow in which the body is at rest in a two-dimensional incompressible time-dependent viscous flow have also been obtained. This work is an extension of the work by Pattani [19] to include the effect of a steady far field flow on an oscillating body.

The numerical model utilizes the finite element method based on a velocity-pressure primitive variable representation of the complete Navier-Stokes equations. Curved isoparametric elements with quadratic interpolation for velocities and bilinear interpolation for pressure are used. Nonlinear boundary conditions on the moving body are represented to the first order in the body amplitude parameter. The method of averaging is used to obtain the resulting periodic motion of the fluid. Three non-dimensional parameters are used to completely characterise the flow problem: the frequency Reynolds number R_ω, the Reynolds number of steady flow R_{e_1} and the Reynolds number for time-dependent flow R_{e_2}.

Numerical results are obtained for a circular body, a square body and an equilateral triangular body. A parametric study is conducted for different values of the Reynolds numbers in the viscous flow regime. In all cases, results are obtained for streamlines, streaklines, added mass, added damping, added force and the drag coefficients. The limiting cases of steady flow over a fixed body and an oscillating body in a stationary fluid are checked with known results. Results for the associated flow are also obtained. The transformations derived, between the two associated flows are checked. Good agreement is obtained between the present results and other known results.

Contents

Figures

Tables

Acknowledgements

Introduction and Literature Survey

1.1 General Remarks

The subject of bluff body flows has been receiving a great deal of attention recently. This is due in large part to its importance in design of offshore structures. In spite of the importance of bluff body flows, relatively little is known about them. The vortex shedding characteristics of even the simplest of bodies like circular and rectangular cylinders are not well understood.

For most applications of practical interest, the forces acting on a structural section in a two-dimensional flow are given by the so-called Morison equation. This is an empirical equation but is extensively used in view of the fact that even in a steady, two-dimensional, separated flow past a smooth cylinder, one does not have a theoretical or numerical solution which explains all the characteristics of the flow as a function of Reynolds number. Many investigators have applied numerical methods to the Morison equation.

Many fluid-structure interaction problems are of such complexity that the method of analysis must be numerical in nature. Although the theory of boundary layer permits us to use the influence of viscosity in many practically important cases, nevertheless some phenomena, important in practice, are not described by boundary layer theory. Among them must firstly be mentioned, flows with separation. This phenomenon occurs sometimes in flows around ships, planes or rockets, in spite of all possible means being used to avoid it.

Solutions for incompressible real viscous fluid flow problems involve the complete Navier-Stokes equations. Two properties of the Navier-Stokes equations are the main

source of difficulty in their numerical solution:

1. The presence of nonlinear terms resulting in nonsymmetric *convection* operators.

2. The unbalanced domain of the solution, together with the elliptical character of the equations.

A variety of efficient numerical methods are now available for the solution of 2D and 3D Navier-Stokes equations using finite difference or finite element methods [4]. These methods however are still only reliable at fairly modest Reynolds numbers. In fact, modern computers are not yet sufficiently effective for solving the Navier-Stokes equations in the fully developed turbulence domain. The finite element method is relatively recent as compared to the finite difference method but is gaining popularity due to its ability to easily model complex boundary geometry. Development of research in applying finite element and finite difference methods to the Navier-Stokes equations has progressed in three basic areas according to the variables used namely,

1 The velocity-pressure primitive variables u, v, p.

2 The stream function Ψ and the vorticity ξ.

3 Stream function Ψ alone.

Few investigators have applied finite element methods to viscous fluid-structure inter-action problems. Olson [17] has presented comparison between these methods in finite elements. Others like Liu [12] and Hughes [9] have adapted finite element methods for var-ious problem configurations. Pattani [18, 19, 16] has conducted numerical investigations for the flow around an elastically supported rigid body. Excellent results have been ob-tained by Davis and Moore [2, 3] for steady and unsteady flow around squares for Reynolds numbers between 100 and 2800 using finite difference techniques. Roache's book, [22] gives a detailed analysis of the various finite difference techniques.

1.2 Fluid-Structure Coupling

Various numerical schemes exist for predicting the forces and the details of the flow around cylindrical bluff bodies in both uniform and oscillatory flow at high Reynolds num-

bers using the Morison equation [24]. The Euromech Colloquium, held in 1980 [8] aimed to bring together research work concerning bluff body flows in a unidirectional stream and those concerning the flow around bluff bodies in an oscillatory free stream. Investigations of the in-line oscillations of bluff bodies began in earnest following the troublesome and sometimes damaging vortex induced oscillations of pilings during the construction of an oil terminal on the Humber Estuary in England during 1960 [20]. Tanida and Okajima [26], conducted experiments for a circular cylinder oscillating in a uniform flow at low and high Reynolds numbers. They measured the lift and drag coefficients as well as determined the stability of the cylinder at different oscillating frequencies. Bertelsen [1], conducted experiments to study the steady streaming induced by an oscillating cylinder in an otherwise still fluid at high values of Reynolds number associated with steady streaming.

Considerable work has been done in recent years to develop numerical solutions for the 2D flow around bluff bodies using finite element and finite difference techniques. Results of acceptable accuracy have been obtained for flows and forces on fixed bodies for a finite range of Reynolds numbers. Goddard, [7] carried out a numerical analysis of the drag response of a cylinder to streamwise fluctuations. This work cannot be generalised to higher Reynolds numbers as it is based on the Navier-Stokes equations and since the diffusion of vorticity in the concentrated vortices for Reynolds numbers larger than about 200 is primarily turbulent. Olson and Pattani [16, 18, 19] addressed the problem of the flow around a rigid body which is elastically supported and obtained solutions using a finite element method based on a velocity-pressure primitive variables representation of the complete Navier-Stokes equations. Various investigators, [21, 5] have applied the techniques of higher order boundary layer theory to study the steady streaming induced by an oscillating cylinder in a still fluid.

In order to solve the governing equations of the fluid-structure system simultaneously, suitable conditions must be prescribed along fluid-solid interfaces to match the velocities, tangential and normal to the solid body without gross distortion of the finite element grid. Hughes et al proposed a mixed Lagrangian-Eulerian approach to achieve this. In this method, each degree of freedom may be assigned to move at a fraction of the fluid particle velocity. Pattani and Olson successfully showed that it is possible to keep the finite element grid fixed, but allow the body to move past the grid. The relevant boundary terms

were expanded by the Taylor series to approximate the velocities at the finite element grid points. The time-dependent character of the Navier-Stokes equation was taken care of by considering the steady state periodic solution. Steady state behaviour of forced oscillations of nonlinear systems can be determined by two basic kinds of techniques.

1 Method of Averaging and Multiple Scales.

2 Lindstédt-Poincaré Techniques.

In the present investigations, the method of averaging has been adapted as outlined by Pattani [18].

1.3 Comparison of the two Associated Flows

Wave flow past a bluff body is similar to a two-dimensional harmonic flow past a similar section. Thus waves can be modelled by harmonically oscillating fluid. Isaacson [10] has further indicated that the solution of harmonic flow past a bluff body is closely related to the solution of a harmonically oscillating body in an otherwise still fluid. This in turn is related to the solution of a rigid bluff body which is elastically supported and subjected to an external harmonic forcing function in an otherwise still fluid. Pattani [18] has modelled an elastically supported bluff body subjected to wave flow by considering a problem configuration of an oscillating body in an otherwise still fluid. He has given an excellent comparision between the two associated flows and derived a transformation from one flow to the other. In the present study, a similar transformation is used to model a combined flow of current and waves over bluff bodies.

1.4 Present Investigations

This thesis extends the investigations conducted by Pattani [18] in the modelling of the interaction of viscous fluid flow over a moving body using the finite element method. He considered the case of a solid body oscillating in an otherwise still fluid. The present study considers the problem configuration of an elastically supported rigid body in a two-dimensional incompressible steady flow.

In chapter 2, the fundamentals of fluid-structure interaction are discussed. The Navier-Stokes equations and continuity equation are derived and represented by the u, v, p primitive variables. A comparison of the two associated flows and the related transformations are derived. Suitable sets of non-dimensional parameters are used to effectively non-dimensionalise the governing equations.

In chapter 3, the finite element formulation of the Navier-Stokes equations is discussed. The restricted variational principle for the governing equations is presented and the finite element matrix equations are obtained for a suitable choice of element. Boundary conditions for the outer fluid boundary and the body-fluid interface are discussed and incorporated into the matrix equations. The method of slowly varying amplitudes as formulated by Pattani [18], is then used to obtain a steady state periodic solution. A Newton-Raphson iteration scheme for the solution of the resulting nonlinear algebraic equations, is outlined. Finite element representation of the other associated flow is also presented.

The finite element flow results can be visualised by plotting the streamlines or streaklines. In chapter 4, a finite element scheme is outlined to obtain the stream functions from the flow results and thus obtain the streamlines and streaklines. The force on a bluff body oscillating in line with a steady fluid flow can be characterised by the drag coefficients or the added mass, added damping and added force. A numerical integration scheme to determine these force characteristics is outlined. Force characteristics for the two associated flows and the transformation from one to the other is also presented. Finally, the Morison equation and the representation of the drag and inertia coefficients in terms of the added mass, added damping and the added force is presented.

The numerical investigations are described in chapter 5. Numerical results are obtained for three different body shapes respectively. 1. A circular body oscillating in the direction of flow. 2. A square body oscillating parallel to one of its sides in the direction of flow. 3. An equilateral triangular shaped body oscillating parallel to one of its bisectors in the direction of flow. In all the cases, the results are presented in the form of streamlines streakline, added mass, added damping and added force. Results for the associated flow of a time-dependent flow over a stationary bluff body is also presented. The transformation between the two associated flows derived in chapters 3 and 4 are verified.

Conclusions and suggestions for further development are presented in chapter 6.

Derivation of Governing Equations

2.1 General Remarks

In this chapter, the equations governing two-dimensional incompressible fluid flow are derived and presented in terms of velocity-pressure primitive variables.

A structural section in a two-dimensional flow can be represented as a spring mass system. The equation of motion of such an elastically supported single degree of freedom system is presented.

Isaacson has indicated that there are strong similarities between the wave flow past a section of a structural member and a two-dimensional harmonic flow past a similar section. Also, the problem configuration of a stationary body subjected to a time-dependent flow is interrelated to that of a body undergoing time-dependent motion in an otherwise still fluid. One configuration can be transformed to the other by simple reference frame transformations.

Pattani has considered the wave flow past a body by considering an elastically supported rigid body of arbitrary shape undergoing specified harmonic oscillations in an otherwise still fluid. In this study, a two-dimensional flow consisting of waves and currents past an elastically supported rigid body is considered. The governing equations are presented in their final non-dimensional form.

2.2 Conservation Equations and Boundary Conditions

The equations governing two-dimensional, incompressible viscous fluid flow are the

Navier-Stokes equations, the continuity equations and the boundary and initial conditions. The solution of the problem will be sought within a plane domain Ω which is bounded by a contour Γ. Γ is composed of two distinct parts :- Γ_u and Γ_s respectively.

Γ_u is the kinematic boundary where boundary conditions on the velocity components are specified.

Γ_s is the natural boundary where tractions are specified.

The equations of motion and boundary conditions are given in the (x,y) cartesian coordinate system.

Equations of Motion:-

$$
\begin{aligned}
\frac{Du}{Dt} &= \frac{1}{\rho}\left(\frac{\partial \sigma_x}{\partial x} + \frac{\partial \tau_{xy}}{\partial y}\right) \\
\frac{Dv}{Dt} &= \frac{1}{\rho}\left(\frac{\partial \tau_{xy}}{\partial x} + \frac{\partial \sigma_y}{\partial y}\right)
\end{aligned}
\qquad (x,y) \in \Omega, \quad t > 0
\tag{2.1}
$$

Constitutive Relations:-

$$
\begin{aligned}
\sigma_x &= -p + 2\mu\frac{\partial u}{\partial x} \\
\sigma_y &= -p + 2\mu\frac{\partial v}{\partial y} \\
\tau_{xy} &= \mu\left(\frac{\partial v}{\partial x} + \frac{\partial u}{\partial y}\right)
\end{aligned}
\tag{2.2}
$$

u,v are fluid velocities in the x and y directions respectively.

p is the fluid pressure.

σ_x, σ_y are normal stresses in the x and y directions respectively.

τ is the shear stress.

ρ is the fluid density. μ is the absolute viscosity.

$$
\frac{D}{Dt} = \frac{\partial}{\partial t} + u\frac{\partial}{\partial x} + v\frac{\partial}{\partial y}
$$

D/Dt is the total material derivative.

Substituting equation (2.2) into (2.1), we get the well known Navier-Stokes equations.

$$
\begin{aligned}
\frac{Du}{Dt} &= -\frac{1}{\rho}\frac{\partial p}{\partial x} + \nu\left(2\frac{\partial^2 u}{\partial x^2} + \frac{\partial^2 u}{\partial y^2} + \frac{\partial^2 v}{\partial x \partial y}\right) \\
\frac{Dv}{Dt} &= -\frac{1}{\rho}\frac{\partial p}{\partial y} + \nu\left(\frac{\partial^2 v}{\partial x^2} + 2\frac{\partial^2 v}{\partial y^2} + \frac{\partial^2 u}{\partial x \partial y}\right)
\end{aligned}
\qquad (x,y)\in\Omega, \quad t>0 \qquad (2.3)
$$

where $\nu = \mu/\rho$ is the kinematic viscosity.

Continuity Equation:-

$$
\frac{\partial u}{\partial x} + \frac{\partial v}{\partial y} = 0 \qquad (2.4)
$$

Boundary Conditions:-

$$
u = U, \quad v = V \qquad (x,y)\in\Gamma_u, \quad t>0 \qquad (2.5a)
$$

$$
\begin{aligned}
\sigma_x n_1 + \tau_{xy} n_2 &= X \\
\tau_{xy} n_1 + \sigma_y n_2 &= Y
\end{aligned}
\qquad (x,y)\in\Gamma_s, \quad t>0 \qquad (2.5b)
$$

n_1, n_2 are the direction cosines of the outward pointing normal to the boundary.

X, Y are the specified tractions on Γ_s.

Substituting equations (2.2) into equations (2.5b), we get the boundary conditions in terms of the velocity components.

Kinematic Boundary Conditions:-

$$
u = U, \quad v = V \qquad (x,y)\in\Gamma_u, \quad t>0 \qquad (2.6a)
$$

Natural Boundary Conditions:-

$$
\begin{aligned}
\left[-p + 2\mu\frac{\partial u}{\partial x}\right]n_1 + \left[\nu\left(\frac{\partial u}{\partial y} + \frac{\partial v}{\partial x}\right)\right]n_2 &= X \\
\left[\nu\left(\frac{\partial u}{\partial y} + \frac{\partial v}{\partial x}\right)\right]n_1 + \left[-p + 2\mu\frac{\partial v}{\partial y}\right]n_2 &= Y
\end{aligned}
\qquad (x,y)\in\Gamma_s, \quad t>0 \qquad (2.6b)
$$

The equations of motion of an elastically supported single degree of freedom rigid body as shown in figure 2.1 is given by

$$
m\ddot{s} + ks = f(t) \qquad (2.7)
$$
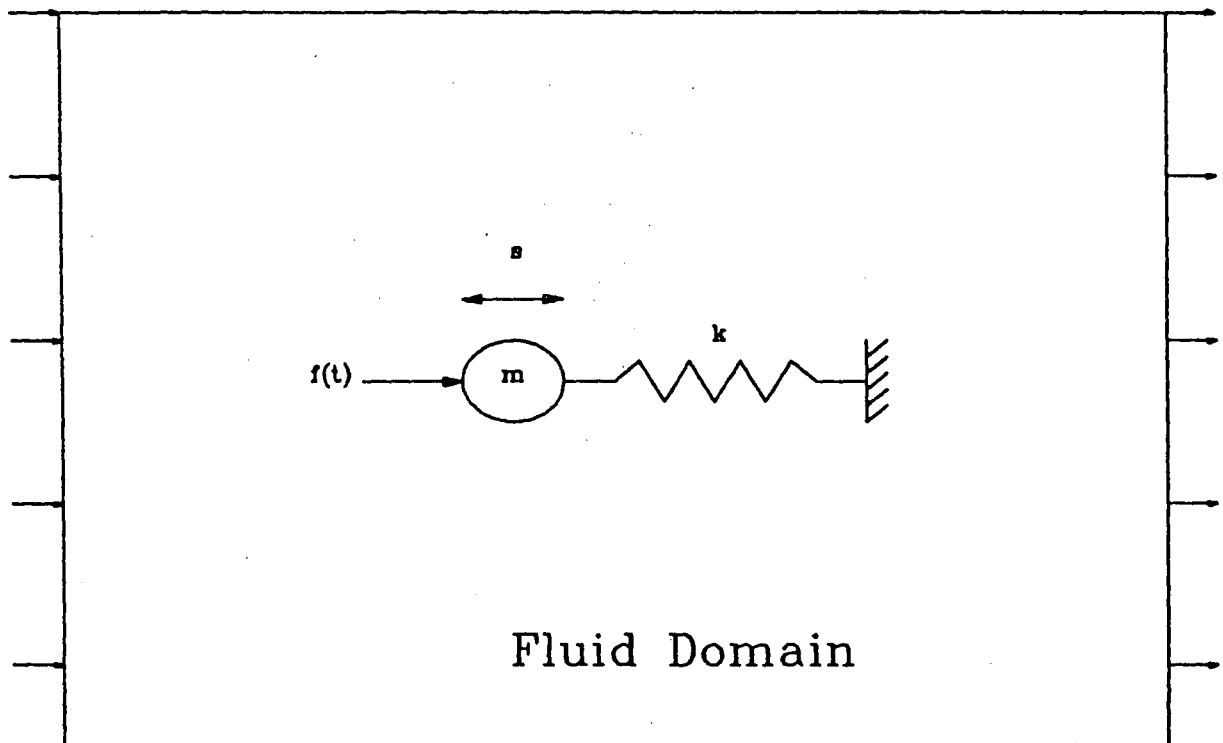
Figure 2.1 Problem Configuration

m is the mass of the body.

k is the elastic spring constant

s is the displacement of body

$f(t) = F_f(t) + F_e(t) =$ Total loading force.

$F_f(t)$ is the fluid force.

$F_e(t)$ is the external force on the body.

2.3 Comparison of the Two Associated Flows

It is sought to model the combined flow of current and waves over a structural section. This is similar to a two dimensional steady flow and a harmonic flow past a similar section [23]. The solution of this reference flow is closely related to the solution of steady flow over a harmonically oscillating structural member. Consider an associated pair of two-dimensional flows as defined in figure 2.2.

Case a   Case b
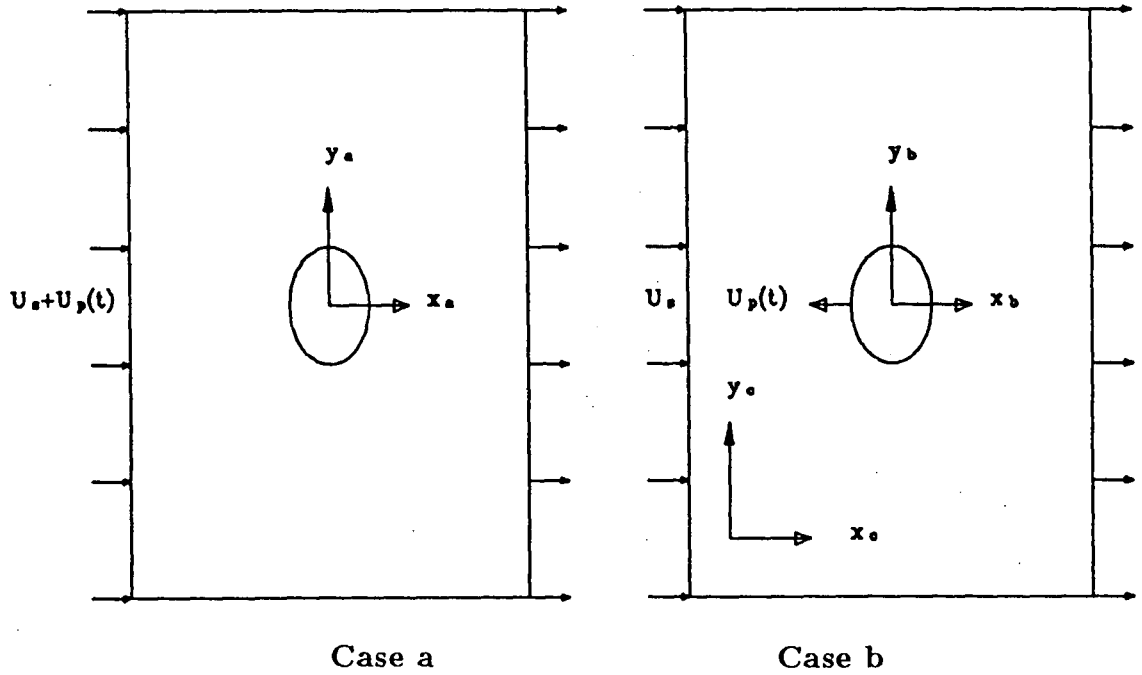
Figure 2.2 The Two Associated Flows

Case a: Fluid remote from the stationary body has two components of velocity in the x direction:-

U_s is the steady component of velocity.

$U_p(t)$ is the uniform time-dependent component of velocity.

Inertial coordinate system (x_a, y_a) is fixed with respect to the body. All flow quantities are denoted by subscript a.

Case b: Inertial coordinate system (x_c, y_c) is stationary. Fluid remote from the body has steady velocity U_s. The body has a velocity $-U_p(t)$ with respect to the inertial

reference frame. All flow quantities in the inertial reference frame are denoted by subscript c.

Non-inertial coordinate system (x_b, y_b) is fixed with respect to the body. All flow quantities in the non-inertial reference frame are denoted by subscript b.

Case a:

Equations of Motion and Continuity:-

$$\frac{Du_a}{Dt} = -\frac{1}{\rho}\frac{\partial p_a}{\partial x_a} + \nu\left(2\frac{\partial^2 u_a}{\partial x_a^2} + \frac{\partial^2 u_a}{\partial y_a^2} + \frac{\partial^2 v_a}{\partial x_a \partial y_a}\right)$$

$$\frac{Dv_a}{Dt} = -\frac{1}{\rho}\frac{\partial p_a}{\partial y_a} + \nu\left(\frac{\partial^2 v_a}{\partial x_a^2} + 2\frac{\partial^2 v_a}{\partial y_a^2} + \frac{\partial^2 u_a}{\partial x_a \partial y_a}\right)$$

$$\frac{\partial u_a}{\partial x_a} + \frac{\partial v_a}{\partial y_a} = 0 \tag{2.8}$$

where

$$\frac{D}{Dt} = \frac{\partial}{\partial t} + u_a\frac{\partial}{\partial x_a} + v_a\frac{\partial}{\partial y_a}$$

Boundary Conditions:-

$$u_a = 0, \qquad v_a = 0 \qquad \text{On body-fluid interface}$$

$$u_a = U_a + U_p(t), \qquad v_a = 0 \qquad \text{On fluid outer boundary}$$

Case b:

Equations of motion and continuity in the (x_c, y_c) system:-

$$\frac{Du_c}{Dt} = -\frac{1}{\rho}\frac{\partial p_c}{\partial x_c} + \nu\left(2\frac{\partial^2 u_c}{\partial x_c^2} + \frac{\partial^2 u_c}{\partial y_c^2} + \frac{\partial^2 v_c}{\partial x_c \partial y_c}\right)$$

$$\frac{Dv_c}{Dt} = -\frac{1}{\rho}\frac{\partial p_c}{\partial y_c} + \nu\left(\frac{\partial^2 v_c}{\partial x_c^2} + 2\frac{\partial^2 v_c}{\partial y_c^2} + \frac{\partial^2 u_c}{\partial x_c \partial y_c}\right)$$

$$\frac{\partial u_c}{\partial x_c} + \frac{\partial v_c}{\partial y_c} = 0 \tag{2.9}$$

where

$$\frac{D}{Dt} = \frac{\partial}{\partial t} + u_c\frac{\partial}{\partial x_c} + v_c\frac{\partial}{\partial y_c}$$

Boundary Conditions:-

$$u_c = -U_p(t), \qquad v_c = 0 \qquad \text{On body-fluid interface}$$

$$u_c = U_s, \qquad v_c = 0 \qquad \text{On fluid outer boundary}$$

Changing from reference frame (x_c, y_c) to reference frame (x_b, y_b), we get the following transformations:-

$$u_b = u_c + U_p(t)$$

$$v_b = v_c$$

$$p_b = p_c \tag{2.10}$$

$$x_b = x_c + \int_0^t U_p(\tau)\, d\tau$$

$$y_b = y_c$$

The absolute acceleration of a fluid particle, in the non-inertial coordinate system (x_b, y_b), moving with velocity $-U_p(t)$ relative to the inertial coordinate system (x_c, y_c) is given by Pattani [18]

$$\frac{Du_c}{Dt} = \frac{Du_b}{Dt} - \frac{dU_p(t)}{dt}$$

$$\frac{Dv_c}{Dt} = \frac{Dv_b}{Dt} \tag{2.11}$$

Substituting equations (2.10) and (2.11) into equation (2.9), and rearranging terms, we get

Equations of motion and continuity in (x_b, y_b) system:-

$$\frac{Du_b}{Dt} = -\frac{1}{\rho}\left(\frac{\partial p_b}{\partial x_b} - \rho\frac{dU_p(t)}{dt}\right) + \nu\left(2\frac{\partial^2 u_b}{\partial x_b^2} + \frac{\partial^2 u_b}{\partial y_b^2} + \frac{\partial^2 v_b}{\partial x_b \partial y_b}\right)$$

$$\frac{Dv_b}{Dt} = -\frac{1}{\rho}\frac{\partial p_b}{\partial y_b} + \nu\left(\frac{\partial^2 v_b}{\partial x_b^2} + 2\frac{\partial^2 v_b}{\partial y_b^2} + \frac{\partial^2 u_b}{\partial x_b \partial y_b}\right)$$

$$\frac{\partial u_b}{\partial x_b} + \frac{\partial v_b}{\partial y_b} = 0 \tag{2.12}$$

where

$$\frac{D}{Dt} = \frac{\partial}{\partial t} + u_b\frac{\partial}{\partial x_b} + v_b\frac{\partial}{\partial y_b}$$

Boundary Conditions:-

$$u_b = 0, \qquad v_b = 0 \qquad \text{On body-fluid interface}$$

$$u_b = U_s + U_p(t), \qquad v_b = 0 \qquad \text{On fluid outer boundary}$$

Comparing equations (2.8) with equations (2.12), we observe that the governing equations of motion, continuity and boundary conditions are the same. Thus assuming a unique solution for all time t, we get

$$u_a = u_b$$

$$v_a = v_b$$

$$\frac{\partial p_a}{\partial x_a} = \frac{\partial p_b}{\partial x_b} - \rho \frac{dU_p(t)}{dt} \qquad (2.13)$$

$$\frac{\partial p_a}{\partial y_a} = \frac{\partial p_b}{\partial y_b}$$

Substitute equation (2.10) into equation (2.13) and get

$$u_a = u_c + U_p(t)$$

$$v_a = v_c$$

$$\frac{\partial p_a}{\partial x_a} = \frac{\partial p_c}{\partial x_c} - \rho \frac{dU_p(t)}{dt} \qquad (2.14)$$

$$\frac{\partial p_a}{\partial y_a} = \frac{\partial p_c}{\partial y_c}$$

Thus we see that the flow quantities and pressure in **case a** and **case b** are interrelated by simple reference transformations. In order to model a combination of steady and harmonic flow past a body as in **case a**, it is possible to model steady flow past a harmonically oscillating body as in **case b** and then use the appropriate transformations to get the solution for **case a**.

2.4 Non-dimensional Form of Governing Equations

Consider a fluid with a velocity $u_s + u_p \cos \omega t$ flowing over a body of arbitrary shape with a characteristic length b. U_s represents steady flow and $u_p \cos \omega t$ represents uniform harmonic flow with an oscillating frequency of ω. The simple harmonic displacement of the fluid is given by

$$s = s_o \sin \omega t$$

$$|U_s| = u_s \qquad (2.15)$$

$$|U_p| = u_p$$

where s_o is the displacement amplitude such that $u_p = \omega s_o$

The problem can be transformed to that of **case b** where fluid with steady velocity u_s is flowing over a body of arbitrary shape with a characteristic length b undergoing uniform harmonic motion with a velocity of $-u_p \cos \omega t$. ω is the frequency of oscillations of the body. The simple harmonic displacement of the body is given by equation (2.15)

Introduce the non-dimensional variables:

$$x' = \frac{x}{b} \qquad y' = \frac{y}{b} \qquad t' = \omega t$$
$$u' = \frac{u}{u_o} \qquad v' = \frac{v}{u_o} \qquad p' = \frac{p}{\mu u_o / b} \qquad (2.16)$$
$$\text{where}$$
$$u_o = u_s + u_p$$

into equations (2.3) and (2.4), we get the non-dimensional form of the Navier-Stokes equations and the continuity equation.

$$R_\omega \frac{\partial u}{\partial t} + R_e \left(u \frac{\partial u}{\partial x} + v \frac{\partial u}{\partial y} \right) = 2 \frac{\partial^2 u}{\partial x^2} + \frac{\partial^2 u}{\partial y^2} + \frac{\partial^2 v}{\partial x \partial y} - \frac{\partial p}{\partial x}$$
$$R_\omega \frac{\partial v}{\partial t} + R_e \left(u \frac{\partial v}{\partial x} + v \frac{\partial v}{\partial y} \right) = \frac{\partial^2 v}{\partial x^2} + 2 \frac{\partial^2 v}{\partial y^2} + \frac{\partial^2 u}{\partial x \partial y} - \frac{\partial p}{\partial y} \qquad (2.17)$$
$$\frac{\partial u}{\partial x} + \frac{\partial v}{\partial y} = 0$$

All quantities are their respective non-dimensional values and the primes have been omitted for convenience.

$R_\omega = \frac{\omega b^2}{\nu} = $ frequency Reynolds number

$R_e = R_{e_1} + R_{e_2}$

$R_{e_1} = \frac{u_s b}{\nu} = $ Reynolds number for steady flow

$R_{e_2} = \frac{u_p b}{\nu} = $ Reynolds number for oscillating flow.

We thus have three non-dimensional parameters which completely characterise the flow problem under consideration. These are the three Reynolds numbers: R_ω, R_{e_1} and R_{e_2}. It should be noted that the pressure has been non-dimensionalised with respect to the characteristic shear stress rather than the dynamic pressure as it is anticipated that the flow regime would be a slow, shear dominated one.

Introducing equations (2.16) and two additional non-dimensional variables

$$X' = \frac{X}{\mu u_o / b} \qquad Y' = \frac{Y}{\mu u_o / b}$$

into equation (2.6), we get the non-dimensional form of boundary conditions

Kinematic Boundary Conditions:-

$$u = U, \quad v = V \qquad (x, y) \in \Gamma_u, \quad t > 0 \tag{2.18a}$$

Natural Boundary Conditions:-

$$
\left[-p + 2\frac{\partial u}{\partial x} \right] n_1 + \left[\left(\frac{\partial u}{\partial y} + \frac{\partial v}{\partial x} \right) \right] n_2 = X
$$
$$
\left[\left(\frac{\partial u}{\partial y} + \frac{\partial v}{\partial x} \right) \right] n_1 + \left[-p + 2\frac{\partial v}{\partial y} \right] n_2 = Y
$$
$$
(x, y) \in \Gamma_s, \quad t > 0 \tag{2.18b}
$$

All quantities are their respective non-dimensional values. The primes have been omitted for convenience.

Introducing equations (2.16) and additional non-dimensional variables

$$\sigma_x' = \frac{\sigma_x}{\mu u_o / b} \quad \sigma_y' = \frac{\sigma_y}{\mu u_o / b} \quad \tau_{xy}' = \frac{\tau_{xy}}{\mu u_o / b}$$

into equations (2.2), we obtain the non-dimensional form of the constitutive relation.

Constitutive Relations:-

$$
\begin{aligned}
\sigma_x &= -p + 2\frac{\partial u}{\partial x} \\
\sigma_y &= -p + 2\frac{\partial v}{\partial y} \\
\tau_{xy} &= \left(\frac{\partial v}{\partial x} + \frac{\partial u}{\partial y} \right)
\end{aligned}
\tag{2.19}
$$

All quantities are their respective non-dimensional values. The primes have been omitted for convenience.

Introduce equations (2.16) and the non-dimensional variables

$$m' = \frac{m}{\rho A_b l} \qquad k' = \frac{k}{\omega^2 \rho A_b l} \qquad F_e' = \frac{F_e}{\mu u_o l} \qquad F_f' = \frac{F_f}{\mu u_o l}$$

into equations (2.7) A_b is the cross-sectional area of the cylinder body and l is the length of the cylinder. We obtain the non-dimensional form of the equation of motion for a single degree of freedom system.

$$m\ddot{s} + ks = J_b(F_e + F_f) \qquad (2.20)$$

where

$$J_b = \frac{\nu u_o}{\omega^2 b A_b} = \frac{R_e}{R_\omega^2}\left(\frac{b^2}{A_b}\right)$$

Finite Element Formulation of the Navier-Stokes Equations

3.1 General Remarks

In this chapter, the Navier-Stokes equations and the continuity equation (eqn 2.17) along with the boundary conditions (2.18) are discretised using the finite element method. The moving body boundary conditions are incorporated into the discretised equations which are then written in matrix form. The steady state solution is obtained using a modified method of averaging. Finally a Newton-Raphson iteration scheme is outlined for solving the resulting nonlinear equations. The whole procedure has been explained in detail for case b associated flow as described in section 2.3 in which the body is oscillating in a fluid domain moving with a steady velocity. A brief description of the finite element formulation of case a associated flow is presented later.

3.2 Restricted Variational Principle

The starting point in the finite element discretisation is the derivation of the functional form of the governing equations (eqns 2.17, 2.18). The *convective* nonlinear terms in the complete Navier-Stokes equations are non-self adjoint terms, due to which no variational principle exists corresponding to these equations. Nevertheless, it is possible to construct

a restricted variational principle of the form :—

$$\Pi = \iint_{\Omega_e} \left\{ \left[R_\omega \frac{\partial u}{\partial t} + R_e \left(u^0 \frac{\partial u^0}{\partial x} + v^0 \frac{\partial u^0}{\partial y} \right) \right] u \right.$$
$$+ \left[R_\omega \frac{\partial v}{\partial t} + R_e \left(u^0 \frac{\partial v^0}{\partial x} + v^0 \frac{\partial v^0}{\partial y} \right) \right] v$$
$$+ \left[\left(\frac{\partial u}{\partial x} \right)^2 + \left(\frac{\partial v}{\partial y} \right)^2 + \frac{1}{2} \left(\frac{\partial u}{\partial y} + \frac{\partial v}{\partial x} \right)^2 \right] \qquad (3.1)$$
$$\left. - p \left(\frac{\partial u}{\partial x} + \frac{\partial v}{\partial y} \right) \right\} dA - \int_{\Gamma_e} (\overline{X} u + \overline{Y} v) \, dS$$

The governing equations (eqn. 2.17 and 2.18) can be retrieved by taking the first variation of Π as shown in appendix A. This is identical to the Galerkin method but allows one to think in the usual terms of seeking a stationary point to some functional. The velocities (u^0, v^0), are associated with the inertial terms and are held constant while taking the first variation of Π. At the end of the process, u^0, v^0 are equated to u, v and there by restoring the governing equations.

3.3 The Discretised Form

The highest order of derivative in the functional Π is unity. Hence an element with only C^0 continuity is required for the interpolation of each of the (u, v, p) variables. Olson [17], has shown that the finite element interpolation for pressure p should be at least one degree less than that for the velocity component u, v. This restriction comes about in order to avoid the spurious singularities for the (u, v, p) integrated formulation. Taking these conditions into consideration, curved isoparametric elements, shown in figure 3.1, with quadratic interpolation for velocities and bilinear interpolation for pressure are used to carry out the finite element discretisation of the Navier-Stokes equations.

In isoparametric elements, the shape functions used are the same both for interpolating the variables u, v, p and for the transformation from s, t natural coordinates to x, y
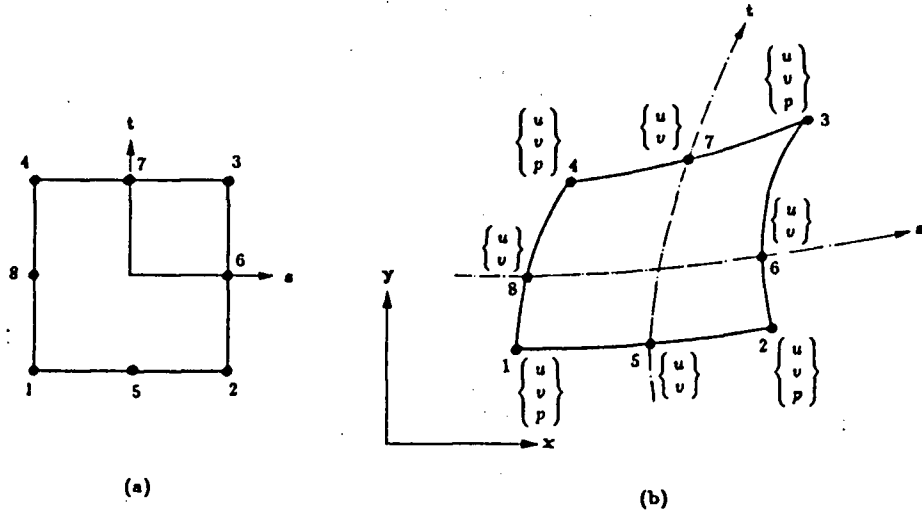
Figure 3.1 Isoparametric element used in present study.

(a.) Element in (s,t) space. (b.) Element in (x,y) space

coordinates. The velocities and pressures are represented by

$$u = N_i u_i(t) \qquad i = 1, 2, \ldots, 8$$
$$v = N_i v_i(t) \qquad i = 1, 2, \ldots, 8 \qquad\qquad (3.2)$$
$$p = M_i v_i(t) \qquad i = 1, \ldots, 4$$

where N_i, M_i are the shape functions and are represented by

$$N_1 = -\frac{1}{4}(1-s)(1-t)(1+s+t) \qquad N_2 = -\frac{1}{4}(1+s)(1-t)(1-s+t)$$

$$N_3 = -\frac{1}{4}(1+s)(1+t)(1-s-t) \qquad N_4 = -\frac{1}{4}(1-s)(1+t)(1+s-t)$$

$$N_5 = \frac{1}{2}(1-s^2)(1-t) \qquad N_6 = \frac{1}{2}(1+s)(1-t^2)$$

$$N_7 = \frac{1}{2}(1-s^2)(1+t) \qquad N_8 = \frac{1}{2}(1-s)(1-t^2)$$

$$M_1 = \frac{1}{4}(1-s)(1-t) \qquad M_2 = \frac{1}{4}(1+s)(1-t)$$

$$M_3 = \frac{1}{4}(1+s)(1+t) \qquad M_4 = \frac{1}{4}(1-s)(1+t)$$

and u_i, v_i, p_i are the time-dependent nodal variables.

Substituting equation 3.2 into the functional Π for one element and carrying out the first variation of each variable, yields

$$\left\{ \begin{array}{c} \frac{\partial \Pi^e}{\partial u_i} \\ \frac{\partial \Pi^e}{\partial v_i} \\ \frac{\partial \Pi^e}{\partial p_i} \end{array} \right\} = \left[\begin{array}{ccc} m_{ij}^{uu} & 0 & 0 \\ 0 & m_{ij}^{vv} & 0 \\ 0 & 0 & 0 \end{array} \right] \left\{ \begin{array}{c} \dot{u}_j \\ \dot{v}_j \\ \dot{p}_j \end{array} \right\} + \left[\begin{array}{ccc} k_{ij}^{uu} & k_{ij}^{uv} & -p_{ij}^{x} \\ k_{ji}^{uv} & k_{ij}^{vv} & -p_{ij}^{y} \\ -p_{ji}^{x} & -p_{ji}^{y} & 0 \end{array} \right] \left\{ \begin{array}{c} u_j \\ v_j \\ p_j \end{array} \right\}$$
$$+ R_e \left\{ \begin{array}{c} \delta_{ijk}^{x} u_j u_k + \delta_{ijk}^{y} v_j u_k \\ \delta_{ijk}^{x} u_j v_k + \delta_{ijk}^{y} v_j v_k \\ 0 \end{array} \right\} = \left\{ \begin{array}{c} 0 \\ 0 \\ 0 \end{array} \right\}$$

$$(3.3)$$

where Π^e denotes the variational principle for one element and Ω_e denotes the domain of the element under consideration.

$$m_{ij}^{uu} = \iint_{\Omega_e} R_\omega N_i N_j \, dA = m_{ij}^{vv}$$

$$k_{ij}^{uu} = \iint_{\Omega_e} 2\frac{\partial N_i}{\partial x}\frac{\partial N_j}{\partial x} + \frac{\partial N_i}{\partial y}\frac{\partial N_j}{\partial y} \, dA$$

$$k_{ij}^{vv} = \iint_{\Omega_e} 2\frac{\partial N_i}{\partial y}\frac{\partial N_j}{\partial y} + \frac{\partial N_i}{\partial x}\frac{\partial N_j}{\partial x} \, dA$$

$$k_{ij}^{uv} = \iint_{\Omega_e} \frac{\partial N_i}{\partial x}\frac{\partial N_j}{\partial y} \, dA \qquad\qquad i,j,k = 1,2,\ldots,8.$$

$$\delta_{ijk}^{x} = \iint_{\Omega_e} N_i N_j \frac{\partial N_k}{\partial x} \, dA$$

$$\delta_{ijk}^{y} = \iint_{\Omega_e} N_i N_j \frac{\partial N_k}{\partial y} \, dA$$

$$p_{ij}^{x} = \iint_{\Omega_e} \frac{\partial N_i}{\partial x} M_j \, dA \qquad i = 1,2,\ldots,8$$

$$p_{ij}^{y} = \iint_{\Omega_e} \frac{\partial N_i}{\partial x} M_j \, dA \qquad j = 1,\ldots,4$$

The derivation of the finite element dicretised form is presented in appendix B.

3.4 Boundary Conditions

For the elements not on the boundary, the line integral in the functional Π cancels out between the adjacent elements. For elements on the boundary where u and v are not specified, the line integral becomes the consistant load vector.

At the fluid outer boundary, u velocity is specified to be the far field uniform flow and v velocity is specified to be zero. Along the fluid-body interface, u and v velocities are spceified to be those of the moving body. The body is oscillating with an amplitude s_o, a frequency ω and a velocity $U_p(t)$.

$$s(t) = s_o \sin \omega t$$
$$U_p(t) = u_p \cos \omega t \tag{3.4}$$
$$u_p = \omega s_o$$

The moving body boundary conditions has been modelled by Pattani [18], where he considered the finite element grid to be fixed at the mean position of the body and the body moves past the grid. The relevant boundary terms are expanded by Taylor series to obtain the velocities at the mean position of the body at any time $t > 0$. We thus obtain

$$u(0) = u_p \cos \omega t - s_o \sin \omega t \left(\frac{\partial u}{\partial x}\right)_0$$
$$v(0) = -s_o \sin \omega t \left(\frac{\partial v}{\partial x}\right)_0 \tag{3.5}$$

The subscript 0 indicates that the derivatives are evaluated at $s = 0$, that is at the mean position of the body. Using the non-dimensional parameters as described in chapter 2 and additional parameters,

$$u_\infty = \frac{R_{e_1}}{R_e} \qquad\qquad u_b = \frac{R_{e_2}}{R_e}$$
$$\beta_1 = \frac{R_{e_1}}{R_\omega} = \frac{u_s}{\omega s_o} \qquad\qquad \beta_2 = \frac{R_{e_2}}{R_\omega} = \frac{s_o}{b}$$

the non-dimensionalised form of equation (3.5) is obtained as

$$u(0) = u_b \cos t - \beta_2 \left(\frac{\partial u}{\partial x}\right)_0 \sin t$$
$$v(0) = -\beta_2 \left(\frac{\partial v}{\partial x}\right)_0 \sin t \tag{3.6}$$

All the quantities are in their respective non-dimensional form and the primes have been omitted for convenience.

u_∞ is the non-dimensional far field fluid velocity.

u_b is the non-dimensional body velocity.

β_2 is the body amplitude parameter which also governs the nonlinear convection terms.

Equation (3.6) is then discretised by substituting equations (3.2) for nodal variables at the edge of the finite element grid interfacing with the mean position of the body. Thus obtain :–

$$u_i = u_b \cos t - \beta_2 C_{ij} u_j \sin t - \beta_2 u_b C_{ik} \sin t \cos t$$

$$v_i = -\beta_2 C_{ij} v_j \sin t$$

where

$$C_{ij} = \left(\frac{\partial N_j}{\partial x} \right)_i$$

(3.7)

1. j is summed over the velocity degrees of freedom other than those on the edge interfacing with the mean position of the body.

2. k is summed over the velocity degrees of freedom on the edge interfacing with the mean position of the body.

3. The subscript i indicates that $\frac{\partial N_j}{\partial x}$ is evaluated at the location of u_j or v_j, which ever is appropriate.

Suppose in a finite element domain, there are net u and v variables numbering n each and net p nodal variables numbering m each. Out of these, the u and v variables each numbering r are located on the fluid-body interface boundary whose values are known from equation (3.7). By suitable matrix manipulation, these variables are segregated and trasformed to the right hand side. This results in the matrix equation of form:–

$$[\mathbf{M} + \beta_2 \mathbf{P} \sin t] \dot{\mathbf{d}} + [\mathbf{K} + (\beta_2 \mathbf{P} + R_e u_b \mathbf{Q}) \cos t + \beta_2 \mathbf{R} \sin t] \, \mathbf{d}$$

$$+ R_e \left\{ \begin{array}{c} \delta^x_{ijk} u_j u_k + \delta^y_{ijk} v_j u_k \\ \delta^x_{ijk} u_j v_k + \delta^y_{ijk} v_j v_k \\ 0 \end{array} \right\} = u_b \mathbf{F} \sin t + u_b \mathbf{G} \cos t$$

(3.8)

$$+ \beta_2 u_b \left[\mathbf{H_1} \cos^2 t + \mathbf{J} \sin^2 t \right] + R_e u_b^2 \mathbf{H_2} \cos^2 t + \beta_2 u_b \mathbf{L} \sin t \cos t$$

where

$$\mathbf{d} = \{ u_1 \quad u_2 \quad \cdots \quad u_{n-r}, \quad v_1 \quad v_2 \quad \cdots \quad v_{n-r}, \quad p_1 \quad p_2 \quad \cdots \quad p_m \}^T$$

is the nodal vector of unknowns.

$$\mathbf{M} = \begin{bmatrix} m_{ij}^{uu} & 0 & 0 \\ 0 & m_{ij}^{vv} & 0 \\ 0 & 0 & 0 \end{bmatrix}$$

$$\mathbf{K} = \begin{bmatrix} k_{ij}^{uu} & k_{ij}^{uv} & -p_{ij}^{x} \\ k_{ji}^{uv} & k_{ij}^{vv} & -p_{ij}^{y} \\ -p_{ji}^{x} & -p_{ji}^{y} & 0 \end{bmatrix}$$

$$\mathbf{P} = -\begin{bmatrix} \sum\limits_{l=n-r+1}^{n} m_{il}^{uu} C_{lj} & 0 & 0 \\ 0 & \sum\limits_{l=n-r+1}^{n} m_{il}^{vv} C_{lj} & 0 \\ 0 & 0 & 0 \end{bmatrix}$$

$$\mathbf{R} = \begin{bmatrix} \sum\limits_{l=n-r+1}^{n} k_{il}^{uu} C_{lj} & \sum\limits_{l=n-r+1}^{n} k_{il}^{uv} C_{lj} & 0 \\ \sum\limits_{l=n-r+1}^{n} k_{li}^{uv} C_{lj} & \sum\limits_{l=n-r+1}^{n} k_{il}^{vv} C_{lj} & 0 \\ -\sum\limits_{l=n-r+1}^{n} p_{li}^{x} C_{lj} & -\sum\limits_{l=n-r+1}^{n} p_{li}^{y} C_{lj} & 0 \end{bmatrix}$$

$$\mathbf{Q} = \begin{bmatrix} \sum\limits_{l=n-r+1}^{n} \left(\delta_{ijl}^{x} + \delta_{ilj}^{x} \right) & \sum\limits_{l=n-r+1}^{n} \delta_{ijl}^{y} & 0 \\ 0 & \sum\limits_{l=n-r+1}^{n} \delta_{ilj}^{x} & 0 \\ 0 & 0 & 0 \end{bmatrix}$$

$$\mathbf{F} = \left\{ \begin{array}{c} \sum\limits_{j=n-r+1}^{n} m_{ij} \\ 0 \\ 0 \end{array} \right\} \qquad \mathbf{G} = -\left\{ \begin{array}{c} \sum\limits_{j=n-r+1}^{n} k_{ij}^{uu} \\ \sum\limits_{j=n-r+1}^{n} k_{ji}^{uv} \\ -\sum\limits_{j=n-r+1}^{n} p_{ji}^{x} \end{array} \right\}$$

Let q be the net number of u and v degrees of freedom, each at the edge of an element which is at the interface between the viscous fluid and the mean position of the body, then

$$\mathbf{H_1} = \left\{ \begin{array}{c} \sum\limits_{l=n-r+1}^{n} m_{il}^{uu} \sum\limits_{j=1}^{q} C_{lj} \\ 0 \\ 0 \end{array} \right\} \qquad \mathbf{H_2} = -\left\{ \begin{array}{c} \sum\limits_{j=n-r+1}^{n} \sum\limits_{k=n-r+1}^{n} \delta_{ijk}^{x} \\ 0 \\ 0 \end{array} \right\}$$

$$\mathbf{L} = \left\{ \begin{array}{c} \displaystyle\sum_{l=n-r+1}^{n} k_{il}^{uu} \sum_{j=1}^{q} C_{lj} \\[2ex] \displaystyle\sum_{l=n-r+1}^{n} k_{li}^{uv} \sum_{j=1}^{q} C_{lj} \\[2ex] - \displaystyle\sum_{l=n-r+1}^{n} p_{li}^{x} \sum_{j=1}^{q} C_{lj} \end{array} \right\} \qquad \mathbf{J} = -\mathbf{H_1}$$

3.5 Steady State Solution

Due to the quadratic nonlinear terms in the Navier-Stokes equations, the velocities have a steady component as well as a time-dependent component. Pattani has modified the method of averaging in order to obtain the steady streaming part of the solution from equation (3.8) which governs the fluid-structure problem under consideration. The same procedure is applied to obtain the steady state solution to equation (3.8).

The starting point in the method of averaging is to assume a form of solution as

$$\mathbf{d} = \mathbf{A} + \mathbf{B}\cos t + \mathbf{C}\sin t \tag{3.9}$$

where $\mathbf{B}(t)$, $\mathbf{C}(t)$ are assumed to be slowly varying functions of non-dimensional time t. Equation (3.9) is substitued into equation (3.8) and method of averaging is applied. The resulting equation is presented in equation 3.10.

$$
\begin{bmatrix} 0 & 0 & \frac{\beta_2}{2}\mathbf{P} \\ 0 & \mathbf{M} & 0 \\ 0 & 0 & \mathbf{M} \end{bmatrix} \begin{Bmatrix} \dot{\mathbf{A}} \\ \dot{\mathbf{B}} \\ \dot{\mathbf{C}} \end{Bmatrix} + \begin{bmatrix} \mathbf{K} & \frac{R_e u_b}{2}\mathbf{Q} & \frac{\beta_2}{2}\mathbf{R} \\ \beta_2\mathbf{P} + R_e u_b\mathbf{Q} & \mathbf{K} & \mathbf{M} \\ \beta_2\mathbf{R} & -\mathbf{M} & \mathbf{K} \end{bmatrix} \begin{Bmatrix} \mathbf{A} \\ \mathbf{B} \\ \mathbf{C} \end{Bmatrix}
$$

$$
+ R_e \left\{ \begin{array}{c} \delta^x_{ijk}(A^u_j A^u_k + B^u_j B^u_k/2 + C^u_j C^u_k/2) + \delta^y_{ijk}(A^v_j A^u_k + B^v_j B^u_k/2 + C^v_j C^u_k/2) \\ \delta^x_{ijk}(A^u_j A^v_k + B^u_j B^v_k/2 + C^u_j C^v_k/2) + \delta^y_{ijk}(A^v_j A^v_k + B^v_j B^v_k/2 + C^v_j C^v_k/2) \\ 0 \\ \delta^x_{ijk}(A^u_j B^u_k + A^u_k B^u_j) + \delta^y_{ijk}(A^v_j B^u_k + A^u_k B^v_j) \\ \delta^x_{ijk}(A^u_j B^v_k + A^v_k B^u_j) + \delta^y_{ijk}(A^v_j B^v_k + A^v_k B^v_j) \\ 0 \\ \delta^x_{ijk}(A^u_j C^u_k + A^u_k C^u_j) + \delta^y_{ijk}(A^v_j C^u_k + A^u_k C^v_j) \\ \delta^x_{ijk}(A^u_j C^v_k + A^v_k C^u_j) + \delta^y_{ijk}(A^v_j C^v_k + A^v_k C^v_j) \\ 0 \end{array} \right\}
$$

$$
= \left\{ \begin{array}{c} \frac{R_e u_b^2}{2}\mathbf{H_2} \\ \\ u_b\mathbf{G} \\ \\ u_b\mathbf{F} \end{array} \right\}
$$

(3.10)

where

$$
\mathbf{A} = \begin{Bmatrix} A^u_j \\ A^v_j \\ A^p_j \end{Bmatrix} \qquad \mathbf{B} = \begin{Bmatrix} B^u_j \\ B^v_j \\ B^p_j \end{Bmatrix} \qquad \mathbf{C} = \begin{Bmatrix} C^u_j \\ C^v_j \\ C^p_j \end{Bmatrix}
$$

The steady state solution corresponds to the singular points of the autonomous system of equations when $\dot{\mathbf{B}} = \dot{\mathbf{C}} = 0$. This results in a set of nonlinear algebraic equations for $\mathbf{A}, \mathbf{B}, \mathbf{C}$ which are solved using Newton-Raphson iteration procedure. The equations obtained for the increments to the solution vector, following the iterative scheme described by Pattani, are of the form

$$
[T]\{\Delta x\} = \{-f\}
$$

(3.11)

$[T]$ is the tangent stiffness matrix.

$\{\Delta x\}$ is the incremental solution vector.

$\{-f\}$ is the unbalanced load vector.

The details of these matrices are given in appendix C.

3.6 Finite Element Formulation for the Associated Flow

So far in this chapter, the finite element representation of **case b** as described in section 2.3 has been derived. The finite element representation of **case a** is similar and in fact simpler than that of **case b**. In this section, the finite element formulation of **case a** is presented.

The fluid remote from the stationary body has a velocity of U_o in the x direction and is given by

$$U_o = U_s + U_p$$
$$|U_o| = u_s + u_p \tag{3.12}$$

U_s is the steady component of the fluid velocity.

$U_p = u_p \cos \omega t$ is the periodic component of the fluid velocity.

The transformation from reference frame (x_a, y_a) to reference frame (x_c, y_c), as given in equation 2.14 can be written as

$$u_a = u_c + u_p \cos \omega t$$

$$v_a = v_c$$

$$\frac{\partial p_a}{\partial x_a} = \frac{\partial p_c}{\partial x_c} + \rho \omega u_p \sin \omega t \tag{3.13}$$

$$\frac{\partial p_a}{\partial y_a} = \frac{\partial p_c}{\partial y_c}$$

Using the non-dimensional variables introduced in sections 2.4 and 3.4, the non-dimensional form of equation 3.13 can be expressed as

$$u_a = u_c + u_b \cos t$$

$$v_a = v_c$$

$$\frac{\partial p_a}{\partial x_a} = \frac{\partial p_c}{\partial x_c} + R_\omega u_b \sin t \tag{3.14}$$

$$\frac{\partial p_a}{\partial y_a} = \frac{\partial p_c}{\partial y_c}$$

All quantities are in their respective non-dimensional form and the primes have been omitted for convenience. Integrating the pressure terms in equation 3.14, the final trans-

formation for u, v, p is obtained.

$$u_a = u_c + u_b \cos t$$

$$v_a = v_c \qquad\qquad (3.15)$$

$$p_a = p_c + R_\omega x_a u_b \sin t + k$$

k is the constant of integration. When p_a at a point (x_{a_o}, y_{a_o}) in the finite element domain is assigned a specified value, say zero, then the value of $k = -R_\omega x_{a_o} u_b \sin t$. Thus the value of p_a at a point (x_a, y_a) is

$$p_a = p_c + R_\omega(x_a - x_{a_o}) u_b \sin t$$

The variational principle Π presented in equation 3.1 is the same in **case a** as in **case b**. The discretised form of Π is identical to **case b** and is given by equation 3.3. In **case a**, no moving body boundary conditions need to be incorporated which makes the formulation simpler. Apply the method of averaging to equation 3.3 as described in section 3.5, and obtain the resulting equations in matrix form as

$$
\begin{bmatrix} 0 & 0 & 0 \\ 0 & \mathbf{M} & 0 \\ 0 & 0 & \mathbf{M} \end{bmatrix} \begin{Bmatrix} \dot{\mathbf{A}} \\ \dot{\mathbf{B}} \\ \dot{\mathbf{C}} \end{Bmatrix} + \begin{bmatrix} \mathbf{K} & 0 & 0 \\ 0 & \mathbf{K} & \mathbf{M} \\ 0 & -\mathbf{M} & \mathbf{K} \end{bmatrix} \begin{Bmatrix} \mathbf{A} \\ \mathbf{B} \\ \mathbf{C} \end{Bmatrix}
$$

$$
+ R_e \begin{Bmatrix}
\delta^x_{ijk}(A^u_j A^u_k + B^u_j B^u_k/2 + C^u_j C^u_k/2) + \delta^y_{ijk}(A^v_j A^u_k + B^v_j B^u_k/2 + C^v_j C^u_k/2) \\
\delta^x_{ijk}(A^u_j A^v_k + B^u_j B^v_k/2 + C^u_j C^v_k/2) + \delta^y_{ijk}(A^v_j A^v_k + B^v_j B^v_k/2 + C^v_j C^v_k/2) \\
0 \\
\delta^x_{ijk}(A^u_j B^u_k + A^u_k B^u_j) + \delta^y_{ijk}(A^v_j B^u_k + A^u_k B^v_j) \\
\delta^x_{ijk}(A^u_j B^v_k + A^v_k B^u_j) + \delta^y_{ijk}(A^v_j B^v_k + A^v_k B^v_j) \\
0 \\
\delta^x_{ijk}(A^u_j C^u_k + A^u_k C^u_j) + \delta^y_{ijk}(A^v_j C^u_k + A^u_k C^v_j) \\
\delta^x_{ijk}(A^u_j C^v_k + A^v_k C^u_j) + \delta^y_{ijk}(A^v_j C^v_k + A^v_k C^v_j) \\
0
\end{Bmatrix}
$$

$$
= \begin{Bmatrix} 0 \\ 0 \\ 0 \end{Bmatrix}
$$

$$(3.16)$$

This equation is similar to equation 3.10, except that the matrices $\mathbf{P}$, $\mathbf{Q}$, $\mathbf{R}$, $\mathbf{F}$, $\mathbf{G}$, $\mathbf{H_1}$, $\mathbf{H_2}$ and $\mathbf{J}$ which are associated with the moving body boundary conditions, are zero. The nodes at the outer boundary of the fluid domain have specified u and v velocities and are imposed as constraint equations in the formulation. The set of nonlinear equations are solved using Newton-Raphson iteration scheme just as described for **case b**. The tangent stiffness matrix and load vector is identical to that given in appendix C, except that $\mathbf{P} = \mathbf{Q} = \mathbf{R} = \mathbf{G} = \mathbf{F} = \mathbf{H_2} = 0$.

Characteristics of Fluid-Structure Interaction

4.1 General Remarks

Once the flow quantitites such as the velocity and pressure are obtained for a fluid domain by the procedure outlined in chapter 3, various other characteristics of the flow can be determined.

Flow characteristics like streamlines, streaklines and forces on the rigid bluff body are discussed and procedures to obtain them are outlined in this chapter. The first step in these procedures is to determine the velocities at the mean position of the body. The overall view of the flow pattern at any instant of time can be obtained by plotting the velocity vectors or the streaklines in the fluid domain. The basic nonlinear phenomenon of steady streaming is obtained by plotting the streamlines of the steady component of the velocity field.

The forces on a rigid body is characterised by the concept of the drag coefficients or the added mass, added damping and added force. The force quantities can be obtained for one case of associated flow and the results can be transformed to the other case of associated flow using simple coordinate transformations.

4.2 Computation of the Body Boundary Velocity

In obtaining the numerical solution of the complete Navier-Stokes equations, we made

the assumption that the fluid flow is periodic and the flow results can be represented as

$$\mathbf{d} = \mathbf{A} + \mathbf{B}\cos t + \mathbf{C}\sin t$$

Thus the velocity at any node in the fluid domain other than at the mean position of the body can be represented as

$$u_j = A_j^u + B_j^u \cos t + C_j^u \sin t$$
$$v_j = A_j^v + B_j^v \cos t + C_j^v \sin t$$

(4.1)

For an element on the body boundary, substitute equation 4.1 into equation 3.7 to obtain the nodal velocities at the mean position of the body. The resulting equations are

$$u_i = -\frac{\beta_2}{2}C_{ij}C_j^u + u_b\cos t - \beta_2 C_{ij}A_j^u\sin t$$
$$- \frac{\beta_2}{2}(C_{ij}B_j^u + u_bC_{ik})\sin 2t + \frac{\beta_2}{2}C_{ij}C_j^u\cos 2t$$

(4.2)

$$v_i = -\frac{\beta_2}{2}C_{ij}C_j^v - \beta_2 C_{ij}A_j^v\sin t - \frac{\beta_2}{2}C_{ij}B_j^v\sin 2t + \frac{\beta_2}{2}C_{ij}C_j^v\cos 2t$$

j is summed over the velocity degrees of freedom other than those on the edge interfacing with the mean position of the body.

k is summed over the velocity degrees of freedom on the edge interfacing with the mean position of the body.

At $t = 0$, when the body is at its mean position, the nodal velocities correspond to the body velocity. Neglecting higher harmonics, we can represent velocity at the mean position of the body as in equation 4.1. In this case

$$A_j^u = -\frac{\beta_2}{2}C_{ij}C_j^u$$
$$B_j^u = u_b$$
$$C_j^u = -\beta_2 C_{ij}A_j^u$$
$$A_j^v = -\frac{\beta_2}{2}C_{ij}C_j^v$$
$$B_j^v = 0$$
$$C_j^v = -\beta_2 C_{ij}A_j^v$$

(4.3)

4.3 Determination of Stream functions, Streamlines and Streaklines

4.3.1 General Remarks

A line in the fluid whose tangent is everywhere parallel to the fluid velocity U_o instantaneously, is a streamline. The family of streamlines at time t are solution of

$$\frac{dx}{u(x,t)} = \frac{dy}{v(x,t)} = \frac{dz}{w(x,t)}$$

where u, v, w are the components of velocity U_o parallel to the rectilinear axes x, y, z. The path of a material element of fluid does not in general coincide with a streamline, although it does so when the motion is steady. Streakline is that on which lie all those fluid elements that at some earlier instant passed through a certain point of space. Thus, when a dye or some other marking material is discharged slowly at some fixed point in a moving fluid, the visible line produced in the fluid is a streakline. When the flow is steady, streaklines, streamlines and pathlines coincide.

The stream function Ψ is defined in terms of the velocity components u and v as

$$u = \frac{\partial \Psi}{\partial y} \qquad v = -\frac{\partial \Psi}{\partial x}$$

The function Ψ can also be regarded as the only nonzero component of *vector potential* for u and can be written as

$$\frac{v(x,t)}{u(x,t)} = \frac{\partial y}{\partial x} \tag{4.4}$$

Thus the lines of constant stream function are streamlines or streaklines as the case may be. The stream function can be obtained by solving the Poisson equation

$$\nabla^2 \Psi = -\varsigma = \frac{\partial u}{\partial y} - \frac{\partial v}{\partial x} \tag{4.5}$$

1. When u and v represent the total velocity field, (i.e the steady as well as the time-dependent components), lines of constant Ψ represent streaklines.

2. When u and v represent only the steady flow component A, lines of constant Ψ represent streamlines.

3. ς is the vorticity for the total velocity field or the steady flow conmponent as the case may be.

4.3.2 Finite Element Representation of the Poisson equation

The Poisson equation 4.5 can be represented in its functional form as

$$I = \iint_\Omega \left\{ \frac{1}{2} \left[\left(\frac{\partial \Psi}{\partial x} \right)^2 + \left(\frac{\partial \Psi}{\partial y} \right)^2 \right] - \varsigma \Psi \right\} dA - \int_{C_s} g(s) \Psi \, dS \qquad (4.6)$$

Ω is the domain of the problem.

$g(s) = \frac{\partial \Psi}{\partial n}$ is the tangential velocity specified on the natural part of the boundary C_s.

The finite element discretisation is done using the same finite element interpolation of Ψ as that for velocities described in section 3.3. The stream funtion Ψ is represented by

$$\Psi = N_i \Psi_i \qquad i = 1, 2, 3, \cdots, 8 \qquad (4.7)$$

N_i are the shape functions given in section 3.3.

Ψ are the nodal variables of stream function.

Substituting equation 4.7 into the functional I for one element, the resulting equation is

$$I^e = \iint_{\Omega_e} \left\{ \frac{1}{2} \left[N_{i,x} N_{j,x} + N_{i,y} N_{j,y} \right] \Psi_i \Psi_j - \varsigma N_i \Psi_i \right\} dA - \int_{C_s} g(s) N_i \Psi_i \, ds \qquad (4.8)$$

Take the first variation of equation 4.8 with respect to Ψ_i and thus minimise the functional I

$$\frac{\partial I^e}{\partial \Psi_i} = \iint_{\Omega_e} \left\{ \left(N_{i,x} N_{j,x} + N_{i,y} N_{j,y} \right) \Psi_j - \varsigma N_i \right\} dA - \int_{C_s} g(s) N_i \, dS = 0 \qquad (4.9)$$

$$N_{i,x} = \frac{\partial N_i}{\partial x} \qquad N_{i,y} = \frac{\partial N_i}{\partial y}$$

I^e denotes the functional I for one element.

Ω_e denotes the domain of element under consideration.

All such elements are assembled to produce a set of global equations pertaining to the fluid domain. These equations can be written in matrix form as

$$[Z_{ij}]\{\Psi\} = \{P_i\} \tag{4.10}$$

$$[Z_{ij}] = \iint_{\Omega_e} \{N_{i,x}N_{j,x} + N_{i,y}N_{j,y}\} \, dA$$

$$\{P_i\} = \iint_{\Omega_e} \varsigma N_i \, dA + \int_{C_e} g(s)N_i \, dS$$

For an element not on the boundary, the line integral in the functional I cancels out between adjacent elements. For elements on the boundary where Ψ is not specified, the line integral becomes the consistant load vector.

4.4 Determination of Force Characteristics

4.4.1 Computation of Added Mass, Added Damping and Added Force

Consider the fluid-structure problem where a bluff body is oscillating in the direction of flow. This can be represented as a spring-mass system as shown in figure 2.1.

1. M_b = Mass of the bluff body.

2. K_b = Stiffness of the bluff body.

3. $F_e(t)$ = External force applied to cause the motion s of the body.

4. $s(t) = s_o \sin \omega t$ = Motion of the body.

5. U_s = Steady velocity of fluid remote from the body.

6. $U_p = u_p \cos \omega t$ = Velocity of body where $u_p = \omega s_o$.

7. $F_f(t)$ = Fluid force on the body

The fluid forces on a rigid body performing harmonic oscillations will in general consist of three components:– 1. a component in phase with the acceleration of the body, 2. a component in phase with the velocity of the body, 3. a constant component. The components are each associated with the added mass, added damping and added force,

respectively. Added mass is defined as the quotient of the additional force required to produce acceleration throughout the fluid domain divided by the acceleration of the body.

The equation of motion of the single degree of freedom is represented in its non-dimensional form as in equation 2.20

$$M_b\ddot{s} + K_b s = J_b(F_e + F_f) \tag{4.11}$$

where

$$J_b = \frac{R_e}{R_\omega^2}\left(\frac{b^2}{A_b}\right)$$

$$s = \beta_2 \sin t$$

$$R_{e_1} = \frac{u_s b}{\nu} \qquad R_{e_2} = \frac{u_p b}{\nu} \qquad R_\omega = \frac{\omega b^2}{\nu}$$

$$\beta_1 = \frac{R_{e_1}}{R_\omega} \qquad \beta_2 = \frac{R_{e_2}}{R_\omega} \qquad u_\infty = \frac{R_{e_1}}{R_e} \qquad u_b = \frac{R_{e_2}}{R_e}$$

b is the characteristic length of the body.

A_b is the cross-sectional area of the body.

All variables are in their respective non-dimensional form. The non-dimensional variables introduced in section 2.4 and section 3.4 have been used.

Substituting the expression for s into equation 4.11, obtain

$$-M_b\beta_2 \sin t + K_b\beta_2 \sin t = \frac{R_e}{R_\omega^2}\left(\frac{b^2}{A_b}\right)(F_e + F_f) \tag{4.12}$$

We expect the fluid force to be of form

$$F_f = P + Q\cos t + R\sin t \tag{4.13}$$

P represents the steady drag force on the body.

Q and R are the periodic components of fluid force.

Substitute equation 4.13 into 4.12 and rearrange terms to obtain an expression for the

external force F_e.

$$F_e = -P - \left(M_b R_\omega u_b \left(\frac{A_b}{b^2} \right) + R \right) \sin t$$

$$+ K_b R_\omega u_b \left(\frac{A_b}{b^2} \right) \sin t - Q \cos t \tag{4.14}$$

Equation 4.12 can be represented in terms of the added mass M_a, the added damping C_a and the added force F_a.

$$-(M_b + M_a) R_\omega u_b \left(\frac{A_b}{b^2} \right) \sin t$$

$$+ K_b R_\omega u_b \left(\frac{A_b}{b^2} \right) \sin t + C_a R_\omega u_b \left(\frac{A_b}{b^2} \right) \cos t = F_e + F_a \tag{4.15}$$

Comparing equations 4.14 and 4.15, the expressions for added mass, added damping and added force are obtained

$$M_a = \frac{R}{R_\omega u_b} \left(\frac{b^2}{A_b} \right) = \text{added mass}$$

$$C_a = -\frac{Q}{R_\omega u_b} \left(\frac{b^2}{A_b} \right) = \text{added damping} \tag{4.16}$$

$$F_a = P = \text{added force}$$

Appendix E presents the solution procedure to solve the equation of motion in **case b** flow configuration using M_a, C_a and F_a.

4.4.2 Determination of Fluid Forces on the Bluff Body

The normal and shear stress at a point along a plane inclined at an angle α with the x-axis (figure 4.2), can be represented in terms of the stress components σ_x, σ_y and τ_{xy} as

$$\sigma = \sigma_x \sin^2 \alpha + \sigma_y \cos^2 \alpha - 2\tau_{xy} \sin \alpha \cos \alpha$$

$$\tau = \tau_{xy}(\sin^2 \alpha - \cos^2 \alpha) + (\sigma_x - \sigma_y) \sin \alpha \cos \alpha \tag{4.17}$$

The resultant fluid force along the x direction on a length l of the cylinder due to σ and τ is given by

$$F_f = -l \oint (\sigma \sin \alpha + \tau \cos \alpha) \, de \tag{4.18}$$
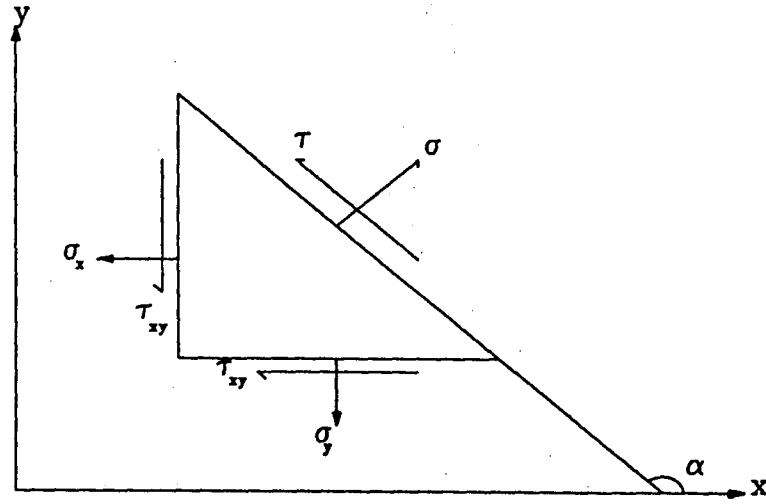
Figure 4.1 Stress Components

The integration around the cross-section is done in the counter- clockwise direction.

The fluid force has two components: F_σ and F_τ.

$$F_\sigma = -l \oint \sigma \sin \alpha \, de$$

$$F_\tau = -l \oint \tau \cos \alpha \, de$$

F_σ is the normal force which is mainly due to pressure and hence is known as the pressure drag.

F_τ is the tangential force which is the result of shearing stresses and hence is known as the friction drag. The drag force is made non-dimensional by dividing it by $0.5\rho u_s^2$ where ρ is the density of the fluid and u_s is its steady velocity. We thus obtain three drag coefficients:

$$C_{d_p} = \frac{F_\sigma}{0.5\rho u_s^2} = \text{the pressure drag coefficient}$$

$$C_{d_f} = \frac{F_\tau}{0.5\rho u_s^2} = \text{the friction drag coefficient}$$

$$C_d = C_{d_p} + C_{d_f} = \text{total drag coefficient}$$

Since at low Reynolds number, flow over bluff bodies is symmetric along the axis normal to the direction of flow, the force along the y axis is zero. That is in our analysis, only the presence of drag force is considered and lift force is neglected. Using the non-dimensional variables

$$e' = \frac{e}{b} \qquad \sigma' = \frac{\sigma}{\mu u_o/b} \qquad \tau' = \frac{\tau}{\mu u_o/b} \qquad F_f' = \frac{F_f}{\mu u_o l}$$

the non-dimensional form of equation 4.18 is obtained as

$$F_f = - \oint (\sigma \sin \alpha + \tau \cos \alpha)\, de$$

All variables are in their respective non-dimensional form and primes have been omitted for convenience.

$$F_\sigma = - \oint \sigma \sin \alpha\, de = \text{fluid force due to } \sigma$$

$$F_\tau = - \oint \tau \cos \alpha\, de = \text{fluid force due to } \tau \qquad (4.19)$$

With this non-dimensionalising, the drag coefficients are redefined as:

$$C_{d_p} = \frac{2}{R_{e_1} u_\infty} F_\sigma \qquad C_{d_f} = \frac{2}{R_{e_1} u_\infty} F_\tau$$

$$C_d = C_{d_p} + C_{d_f}$$

R_{e_1} is the Reynolds number for steady flow and u_∞ is the far field fluid veloicty. All the variables are in their respective non-dimensional form and the primes have been omitted for convenience. The velocities and pressures are represented by the finite elements by

$$u = N_i u_i \qquad i = 1, 2, \cdots, 8$$

$$v = N_i v_i \qquad i = 1, 2, \cdots, 8$$

$$p = M_i P_i \qquad i = 1, \cdots, 4$$

N_i, M_i are the interpolating functions given in section 3.3.

u_i, v_i, p_i are the nodal variables.

The stress components given by equation 2.19 can be represented in matrix form as

$$\left\{ \begin{array}{c} \sigma_x \\ \sigma_y \\ \tau_{xy} \end{array} \right\} = \begin{bmatrix} 2N_{i,x} & 0 & -M_i \\ 0 & 2N_{i,y} & -M_i \\ M_{i,y} & M_{i,x} & 0 \end{bmatrix} \left\{ \begin{array}{c} u_i \\ v_i \\ p_i \end{array} \right\} \qquad (4.20)$$

$$N_{i,x} = \frac{\partial N_i}{\partial x} \qquad\qquad N_{i,y} = \frac{\partial N_i}{\partial y}$$

$$M_{i,x} = \frac{\partial M_i}{\partial x} \qquad\qquad M_{i,y} = \frac{\partial M_i}{\partial y}$$

Thus equation 4.19 can be written in matrix form as

$$\left\{ \begin{array}{c} \sigma \\ \tau \end{array} \right\} = \left[\begin{array}{ccc} \sin^2\alpha & \cos^2\alpha & -2\sin\alpha\cos\alpha \\ \sin\alpha\cos\alpha & -\sin\alpha\cos\alpha & \sin^2\alpha - \cos^2\alpha \end{array} \right] \left\{ \begin{array}{c} \sigma_x \\ \sigma_y \\ \tau_{xy} \end{array} \right\} \tag{4.21}$$

Equation 4.19 can be written as

$$\left\{ \begin{array}{c} F_\sigma \\ F_\tau \end{array} \right\} = -\oint \left[\begin{array}{ccc} \sin^3\alpha & \cos^2\alpha\sin\alpha & -2\sin^2\alpha\cos\alpha \\ \sin\alpha\cos^2\alpha & -\sin\alpha\cos^2\alpha & \cos\alpha(\sin^2\alpha - \cos^2\alpha) \end{array} \right]$$

$$\left[\begin{array}{ccc} 2N_{i,x} & 0 & -M_i \\ 0 & 2N_{i,y} & -M_i \\ M_{i,y} & M_{i,x} & 0 \end{array} \right] de \left\{ \begin{array}{c} u_i \\ v_i \\ p_i \end{array} \right\} \tag{4.22}$$

For an isoparametric element, the coordinates of a point in the element are also given by

$$x = N_i x_i \qquad i = 1, 2, \cdots, 8$$

$$y = N_i y_i \qquad i = 1, 2, \cdots, 8$$

where x_i and y_i are the nodal variables.

Thus the derivatives can be obtained as

$$\left\{ \begin{array}{c} \frac{\partial N_i}{\partial x} \\ \frac{\partial N_i}{\partial y} \end{array} \right\} = J^{-1} \left\{ \begin{array}{c} \frac{\partial N_i}{\partial s} \\ \frac{\partial N_i}{\partial t} \end{array} \right\} \tag{4.23}$$

J is termed the Jacobian of the transformation and is given by

$$J = \left[\begin{array}{cc} N_{j,s}x_j & N_{j,s}y_j \\ N_{j,t}x_j & N_{j,t}y_j \end{array} \right]$$

where

$$N_{j,s} = \frac{\partial N_j}{\partial s} \qquad\qquad N_{j,t} = \frac{\partial N_j}{\partial t}$$

Substituting equation 4.23 into equation 4.22 and using two point Gauss quadrature for numerical integration, P, Q, R of F_f is obtained from which M_a, C_a and F_a and the drag coefficients can be calculated.

4.4.3 Force Characteristics of the Associated Flow

The force characteristics for the case **b** where the body is oscillating in-line with a steady fluid flow has been considered. The force quantities for the **case a** where the body is at rest in an oscillating fluid flow can be easily determined by transforming the results obtained from **case b**.

The transformation from reference frame a to c is obtained from equation 3.15. Subscripts a and c denote **case a** and **case b** flow configurations respectively. The transformation for stresses is obtained as

$$\sigma_{x_a} = \sigma_{x_c} - R_\omega x_a u_b \sin t$$
$$\sigma_{y_a} = \sigma_{y_c} - R_\omega x_a u_b \sin t \qquad (4.24)$$
$$\tau_{xy_a} = \tau_{xy_c}$$

The fluid forces in the two reference frames can be expressed as

$$F_{f_a} = -\oint (\sigma_a \sin \alpha + \tau_a \cos \alpha)\, de$$
$$F_{f_c} = -\oint (\sigma_c \sin \alpha + \tau_c \cos \alpha)\, de$$

The transformation for the fluid force in the two associated flows is written as

$$F_{f_a} = F_{f_c} + R_\omega u_b \left(\frac{A_b}{b^2} \right) \sin t \qquad (4.25)$$

$$F_{f_a} = P_a + Q_a \cos t + R_a \sin t$$
$$F_{f_c} = P_c + Q_c \cos t + R_c \sin t$$

Thus the transformation for the fluid force components P, Q, R is expressed as

$$P_a = P_c$$
$$Q_a = Q_c \qquad (4.26)$$
$$R_a = R_c + R_\omega u_b \left(\frac{A_b}{b^2} \right)$$

The added mass is associated with R, the added damping with Q and the added force is associated with P. The *added mass* in **case b** is termed as the *inertia force* in case

a. Thus the transformation for added mass, added damping and added force for the two associated flows is expressed as

$$M_{a_a} = M_{a_c} + 1$$

$$C_{a_a} = C_{a_c} \tag{4.27}$$

$$F_{a_a} = F_{a_c}$$

M_{a_a} is the inertia force in **case a** and M_{a_c} is the added mass in **case b**. From equation 4.27, it is noted that there is no change in the added damping and added force between the two associated flows. M_{a_a} is greater than M_{a_c} by unity.

The transformation for C_{d_p}, C_{d_f} and C_d for the two associated flows is expressed as:

$$C_{d_{pa}} = C_{d_{pc}} + \frac{2}{R_{e_1} u_\infty} R_\omega u_b \left(\frac{A_b}{b^2} \right) \sin t$$

$$C_{d_{fa}} = C_{d_{fc}} \tag{4.28}$$

$$C_{d_a} = C_{d_c} + \frac{2}{R_{e_1} u_\infty} R_\omega u_b \left(\frac{A_b}{b^2} \right) \sin t$$

From equation 4.28, it is evident that there is no change in the friction drag coefficient but there is change in the pressure and total drag coefficients in the sine component.

4.5 The Morison Equation

In most applications of practical interest, the fluid forces acting on a body in a two-dimensional flow are determined by the Morison equation. The empirical coefficients used in the equation can be represented in terms of M_a, C_a and F_a.

Consider a cylinder of length l, characteristic cross-sectional size b and cross-sectional area A_b, in a viscous fluid. The fluid has a velocity U which consists of a steady component U_s and an oscillating component U_p and is given by

$$U = U_s + U_p$$

$$|U| = u_o = u_s + u_p$$

where $u_s = |U_s|$ and $U_p = u_p \cos \omega t$ and ω is the frequency of oscillations. The fluid force

F_f on the cylinder is given by the Morison equation as

$$\frac{F_f}{l} = \frac{1}{2}\rho b C_d U |U| + \rho A_b C_m \frac{dU}{dt}$$

$$= \frac{1}{2}\rho b C_d (u_s + u_p \cos\omega t)|(u_s + u_p \cos\omega t)| - \rho A_b C_m \omega u_p \sin\omega t \qquad (4.29)$$

$$= F_D + F_I$$

C_d is the drag coefficient associated with the drag force F_D, and C_m is the inertia coefficient associated with the inertia force F_I. The drag force can be linearised by representing $U|U|$ in terms of a fourier series. Considering only the first two terms of the series, we obtain

$$\frac{F_D}{l} = \frac{1}{2}\rho b C_d u_o^2 (a_o + a_1 \cos\omega t) \qquad (4.30)$$

a_o and a_1 are constants determined by R_{e_1} and R_{e_2}. Hence we can associate two drag coefficients with the drag force on a body.

1. $C_d(1) = a_o C_d$ = Drag coefficient associated with the steady drag force.

2. $C_d(2) = a_1 C_d$ = Drag coefficient associated with the oscillating drag force.

The linearised form of the Morison equation is written as

$$\frac{F_f}{l} = \frac{1}{2}\rho b u_o^2 [C_d(1) + C_d(2)\cos\omega t] - \rho A_b C_m \omega u_p \sin\omega t \qquad (4.31)$$

From the present investigation, the fluid force is obtained as described in section 4.4 as

$$\frac{F_f}{l} = \mu u_o (P + Q\cos\omega t + R\sin\omega t)$$

The coefficients used in the Morison equation can be represented in terms of the added mass M_a, added damping C_a and the added force F_a.

$$C_d(1) = \frac{2}{R_e} F_a$$

$$C_d(2) = \frac{\pi}{2}\frac{R_\omega R_{e_2}}{R_e^2} C_a \qquad (4.32)$$

$$C_m = M_a + 1$$

where R_{e_1}, R_{e_2}, R_ω and R_e are as defined in section 2.4.

<div align="right">

CHAPTER 5

</div>

Numerical Investigations

5.1 Introduction

In this chapter, numerical results are presented for three different body shapes, namely

1. Circular body oscillating in the direction of the flow.

2. Square body oscillating parallel to one of its sides in the direction of the flow.

3. Equilateral triangular body oscillating parallel to one of its bisectors in the direction of the flow.

The investigation is carried out in the viscous flow regime up to Reynolds number $R_{e_1} = 100$ with various values of R_{e_2} and R_ω, keeping the body amplitude parameter β_2 less than 0.2. The limiting cases of the body oscillating in an otherwise still fluid and that of a steady flow over a fixed body are verified with known results.

No experimental or analytical results are available at such low values of Reynolds numbers for the combined problem of a body oscillating in line with a steady fluid flow. Hence a parametric study is conducted for this combined flow problem and is classified into four groups.

Group 1.a: R_{e_1} is kept constant and R_{e_2} and R_ω are changed such that β_2 is kept constant. The effect of R_{e_2}/R_{e_1} on the flow pattern is observed.

Group 1.b: β_2 is kept constant by keeping R_ω and R_{e_2} constant. R_{e_2}/R_{e_1} is changed by changing R_{e_1}

Group 2: The effect of β_2 on the flow pattern is observed. R_{e_1} and R_{e_2} are kept constant and β_2 is changed by changing R_ω .

<div align="center">

42

</div>

Group 3: Effect of R_{e_2} on the flow pattern is observed. R_ω and R_{e_1} are kept constant. R_{e_2}/R_{e_1} and β_2 are changed due to the change in R_{e_2} .

The numerical results are also presented for the associated flow configuration of **case a** as described in section 2.3. These results are compared with those of **case b** and the transformations presented in equations 3.15 and 4.27 are checked.

The flow results are presented in the form of streamlines and streaklines. Streamlines are the stream function contours of the steady part of the velocity field and streaklines are the stream function contours of the total velocity field at one instant in time. The contour plots are obtained by plotting 31 equally spaced contours between the maximum and minimum values of the stream function in the plotted domain. In order to plot stream function contours, the stream function at each node of the plotting grid is required. A procedure for obtaining these nodal values is outlined in appendix D. The forces on the rigid body are computed in terms of added mass, added damping, added force and the drag coefficients.

All the computer programs are implemented on a 48-megabyte Amdahl 5840 system with double accelerator at the University of British Columbia. Double precision arithmetic is used throughout to reduce the effect of round-off errors. The solution of the linear algebraic equations and the matrix inversions are performed using a sparse matrix solving package called SPARSPAK.

5.2 Results for a Circular Body

5.2.1 General Remarks

A considerable amount of work has been conducted on an oscillating circular body in a fluid. Bertelsen [1] conducted experiments to study the steady streaming phenomenon in the boundary layer on a cylinder performing simple harmonic motion in a viscous incompressible fluid at rest. Riley [21] and Stuart tackled the same problem analytically using perturbation techniques to boundary layer theory. The experimental and analytical results are for very high values of R_ω and R_{e_2} , of the order of 100,000 and 5,000 respectively.

The present numerical model is not accurate at such high values of R_ω and R_{e_2}.

Pattani [18] has modelled the problem of a circular body oscillating in an otherwise still fluid and has obtained excellent agreement with Tatsuno's experimental results of the same problem configuration [28]. Tatsuno [27] and Tanida [26] have studied the problem of a circular cylinder oscillating in a steady viscous flow. But their experiments are conducted in the flow regime of a well developed vortex street behind the cylinder and at very high values of the body amplitude parameter in the range $\beta_2 > 0.5$.

Hence a parametric study is conducted as described in section 5.1 for the combined problem. The limiting case of steady flow over a circular fixed body is verified with the results obtained from Olson [31]. The limiting case of a circular body oscillating in a stationary fluid is verified with the results obtained from Pattani [18].

5.2.2 Finite Element Grid and Boundary Conditions

The numerical results are obtained for a circular body with a diameter b of unity. This diameter is also the characteristic length of the body. The centroid of the body is located at the origin of the x-y axis system and the body is performing oscillations parallel to the x-axis. Using symmetry in the flow problem, only one half of the domain is modelled.

Three finite element grids are developed as shown in figure 5.1. Grid 1 and Grid 2 have the same ratio of D/b=15.5, where D is the total length of the flow domain. Grid 3 has D/b=30.0. Grid 2 has a rectangular outer boundry while Grid 1 and Grid 3 have a circular outer boundary.

In finite element formulation, only the kinematic boundary conditions need to be specified and the homogenous natural boundary conditions come out as a part of the solution in the limit of grid refinement. Thus the symmetry condition is obtained by letting the velocity $v = 0$ and the shear stress $\tau_{xy} = 0$ (which is implemented by letting the velocity u float, $u =$?) on the symmetry line Γ_s. Though there is no symmetry in the pressure distribution, the pressure is specified to be zero at two symmetric locations: points 1 and 2 shown in figure 5.1. The fluid outer boundary is assumed to be far enough so that the pressure at these two points is approximately zero. Negligible change in the numerical

results is observed when the pressure is specified to be zero at only one point.

Boundary Conditions for Grid 1 and Grid 3

Grid 1 and 3 have the same velocity and pressure boundary conditions.

1. $u = u_\infty$, $v = 0$ all along the fluid outer boundary.

2. u and v velocities at the body boundary are specified according to equation 3.7.

3. $u=?$, $v=0$ all along the symmetry line Γ_s.

4. $p = 0$ at points 1 and 2 shown in the figure 5.1a and c.

Boundary Condition for Grid 2

1. $u = u_\infty$, $v = 0$ along Γ_i, the inflow boundary.

2. $u = u_\infty$, $v=?$ along Γ_u.

3. $u=?$, $v = 0$ along Γ_o, the outflow boundary.

4. $u=?$, $v = 0$ along Γ_s, the symmetry line.

5. $p = 0$ at points 1 and 2 shown in figure 5.1b.

Along Γ_o, the velocity u is allowed to float $(u=?)$. This implies that the associated stress, $\sigma_x = -p + \mu\frac{\partial u}{\partial x}$ is zero. The pressure $p = 0$ at point 2 and hence is approximately zero all along Γ_o. Thus $\frac{\partial u}{\partial x} = 0$ all along Γ_o.

For the flow problem of a body oscillating in a steady fluid flow, Grid 1 and Grid 3 have 368 net degrees of freedom of which 307 are for the velocities and 61 are for the pressure. Grid 2 has 370 net degrees of freedom of which 309 are for the velocities and 61 are for the pressure. There are three coefficients A, B, C for each degree of freedom. This results in 1104 variables in Grid 1 and Grid 3 and 1110 variables in Grid 2.
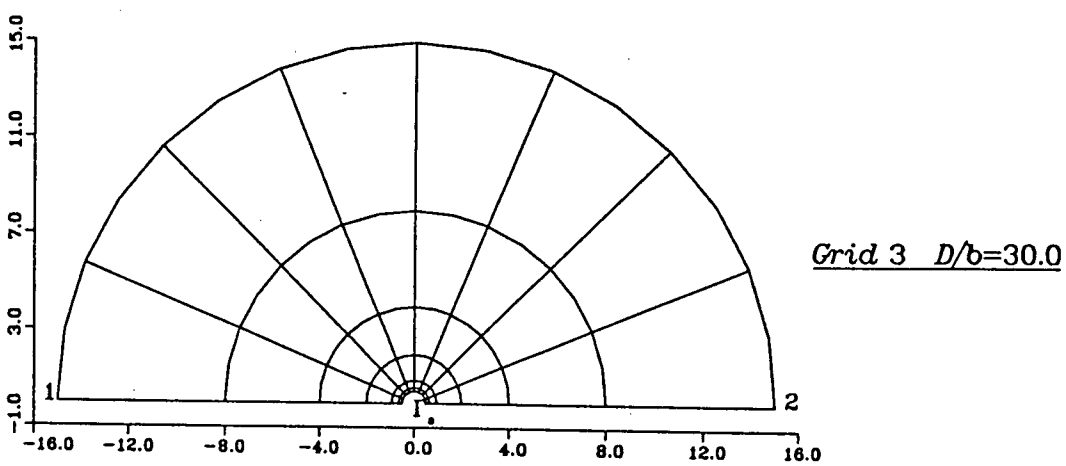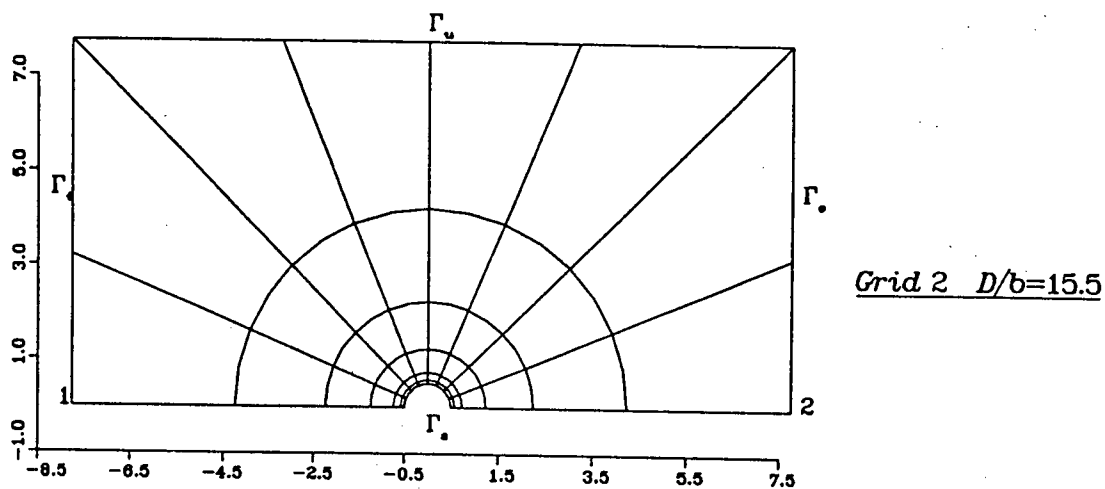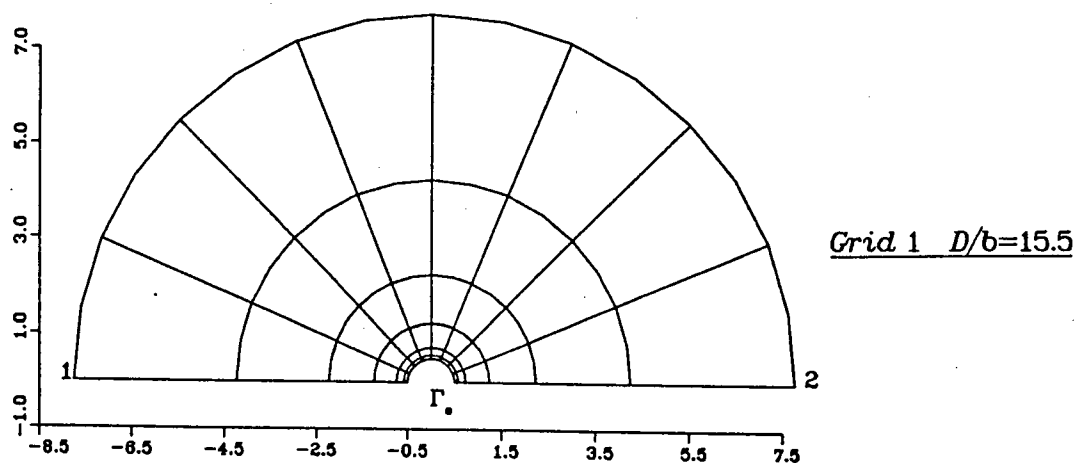
Figure 5.1 Finite Element Grids for Circular Body

5.2.3 Flow Results

Limiting Cases:-

The limiting case of a circular bluff body oscillating in an otherwise still fluid is verified with [18] for R_ω =250.0, R_{e_1} =0.0 and R_{e_2} =20.0 using Grid 1 and R_ω =278.2, R_{e_1} =0.0 and R_{e_2} =10.572 using Grid 3. Identical numerical results are obtained in both cases. Streamlines are plotted for the first case in figure 5.2.
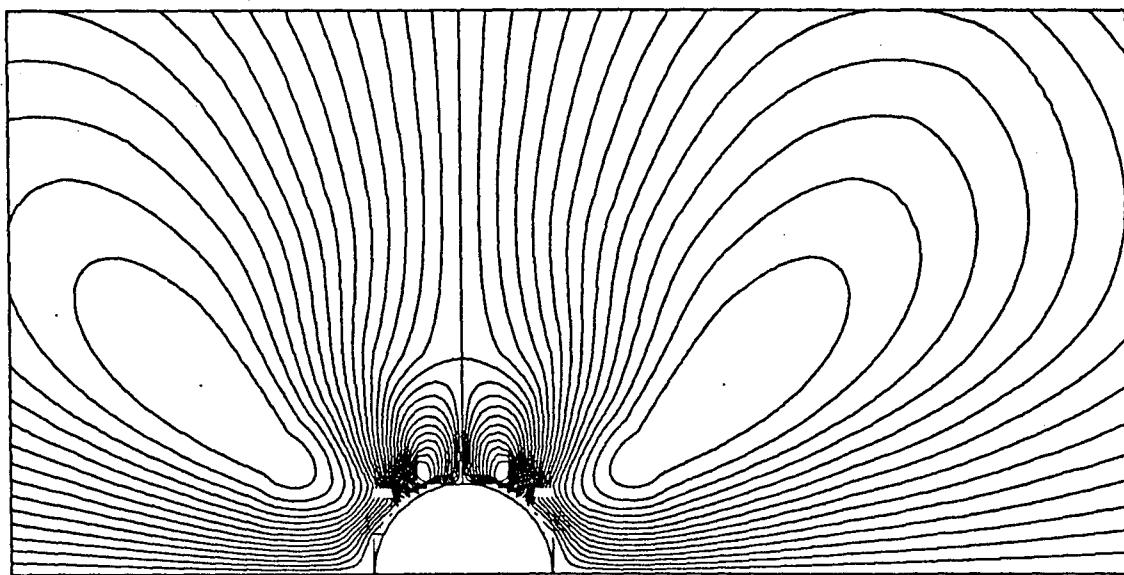

Figure 5.2 Limiting Case of an Oscillating Circular
Body in Still Fluid. R_ω =250.0 R_{e_1} =0.0 R_{e_2} =20.0

The limiting case of a steady flow over a stationary body is verified with [31] for values of R_{e_1} ranging from 2 to 70. The streamline plots for R_{e_1} =20 and 70 are presented in figures 5.3 and 5.4 respectively. The same contour values are plotted in the present study results as that of [31]. The kinks in the streamlines near the body in the present study are due to the coarseness of the grid. On refining the finite element grid, more stream function contours can be plotted and the kinks can be eliminated. Good agreement is obtained in the streamline plots.

The pressure distribution around the body at R_{e_1} =20 is presented in figure 5.5. The drag coefficients for R_{e_1} =5, 20, 40, and 70 are presented in table 5.1. Good agreement is obtained with [31] for the pressure distribution and the drag coefficients.
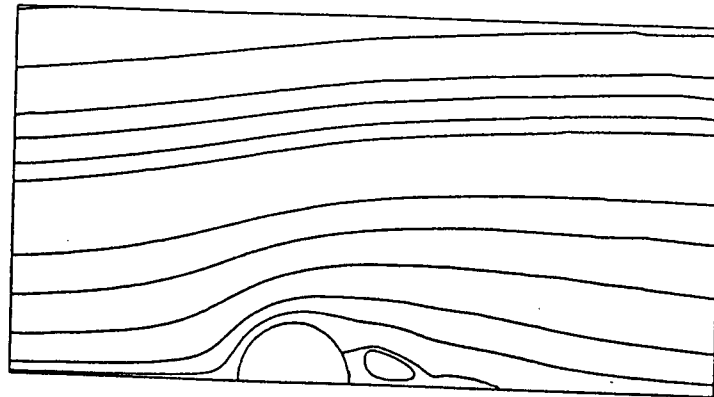
Present Study
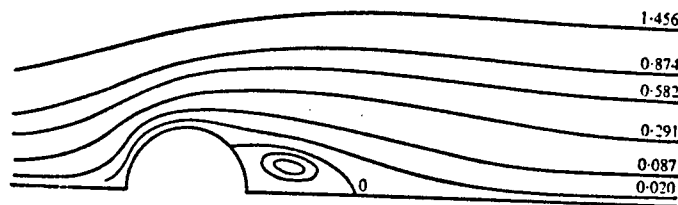
Reference [31]

Figure 5.3 Limiting Case of Steady Flow over a Circular Body. $R_\omega = 0.0$ $R_{e_1} = 20.0$ $R_{e_2} = 0.0$

Present Study

Reference [31]
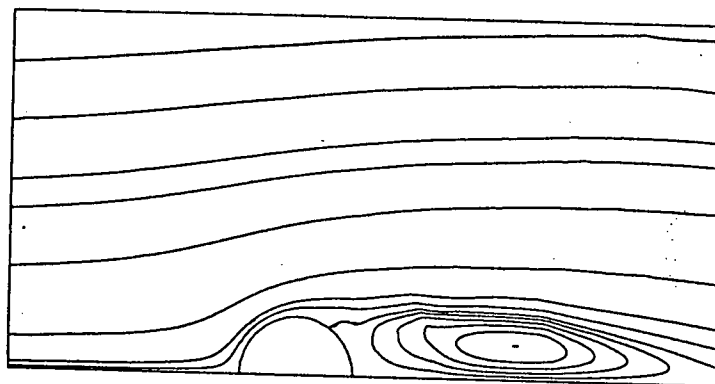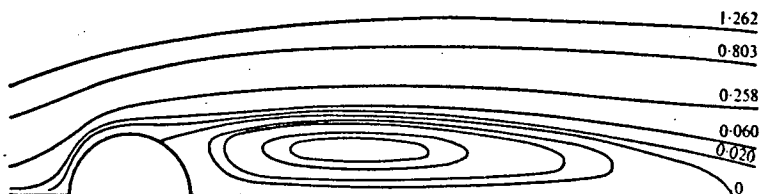
Figure 5.4 Limiting Case of Steady Flow over a Circular Body. $R_\omega = 0.0$ $R_{e_1} = 70.0$ $R_{e_2} = 0.0$
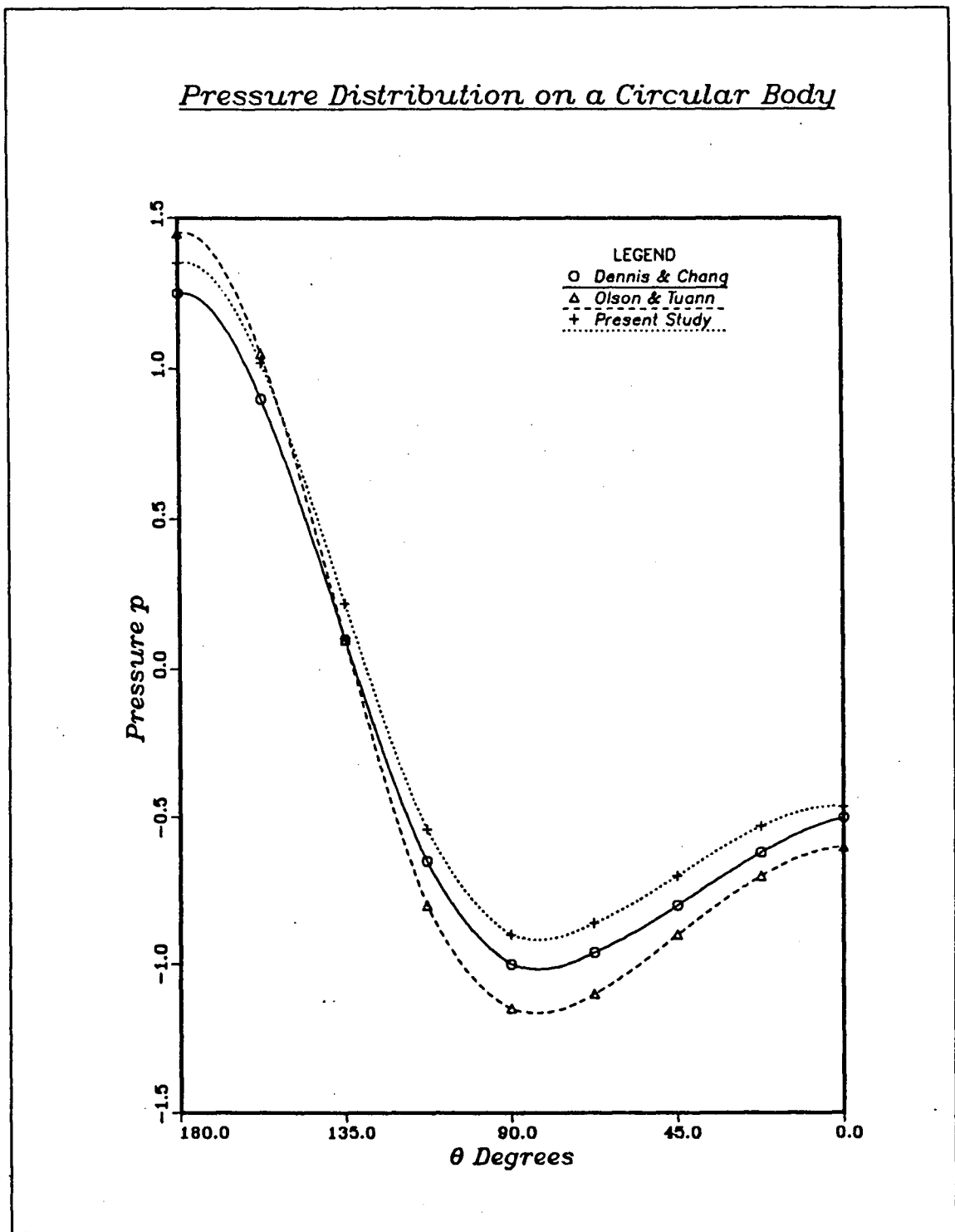
Figure 5.5 Pressure Distribution along the Circular

Body Wall for $R_\omega = 0.0$ $R_{e_1} = 20.0$ $R_{e_2} = 0.0$

Table 5.1

Drag Coefficients for Different Values of R_{e_1}
for a Circular Body $R_\omega = 0.0$ $R_{e_2} = 0.0$

R_{e_1}		Pressure Drag	Friction Drag	Total Drag
5.0	Present Study	2.382	2.020	4.402
	Olson & Tuann	2.199	1.917	4.116
20.0	Present Study	1.211	0.791	2.002
	Olson & Tuann	1.233	0.812	2.045
40.0	Present Study	0.987	0.521	1.508
	Olson & Tuann	0.998	0.524	1.522
70.0	Present Study	0.870	0.372	1.242
	Olson & Tuann	0.852	0.360	1.212

Parametric Study:-

The parameters investigated and their groupings are given in table 5.2. Grid 1 is used in all the cases. Streamlines of the steady component of the velocity field are plotted for each of the groups.

Group 1.a set of results are presented in figures 5.6a to 5.6e. R_{e_1} and β_2 are kept constant at 20.0 and 0.08 respectively. R_{e_2}/R_{e_1} varies in the range 0.1 to 2. This set of results is at low values of R_{e_2}/R_{e_1} , hence the flow pattern is dominated by the steady fluid flow. On introducing small oscillations $(R_{e_2}/R_{e_1}$ =0.1) to the body, a small vortex appears at the front of the body but the wake behind the body remains intact (Fig. 5.6a). At R_{e_2}/R_{e_1} =0.75, the wake behind the body becomes very small and a small vortex at the top right of the body is formed (Fig 5.6c). At higher values of R_{e_2}/R_{e_1} , (Fig. 5.6d and e) the vortex behind the body dimnishes and that at the front and top right grow in size. All these vortices are at very localized regions near the body.

Group 1.b set of results are presented in figures 5.7a to 5.7c. R_ω and R_{e_2} are constant at 250.0 and 20.0 respectively. R_{e_2}/R_{e_1} is varied in the range 1.0 to 10.0 by changing R_{e_1} . On increasing R_{e_2}/R_{e_1} , the vortex at the front and top right of the body grow in size. It is interesting to compare this to the case when there is no steady flow around the body and two huge symmetric vortices appear on either side of the body as shown in figure 5.2.

Table 5.2

Parametric Study of the Flow Pattern for a Circular Body

Group	R_ω	R_{e_1}	R_{e_2}	$\frac{R_{e_2}}{R_{e_1}}$	β_2	Figure
	0.0*	20.0*	0.0*			5.3
	25.0	20.0	2.0	0.1	0.08	5.6a
1a	62.5	20.0	5.0	0.25	0.08	5.6b
	187.5	20.0	15.0	0.75	0.08	5.6c
	250.0	20.0	20.0	1.0	0.08	5.6d
	500.0	20.0	40.0	2.0	0.08	5.6e
	250.0	20.0	20.0	1.0	0.08	5.6d
	250.0	15.0	20.0	1.333	0.08	5.7a
1b	250.0	5.0	20.0	4.0	0.08	5.7b
	250.0	2.0	20.0	10.0	0.08	5.7c
	250.0**	0.0**	20.0**			5.2
	0.0*	2.0*	0.0*			5.8a
	1000.0	2.0	20.0	10.0	0.02	5.8b
	500.0	2.0	20.0	10.0	0.04	5.8c
2	333.33	2.0	20.0	10.0	0.06	5.8d
	250.0	2.0	20.0	10.0	0.08	5.8e
	200.0	2.0	20.0	10.0	0.1	5.8f
	250.0	2.0	10.0	5.0	0.04	5.9a
	250.0	2.0	15.0	7.5	0.06	5.9b
3	250.0	2.0	20.0	10.0	0.08	5.8e
	250.0	2.0	25.0	12.5	0.1	5.9c

*   Limiting case of steady flow over a fixed body.
** Limiting case of an oscillating body in stationary fluid.

Group 2 set of results are presented in figures 5.8a to 5.8f. R_{e_1} and R_{e_2} are kept constant at 2.0 and 20.0 respectively. R_ω is changed such that β_2 varies in the range 0.02 to 0.1. This set of results is at a very high value of R_{e_2}/R_{e_1} (R_{e_2}/R_{e_1} =10.0). Thus the flow is dominated by the oscillations of the body. At R_{e_1} =2.0 and R_{e_2} =R_ω =0.0 (Fig.

5.8a), no wake is formed behind the body. On introducing oscillations to the body (β_2 =0.02), a small vortex develops at the front of the body (Fig 5.8b). At β_2 =0.04 (Fig. 5.8c), the localized vortex at the front of the body disappears and a huge vortex develops behind the body. At β_2 =0.06, the vortex at the back moves to the front of the body (Fig. 5.8d). For higher values of β_2 =0.1 (Fig 5.8e), the vortex at the front of the body grows in size.

Group 3 set of results are presented in figures 5.9a to 5.9c. R_ω and R_{e_1} are kept constant at 250.0 and 2.0 respectively. R_{e_2} is changed such that β_2 varies in the range 0.04 to 0.1. and R_{e_2}/R_{e_1} varies in the range 5 to 12.5. Just as in group 2, this set of results are at high R_{e_2}/R_{e_1} values. The phenomenon of the vortex moving from the back to the front of the body is observed to occur at β_2 =0.06, just as in Group 2 set of results. It is observed that irrespective of different values of R_ω and R_{e_2} , for the same β_2 values, the flow patterns in group 2 and group 3 set of results are quite similar. This indicates the significant effect of the β_2 parameter.

The minimum and maximum values of the stream functions and their respective locations for different cases of R_ω , R_{e_1} and R_{e_2} are tabulated in table 5.3. In all the cases, a plotting domain from -2.5 to 3.7 along the x-axis and 0.0 to 3.1 along the y-axis is used. The dot (.) in the streamline plots represents the location of the minimum value of the stream function.

The following observations are made from the foregoing flow results.

1. At low values of R_{e_2}/R_{e_1} (R_{e_2}/R_{e_1} <1), the flow pattern is dominated by the steady stream flow. Hence the body amplitude parameter β_2 has little effect on the flow pattern except in a localized region near the body.

2. At high values of R_{e_2}/R_{e_1} (R_{e_2}/R_{e_1} >1), the flow pattern is dominated by the oscillations of the body. Thus R_ω and R_{e_2} and as a consequence β_2 influence the flow pattern significantly.

3. For a constant low value of R_{e_1} (R_{e_2}/R_{e_1} <1), the flow pattern for different cases of R_ω and R_{e_2} which result in the same value of β_2 , are quite similar. This implies that the body amplitude parameter characterises the flow pattern to a greater extent than either R_ω or R_{e_2} alone.
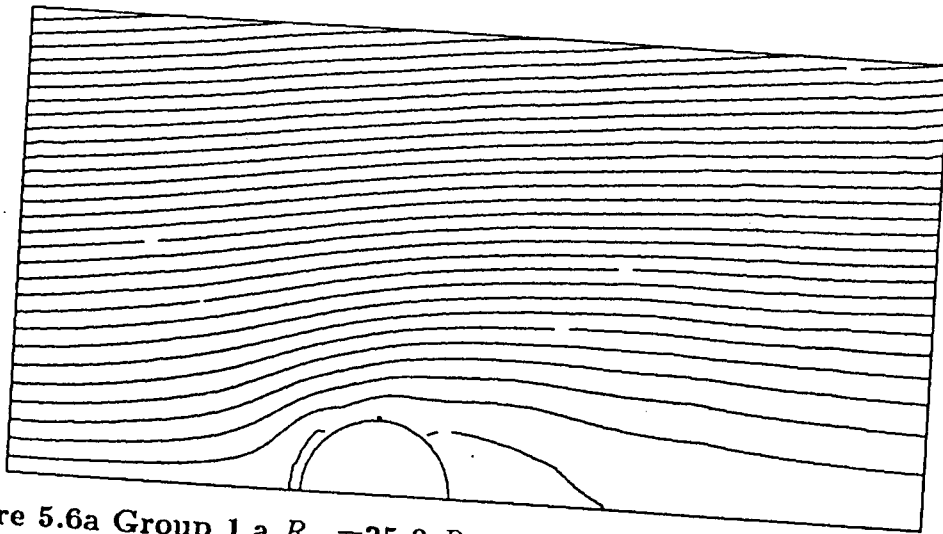
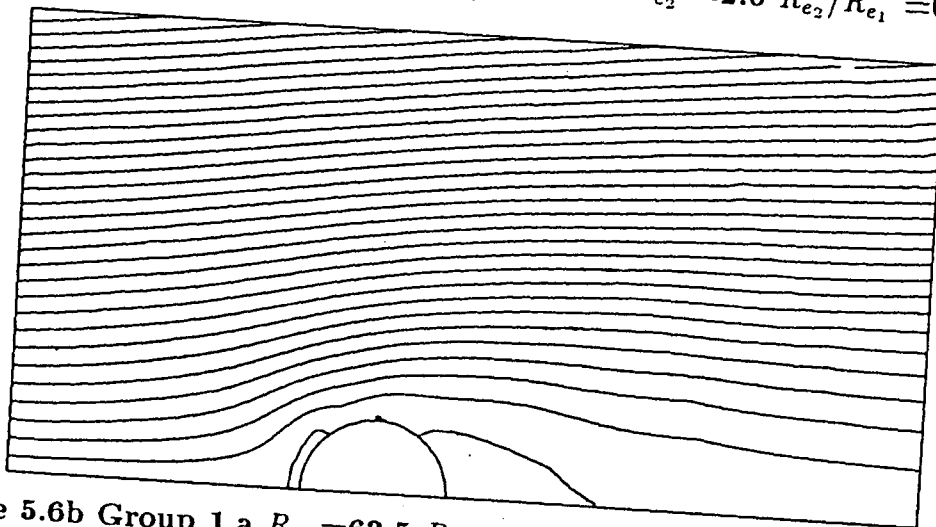Figure 5.6a Group 1.a $R_\omega = 25.0$ $R_{e_1} = 20.0$ $R_{e_2} = 2.0$ $R_{e_2}/R_{e_1} = 0.1$ $\beta_2 = 0.08$

Figure 5.6b Group 1.a $R_\omega = 62.5$ $R_{e_1} = 20.0$ $R_{e_2} = 5.0$ $R_{e_2}/R_{e_1} = 0.25$ $\beta_2 = 0.08$
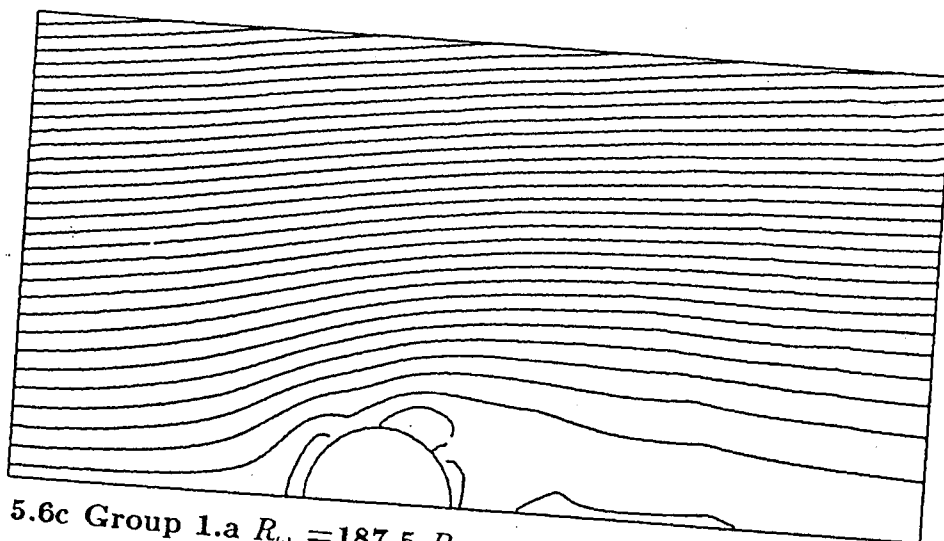
Figure 5.6c Group 1.a $R_\omega = 187.5$ $R_{e_1} = 20.0$ $R_{e_2} = 15.0$ $R_{e_2}/R_{e_1} = 0.75$ $\beta_2 = 0.08$
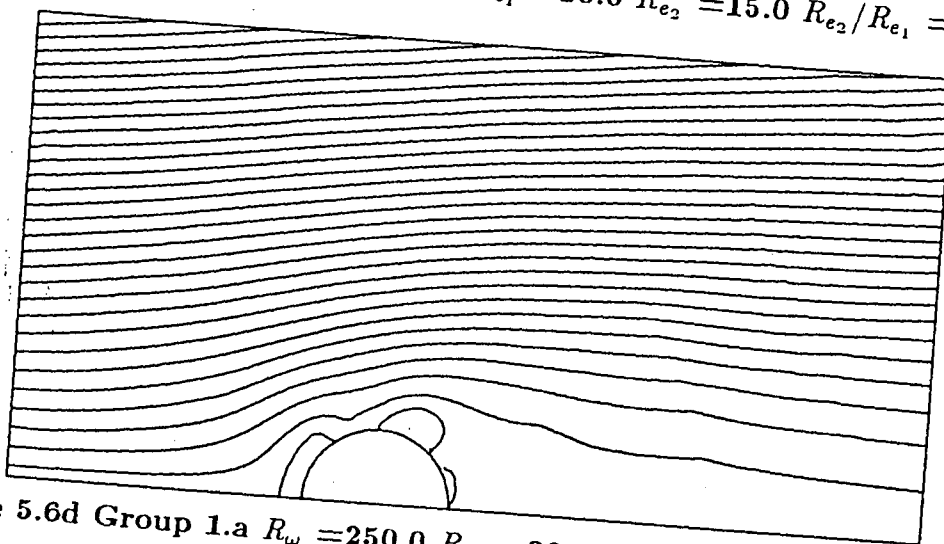
Figure 5.6d Group 1.a $R_\omega = 250.0$ $R_{e_1} = 20.0$ $R_{e_2} = 20.0$ $R_{e_2}/R_{e_1} = 1.0$ $\beta_2 = 0.08$

Figure 5.6e Group 1.a $R_\omega = 500.0$ $R_{e_1} = 20.0$ $R_{e_2} = 40.0$ $R_{e_2}/R_{e_1} = 2.0$ $\beta_2 = 0.08$
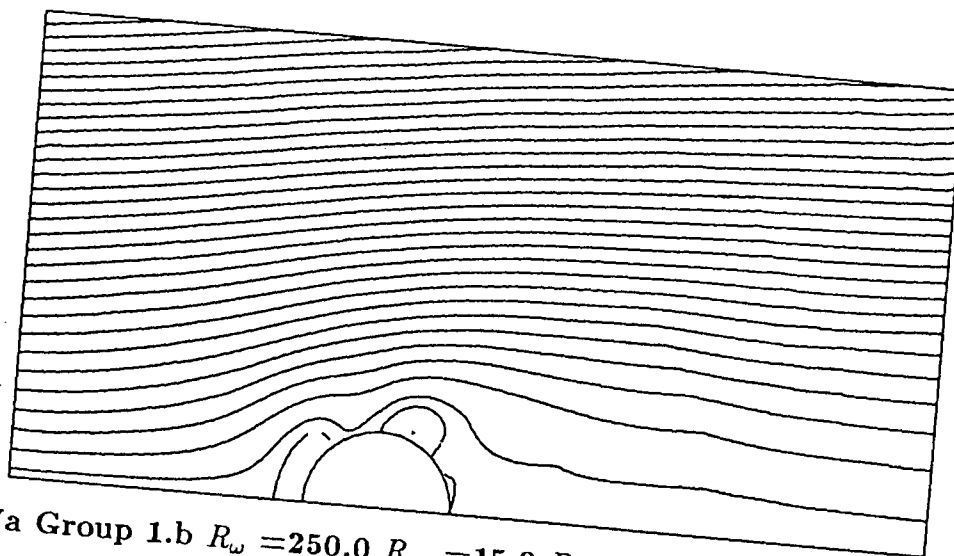
Figure 5.7a Group 1.b R_ω =250.0 R_{e_1} =15.0 R_{e_2} =20.0 R_{e_2}/R_{e_1} =1.33 β_2 =0.08
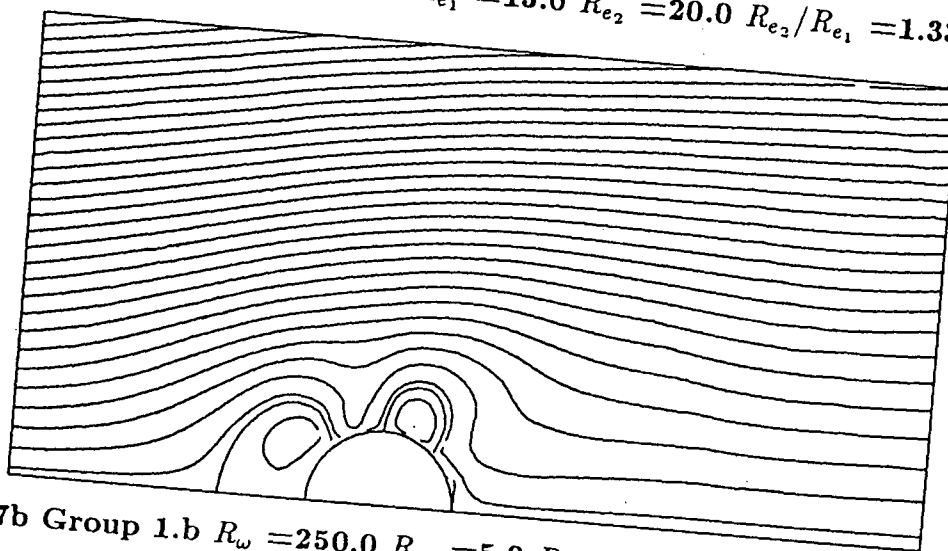
Figure 5.7b Group 1.b R_ω =250.0 R_{e_1} =5.0 R_{e_2} =20.0 R_{e_2}/R_{e_1} =4.0 β_2 =0.08
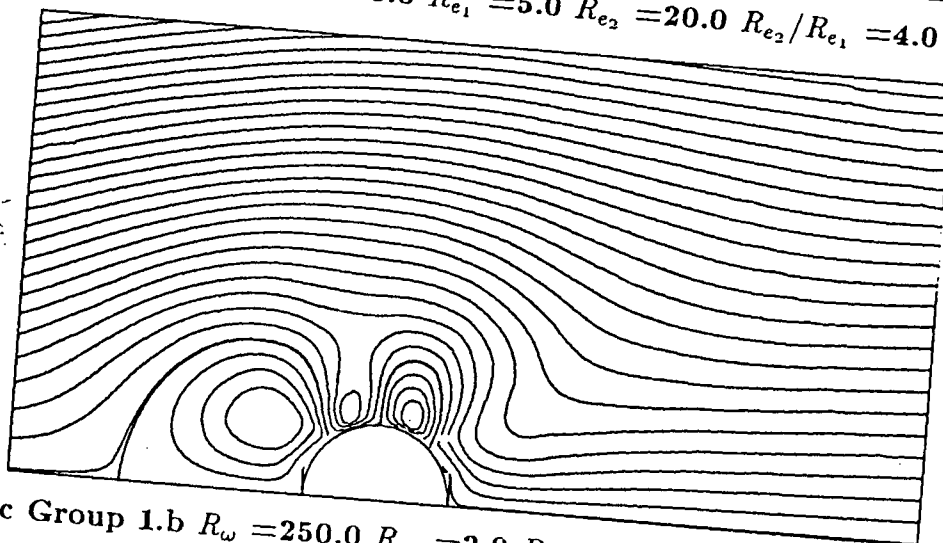
Figure 5.7c Group 1.b R_ω =250.0 R_{e_1} =2.0 R_{e_2} =20.0 R_{e_2}/R_{e_1} =10.0 β_2 =0.08
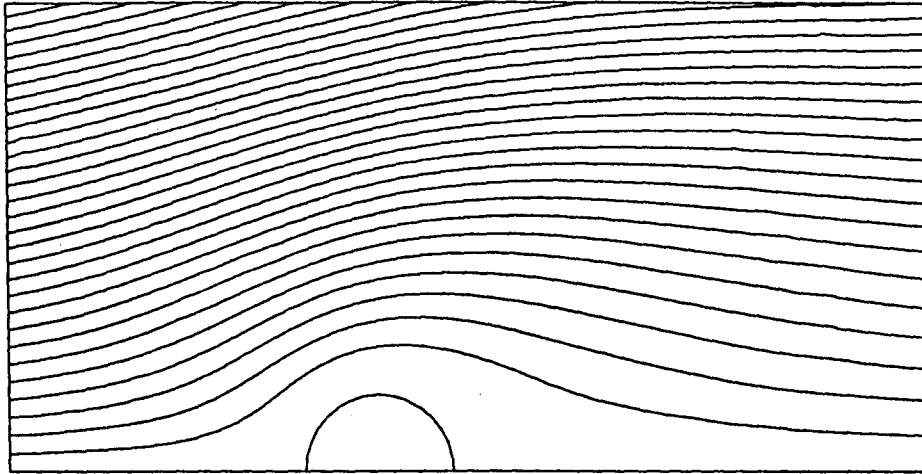
Figure 5.8a Group 2 $R_\omega =0.0$ $R_{e_1} =2.0$ $R_{e_2} =0.0$
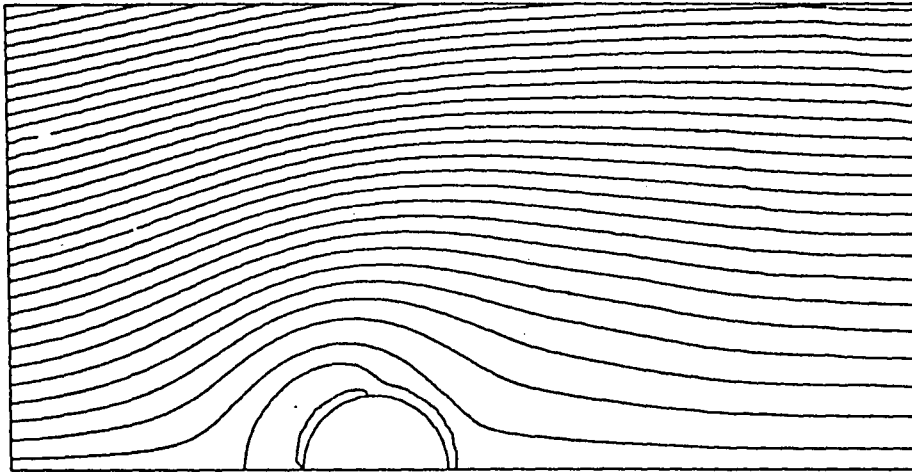
Figure 5.8b Group 2 $R_\omega =1000.0$ $R_{e_1} =2.0$ $R_{e_2} =20.0$ $R_{e_2}/R_{e_1} =10.0$ $\beta_2 =0.02$
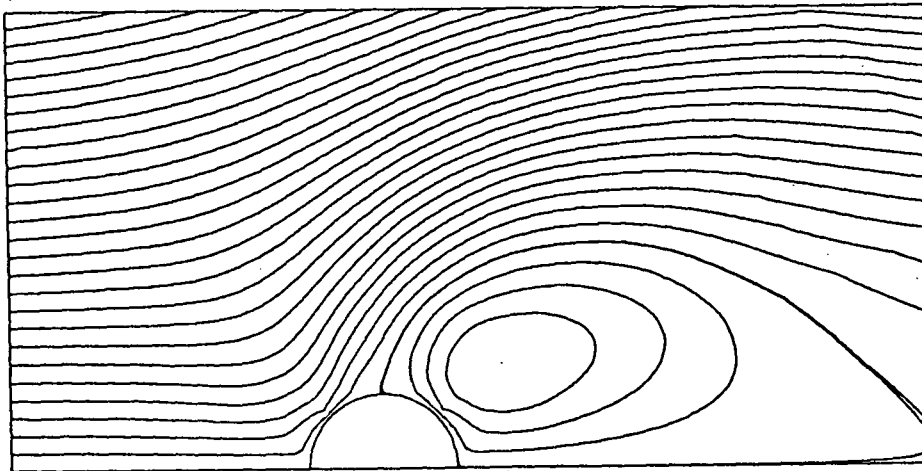
Figure 5.8c Group 2 $R_\omega =500.0$ $R_{e_1} =2.0$ $R_{e_2} =20.0$ $R_{e_2}/R_{e_1} =10.0$ $\beta_2 =0.04$
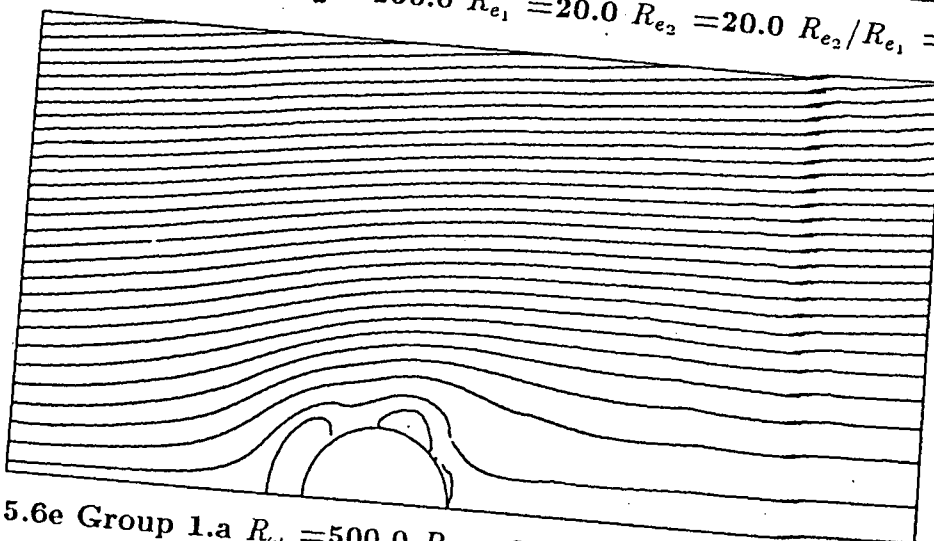
Figure 5.8d Group 2 R_ω =333.33 R_{e_1} =2.0 R_{e_2} =20.0 R_{e_2}/R_{e_1} =10.0 β_2 =0.06

Figure 5.8e Group 2 R_ω =250.0 R_{e_1} =2.0 R_{e_2} =20.0 R_{e_2}/R_{e_1} =10.0 β_2 =0.08
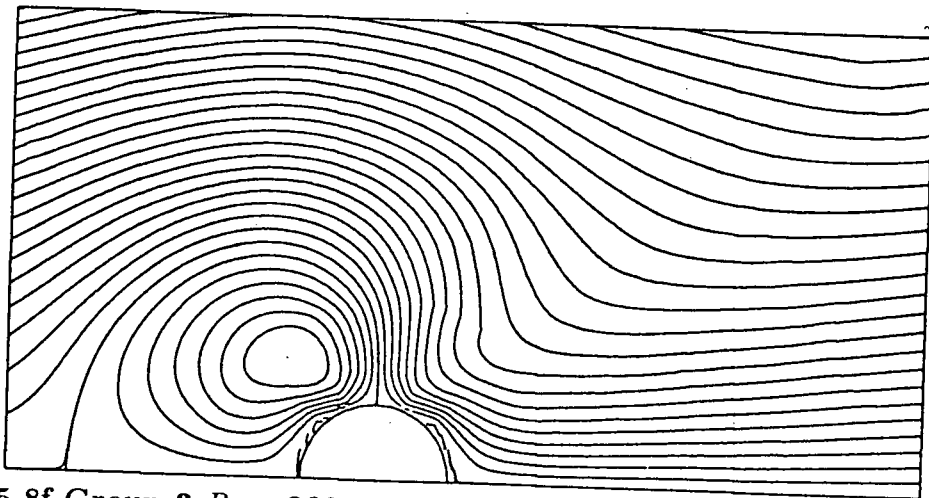
Figure 5.8f Group 2 R_ω =200.0 R_{e_1} =2.0 R_{e_2} =20.0 R_{e_2}/R_{e_1} =10.0 β_2 =0.1
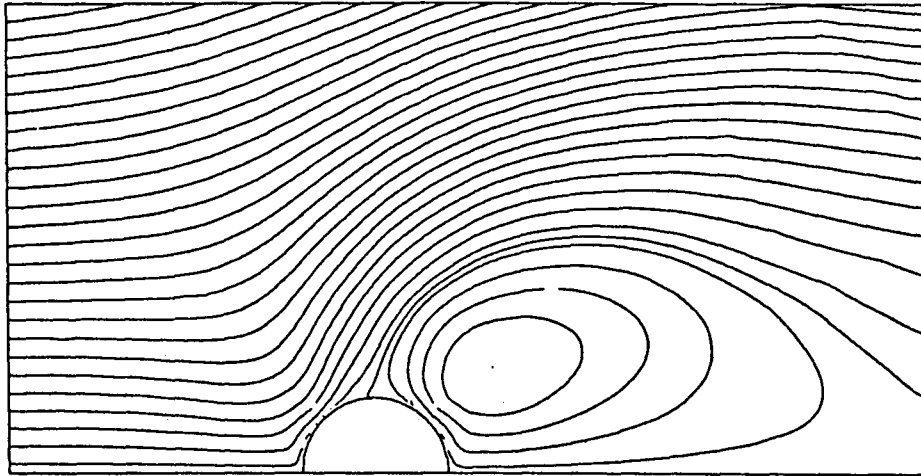
Figure 5.9a Group 3 R_ω =250.0 R_{e_1} =2.0 R_{e_2} =10.0 R_{e_2}/R_{e_1} =5.0 β_2 =0.04
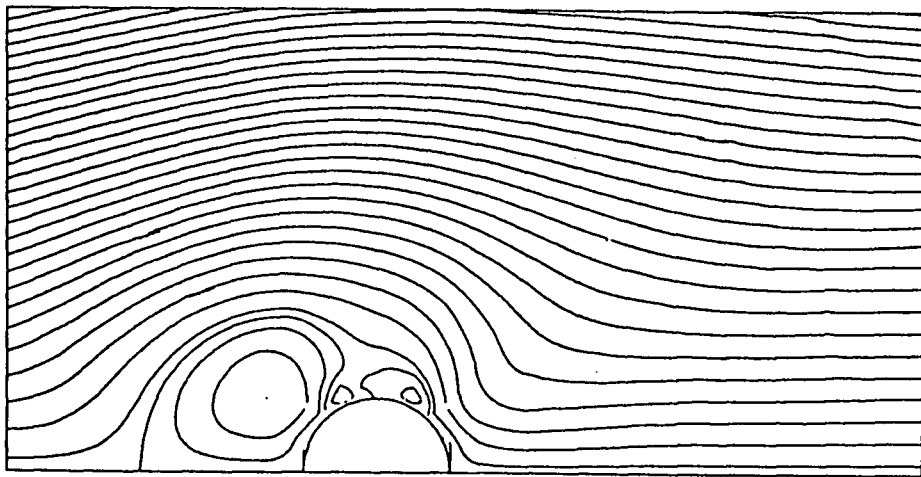
Figure 5.9b Group 3 R_ω =250.0 R_{e_1} =2.0 R_{e_2} =15.0 R_{e_2}/R_{e_1} =7.5 β_2 =0.06
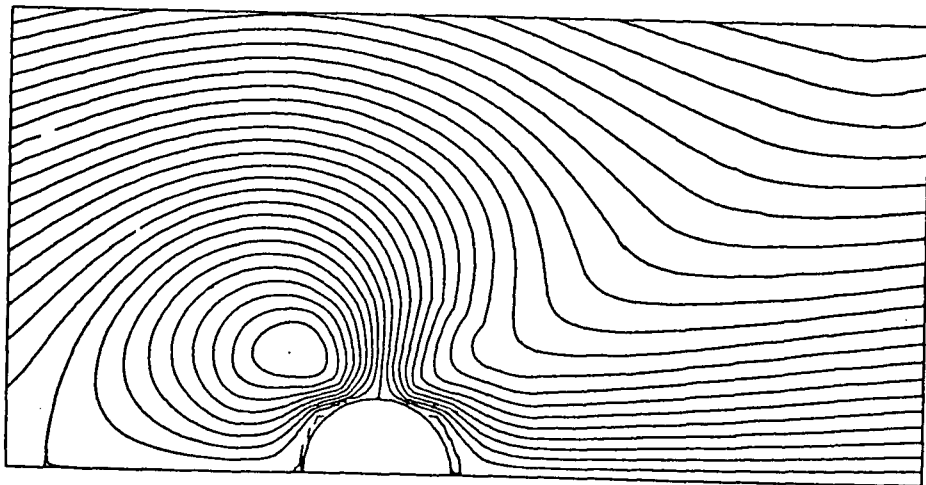
Figure 5.9c Group 3 R_ω =250.0 R_{e_1} =2.0 R_{e_2} =25.0 R_{e_2}/R_{e_1} =12.5 β_2 =0.1

Table 5.3
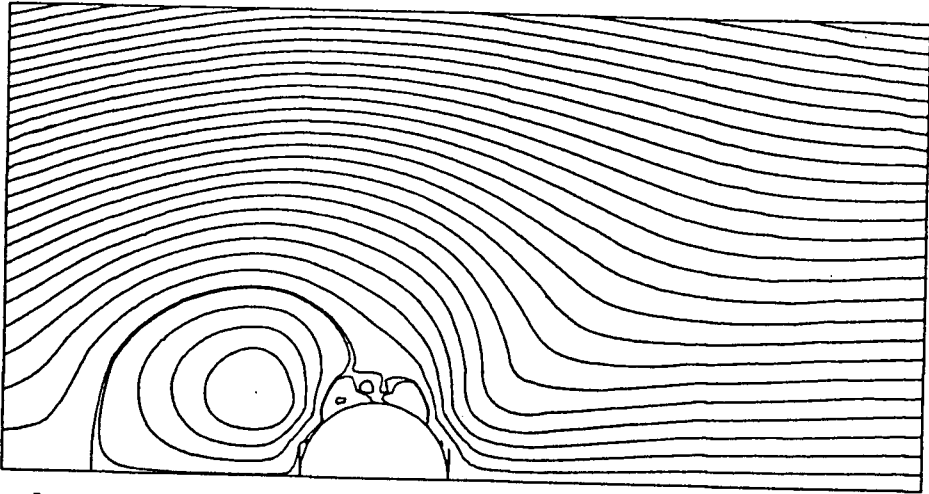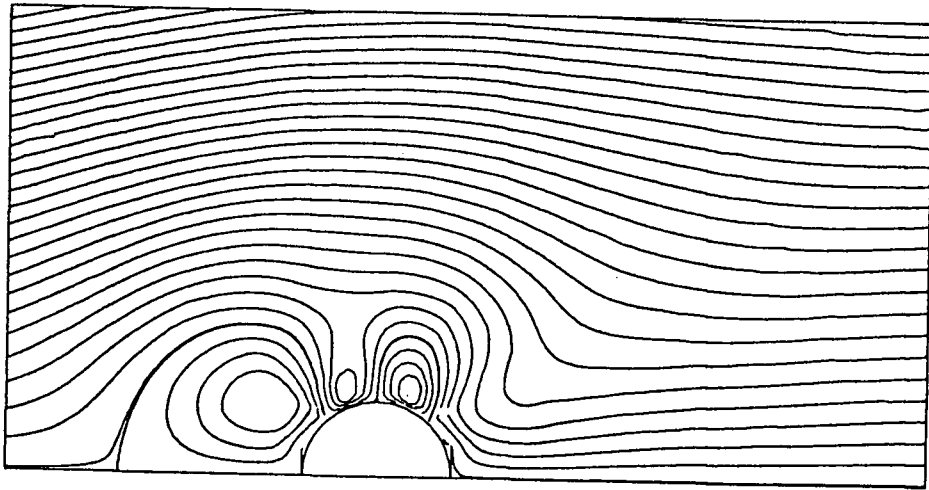
Maximum and Minimum Stream Function Values of the
Steady Component of the Velocity Field

R_ω	R_{e_1}	R_{e_2}	Stream Function	location	
				x	y
0.0	2.0	0.0	min. val.=0.0000 max. val.=2.6750	0.0 -2.5	0.5 3.1
25.0	20.0	2.0	min. val.=-0.0121 max. val.=2.5040	0.65 -2.5	0.3 3.1
62.5	20.0	5.0	min. val.=-0.0086 max. val.=2.2000	0.65 -2.5	0.3 3.1
187.5	20.0	15.0	min. val.=-0.0183 max. val.=1.5510	0.2 -2.5	0.525 3.1
250.0	20.0	20.0	min. val.=-0.0189 max. val.=1.3560	0.2 -2.5	0.525 3.1
250.0	15.0	20.0	min. val.=-0.0219 max. val.=1.1610	0.2 -2.5	0.525 3.1
250.0	5.0	20.0	min. val.=-0.0309 max. val.=0.5410	0.2 -2.5	0.55 3.1
250.0	2.0	20.0	min. val.=-0.0350 max. val.=0.2326	0.2 -2.5	0.55 3.1
250.0	0.0	20.0	min. val.=-0.0519 max. val.=0.0519	-1.45 1.45	1.05 1.05
1000.0	2.0	20.0	min. val.=-0.0305 max. val.=0.2442	-0.55 -2.5	0.425 3.1
500.0	2.0	20.0	min. val.=-0.0394 max. val.=0.2547	0.8 -2.5	0.7 3.1
333.33	2.0	20.0	min. val.=-0.0330 max. val.=0.2087	-0.8 -2.5	0.55 3.1
200.0	2.0	20.0	min. val.=-0.0746 max. val.=0.2454	-0.6 3.25	0.80 3.1
250.0	2.0	10.0	min. val.=-0.0825 max. val.=0.4748	0.8 -2.5	0.7 3.1
250.0	2.0	25.0	min. val.=-0.0928 max. val.=0.2163	-0.6 3.3	0.8 3.1

4. Dramatic changes are observed as β_2 changes at a constant low value of R_{e_1} . For instance, at low values of β_2 (≤ 0.04), a vortex develops behind the body. At higher values of β_2 (≥ 0.06), the vortex moves to the front of the body.

5. At a constant low value of R_{e_2}/R_{e_1} , the flow is dominated by the steady stream flow. On increasing β_2 gradually by changing R_ω , the following changes are observed in the flow pattern

   - The wake behind the body grows considerably in size.

   - The apparent separation point moves to the front of the body.

   - At R_{e_2}/R_{e_1} =0.25, there is a drastic decrease in the wake behind the body. At higher values of R_{e_2}/R_{e_1} the wake again increases in size.

   - At still higher values of R_{e_2}/R_{e_1} , a small vortex appears in a localized region at the front of the body.

The streaklines of the total velocity field are plotted for t=0, $\frac{\pi}{2}$, π, $\frac{3\pi}{2}$, that is, equal time steps over one half cycle of the body motion. Streakline plots for R_ω =250.0, R_{e_1} =20.0 and R_{e_2} =20.0 are presented in figure 5.10. The streamline plot at these values of Reynolds numbers indicates two small vortices at the front and at the top right of the body (Fig. 5.6d). At $t = \pi/2$, two small vortices appear at the front and back of the body. At t=π, and $3\pi/2$, the body is enveloped by these vortices. At t=2π, the streaklines are the same as at $t = 0$.

Streakline plots for R_ω =250.0, R_{e_1} =2.0 and R_{e_2} =20.0 are presented in figure 5.11. The streamline plot for the same values of Reynolds numbers (Fig. 5.7c) shows a large vortex at the front of the body. At t=0, the streakline plot shows small vortices on the top of the body and a big vortex at the front of the body. At t=π and t=$3\pi/2$, the body is enveloped by the vortices which grow in size. There is a dominant vortex at the front of the body.

The minimum and maximum values of stream function and their respective locations at different times t for these two case are presented in table 5.4.

The following observations are made from the foregoing streaklines:

1. At low values of R_{e_2}/R_{e_1} ($R_{e_2}/R_{e_1} \leq 1$), the streaklines are quite similar to the stream-

lines for the same values of Reynolds numbers except for small vortices near the body. This is expected as the flow pattern is dominated by the steady component of the velocity field.

2. At higher values of R_{e_2}/R_{e_1} , the streaklines show signifincant change in vortex at different time t. The overall flow pattern still resembles the streamline plots for the same values of Reynolds numbers. At different time t, the vortex moves to and fro from the front to the back and to the front again in one cycle.

5.2.4 Added Mass, Added Damping and Added Force

The values of added mass, added damping and added force are tabulated for different cases of R_ω , R_{e_1} and R_{e_2} in table 5.5. The force quantities are observed to be intimately related to the flow pattern. A similar parametric study as described for the streamlines is carried out for the force quantities. Figures 5.12, 5.13 and 5.14 show the variation of the force quantities with change in β_2 and R_{e_2}/R_{e_1} for Group 1 and Group 2, respectively.

Figure 5.12 presents the variation of the force quantities with change in R_{e_2}/R_{e_1} for Group 1.a. R_{e_1} is constant at 20.0. It is observed that with an increase in R_{e_2}/R_{e_1} , there is a decrease in added force while the added mass and added damping remain relatively constant. Figure 5.13 presents the variation of the force quantities with R_{e_2}/R_{e_1} for Group 1.b. R_ω and R_{e_2} are kept constant at 250.0 and 20.0 respectively. In both Group 1.a and Group 1.b, β_2 is contant at 0.08. From figure 5.13 it is evident that the added mass and added damping are constant while there is a decrease in added force with increase in R_{e_2}/R_{e_1} .

Figure 5.14 presents the variation of the force quantities with change in β_2 for Group 2. R_{e_1} and R_{e_2} are kept constant at 2.0 and 20.0 respectively. At β_2 =0.06, there is a sharp decrease in the added mass and added damping and a sharp increase in the added force. At this value of β_2 , the vortex moves from the back to the front of the body. Thus the flow pattern has a great influence on the forces on a body.

The following observations are made from this parametric study:-

1. The added mass and added damping are influenced by R_ω and R_{e_2} , while the added

$t=0.0$

$t=\frac{\pi}{2}$

$t=\pi$

$t=\frac{3\pi}{2}$
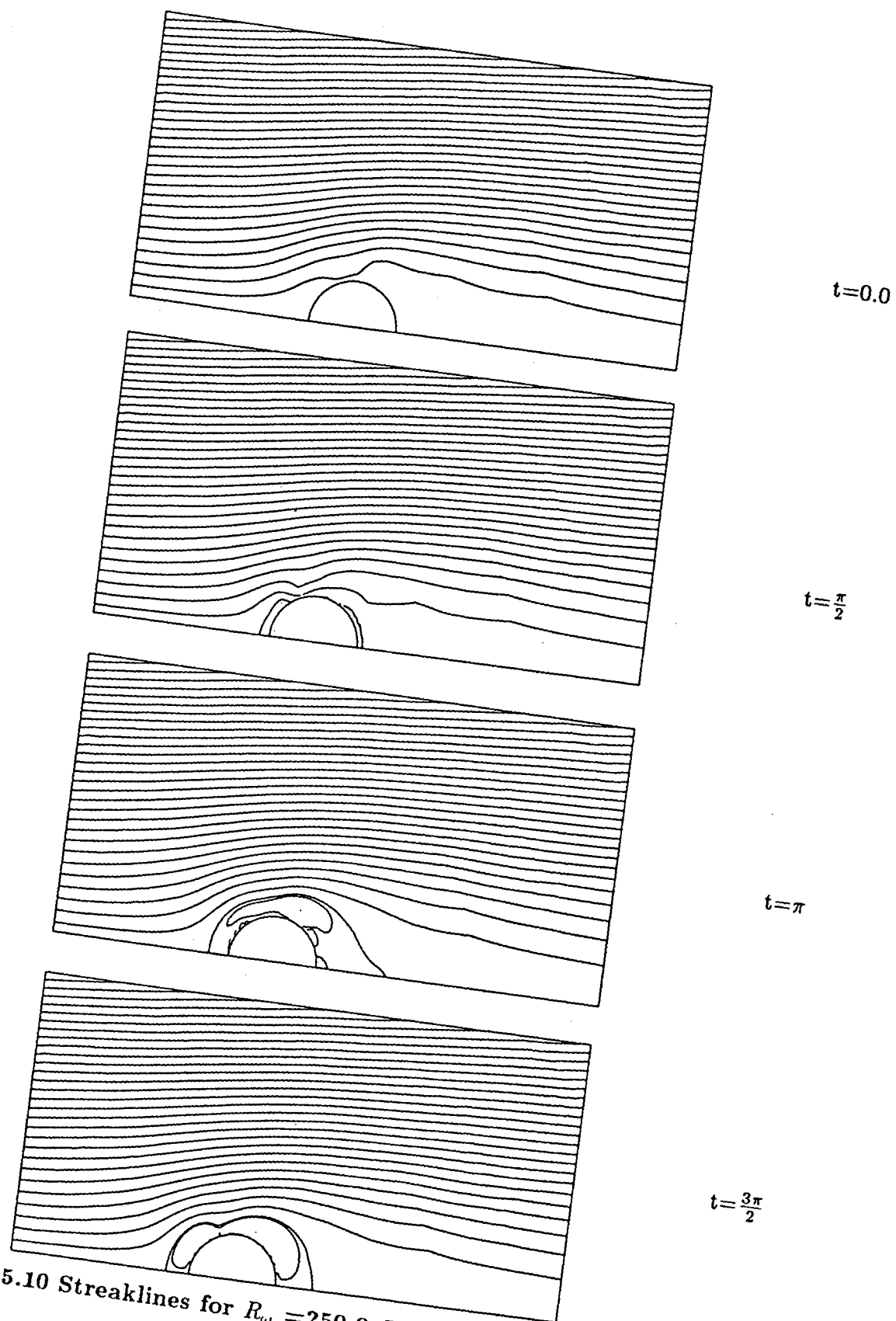
Figure 5.10 Streaklines for $R_\omega =250.0$ $R_{e_1} =20.0$ $R_{e_2} =20.0$ at $t=0.0$, $\frac{\pi}{2}$, π, $\frac{3\pi}{2}$ respectively

t=0.0

$t=\frac{\pi}{2}$

$t=\pi$

$t=\frac{3\pi}{2}$
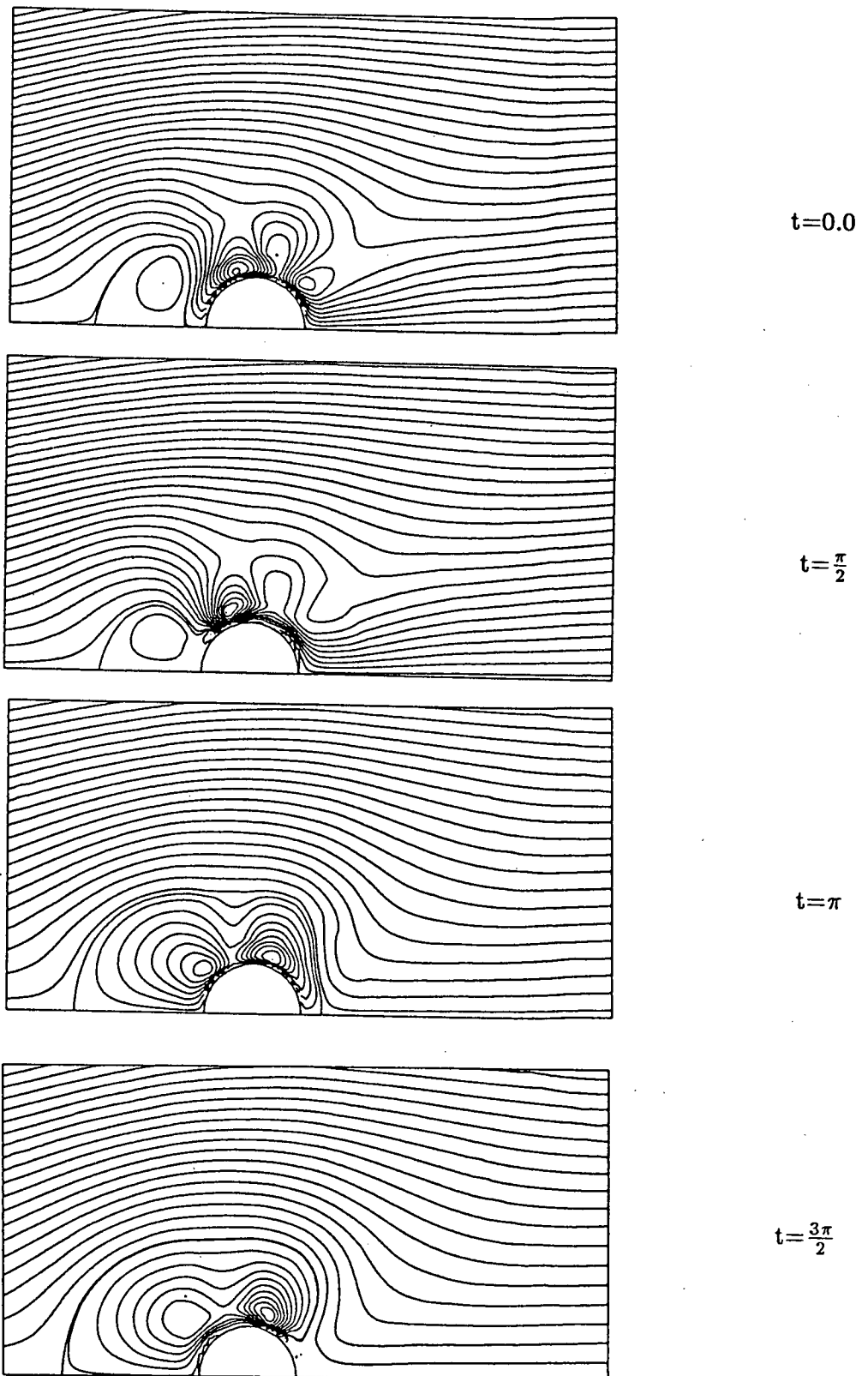
Figure 5.11 Streaklines for $R_\omega =250.0$ $R_{e_1} =2.0$ $R_{e_2} =20.0$
at t=0.0, $\frac{\pi}{2}$, π, $\frac{3\pi}{2}$ respectively

Table 5.4

Maximum and Minimum Stream Function Values of the Total Velocity Field at Different Times t

R_ω=250.0 R_{e_1}=20.0 R_{e_2}=20.0			
t	Stream Function	location	
		x	y
0	min. val.=-0.0020	-0.3	0.4
	max. val.=1.3550	-2.5	3.1
$\frac{\pi}{2}$	min. val.=-0.0119	-0.4	0.375
	max. val.=1.3610	-2.5	3.1
π	min. val.=-0.0523	0.2	0.55
	max. val.=1.3580	-2.5	3.1
$\frac{3\pi}{2}$	min. val.=-0.0563	0.25	0.6
	max. val.=1.3520	-2.5	3.1
R_ω=250.0 R_{e_1}=2.0 R_{e_2}=20.0			
0	min. val.=-0.0161	-0.95	0.425
	max. val.=0.2291	-2.5	3.1
$\frac{\pi}{2}$	min. val.=-0.0138	-0.4	0.375
	max. val.=0.2408	-2.5	3.1
π	min. val.=-0.0495	-0.4	0.4
	max. val.=0.2405	-2.5	3.1
$\frac{3\pi}{2}$	min. val.=-0.1133	0.25	0.6
	max. val.=0.2239	-2.5	3.1

Table 5.5

Added Mass, Added Damping and Added Force
for a Circular Body

R_ω	R_{e_1}	R_{e_2}	Added Mass	Added Damping	Added Force
0.0*	2.0*	0.0*	-	-	7.1769
0.0*	20.0*	0.0*	-	-	20.0221
0.0*	40.0*	0.0*	-	-	30.1568
250.0**	0.0**	20.0**	1.2696	0.4260	0.0000
25.0	20.0	2.0	2.1312	1.6045	13.1090
62.5	20.0	5.0	1.5815	0.9020	11.7870
187.5	20.0	15.0	1.3003	0.4828	9.3309
250.0	20.0	20.0	1.2827	0.4014	7.9780
500.0	20.0	40.0	1.2161	0.2665	4.5587
250.0	15.0	20.0	1.2776	0.4107	5.8885
250.0	5.0	20.0	1.2706	0.4237	1.6123
250.0	2.0	20.0	1.2697	0.4259	0.4372
1000.0	2.0	20.0	1.1383	0.2093	0.7381
500.0	2.0	20.0	1.1723	0.3874	1.0247
333.33	2.0	20.0	1.3306	0.2161	0.3467
200.0	2.0	20.0	1.5158	0.3827	-0.0370
250.0	2.0	10.0	1.1873	0.7151	1.9281
250.0	2.0	15.0	1.3852	0.2793	0.6197
250.0	2.0	25.0	1.4734	0.3396	-0.3898

* Limiting case of steady flow over a fixed body.
** Limiting case of an oscillating body in stationary fluid.

force is predominantly influenced by R_{e_1} .

2. At constant values of β_2 , the added mass and added damping remain fairly constant indicating their relative insensitivity to the other parameters. On the other hand, they are affected significantly by changes in β_2 itself.

3. At high values of R_{e_2}/R_{e_1} , the added force is also influenced considerably by β_2 .

4. The force quantities are related to the flow pattern. Drastic changes in the flow pattern result in drastic changes in the added mass, added damping and added force.

Force Quantities for a Circular Body

Class 1a $Re_1=20.0$

$\beta_2=0.08$

LEGEND
o *Added Mass*
△ *Added Damping*
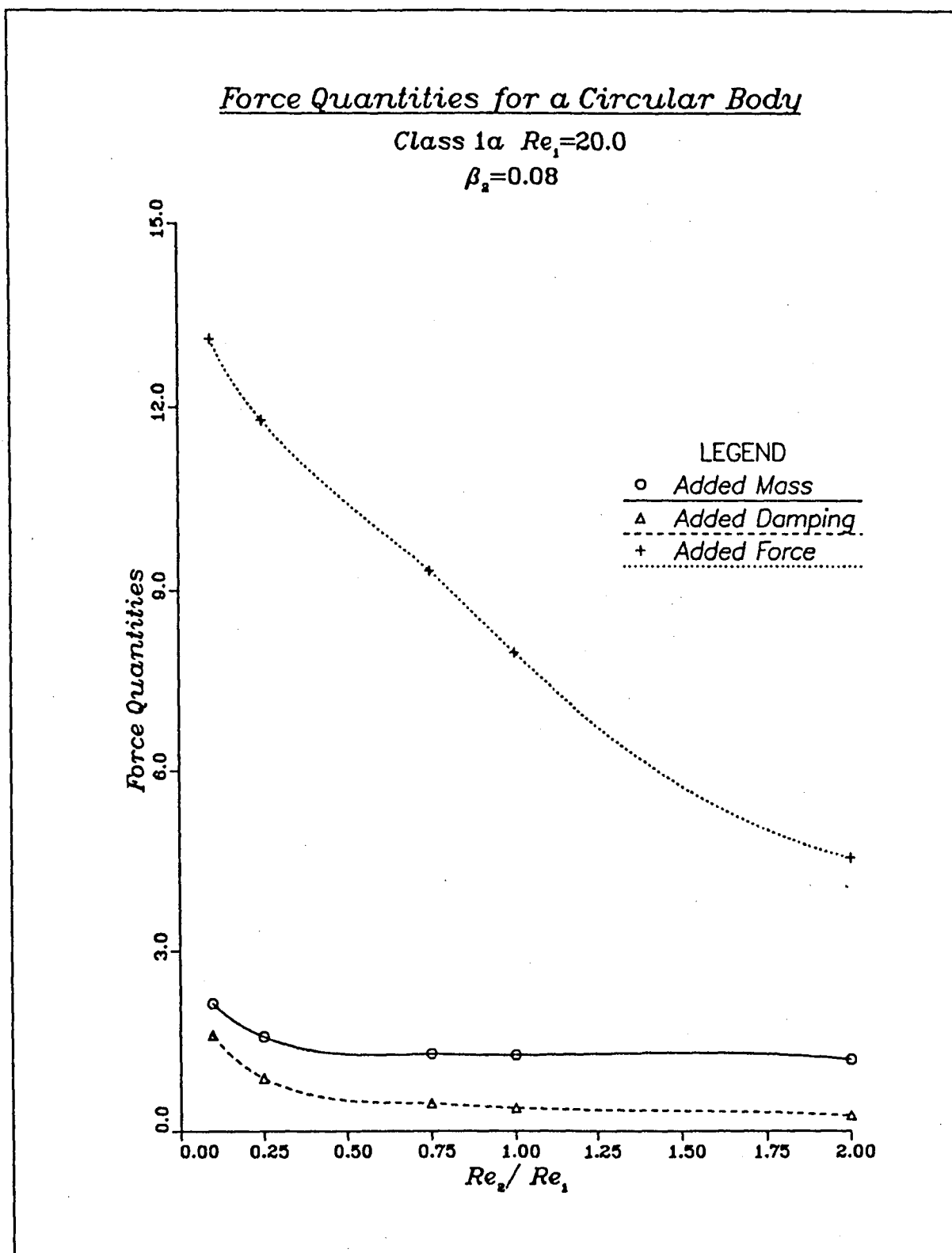+ *Added Force*

Force Quantities

Re_2/Re_1

Figure 5.12   Variation of Force Quantities with R_{e_2}/R_{e_1} in Group 1.a
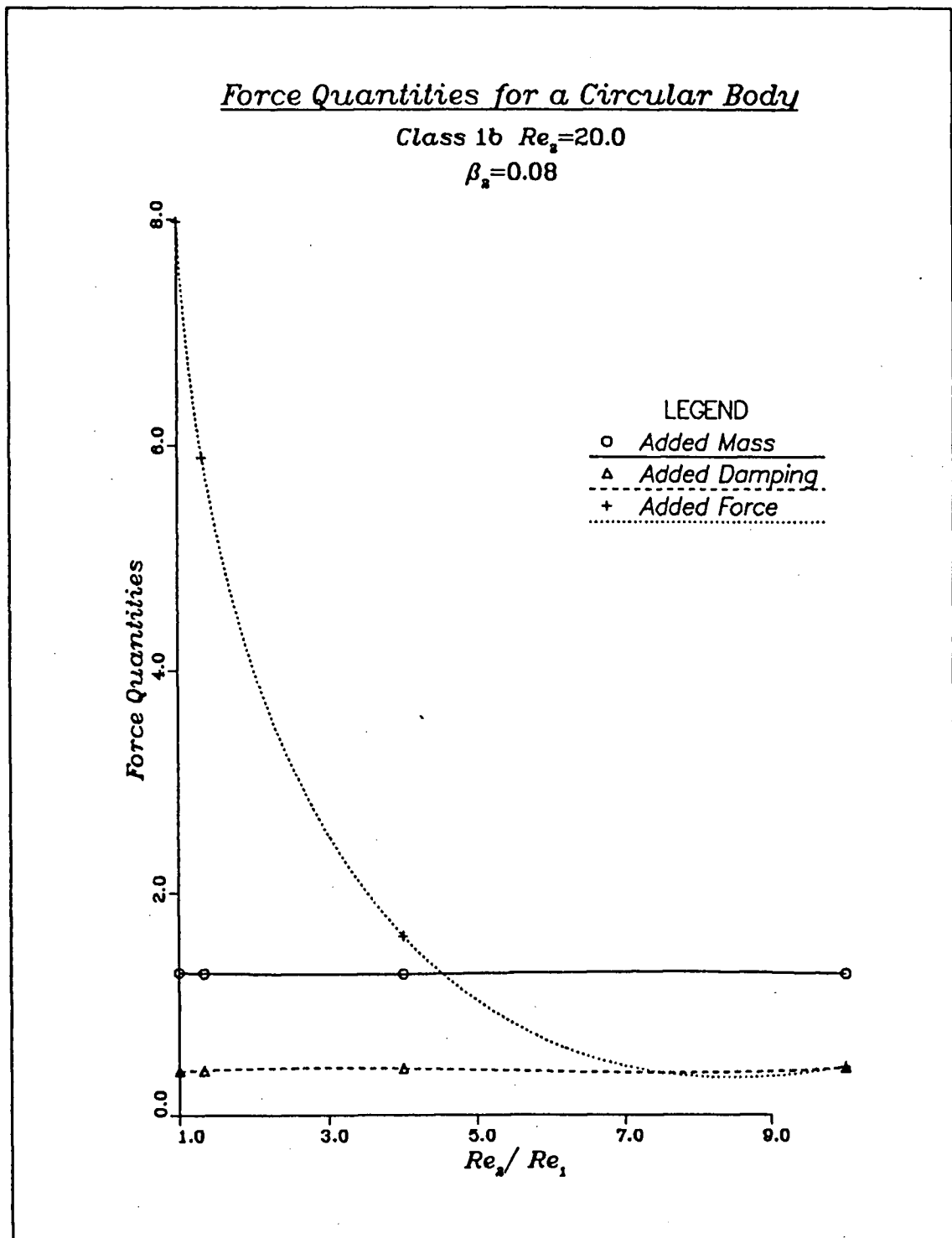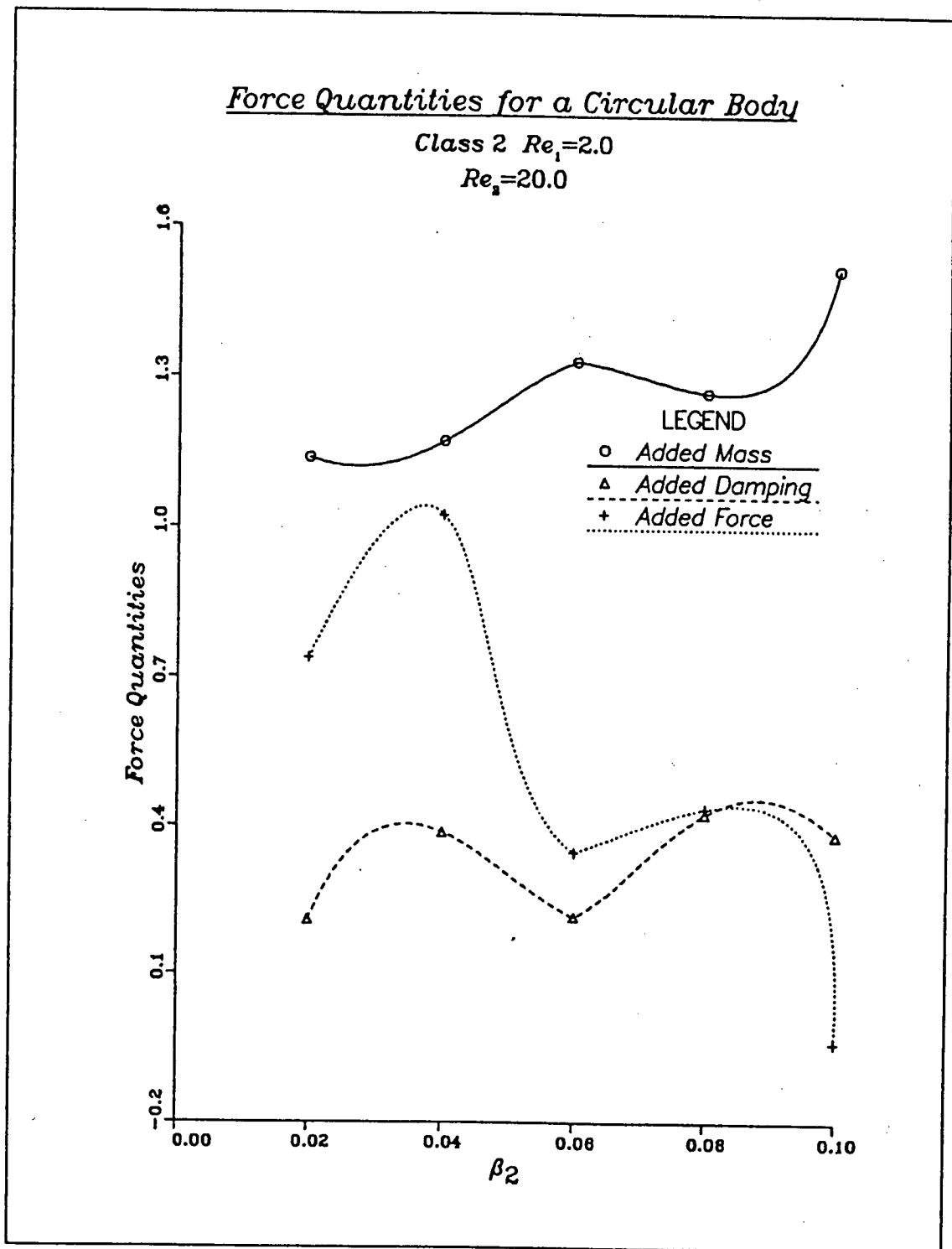
Figure 5.13 Variation of Force Quantities with R_{e_2}/R_{e_1} in Group 1.b

Figure 5.14 Variation of Force Quantities with β_2 in Group 2

5.3 Results for a Square Body

5.3.1 General Remarks

A parametric study is conducted as described in section 5.1 for a square body. The limiting case of a square body oscillating in an otherwise still fluid is verified with the results obtained by Pattani [18]. No experimental or analytical results seem to be available for the limiting case of a steady flow around fixed square bodies at such low values of R_{e_1} .

5.3.2 Finite Element Grid and Boundary Conditions

The numerical results are obtained for a square body having sides of unity with the centroid of its area located at the origin of the x-y coordinate system and the sides parallel to the axis. The body is performing harmonic oscillations parallel to the x-axis. Using symmetry, only one half of the domain is modelled. The finite element grid used is shown in figure 5.15. The grid has a circular outer boundary and a D/b ratio of 15.5. Similar boundary conditions are used as that of grid 1 and 3 for a circular body.

Boundary Conditions:-

1. $u = u_\infty$, $v = 0$ along the fluid outer boundary.

2. u and v velocities at the body boundary are specified according to equation 3.7.

3. u=?, $v = 0$ along Γ_s, the symmetry line.

4. $p = 0$ at points 1 and 2 shown in figure 5.15.

For the flow problem under consideration, there are 368 net degrees of freedom of which 307 are for the velocities and 61 are for the pressure. There are three coefficients A, B, C, for each degree of freedom resulting in 1104 variables in total.

5.3.3 Flow Results

The limiting case of a square bluff body oscillating in an otherwise still fluid is verified
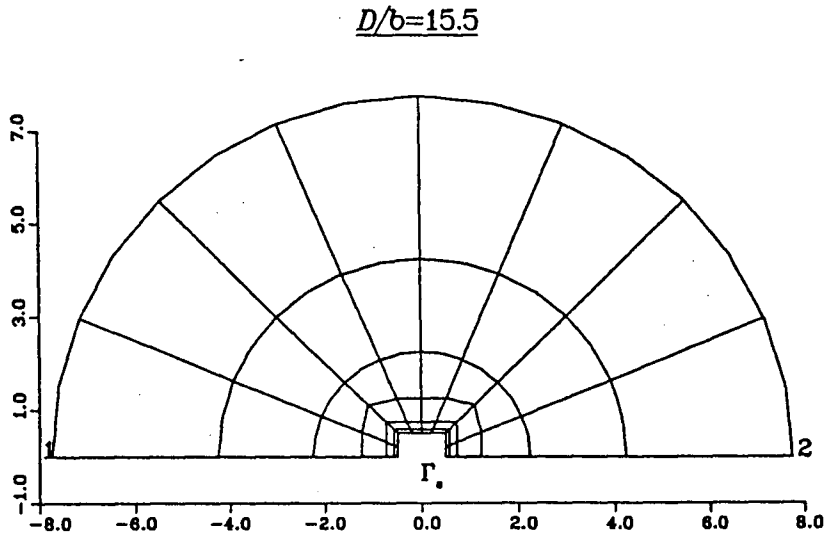
Figure 5.15 Finite Element Grid for Square Body

with [18] for R_ω =150.0, R_{e_1} =0.0 and R_{e_2} =10.0. Identical numerical results are obtained. Streamlines are plotted for this limiting case in Figure 5.17d.

A listing of the parameters investigated and their groupings for a square body are shown in table 5.6. Streamlines of the steady component of the velocity field are plotted for each of the groups.

Group 1.a set of results are presented in figures 5.16a to 5.16e. R_{e_1} and β_2 are kept constant at 10.0 and 0.067 respectively. R_{e_2}/R_{e_1} is varied in the range 0.1 to 1.0. At R_{e_1} =10.0 and R_{e_2} =0.0 (Fig. 5.16a), a wake is present behind the body and the separation point is just after the front corner. When small oscillations are introduced on the body (R_{e_2}/R_{e_1} =0.1), the separation point moves to the front of the body (Fig. 5.16b). At R_{e_2}/R_{e_1} =0.75 (Fig. 5.16d), the wake behind the body becomes very small and a small vortex at the front corner of the body develops. At R_{e_2}/R_{e_1} =1.0 (Fig. 5.16e), the vortex behind the body is negligible while that at the front corner of the body grows in size.

Group 1.b set of results are presented in figures 5.17a to 5.17d. R_ω and R_{e_2} are kept constant at 150.0 and 10.0 respectively. R_{e_2}/R_{e_1} is varied in the range of 1.0 to 10.0. With increase in R_{e_2}/R_{e_1} values, the vortex at the left corner of the body increases and becomes well developed. It is no longer at a localized region near the body.

Table 5.6

Parametric Study of the Flow Pattern For a Square Body

Group	R_ω	R_{e_1}	R_{e_2}	$\frac{R_{e_2}}{R_{e_1}}$	β_2	Figure
	0.0*	10.0*	0.0*			5.16a
	15.0	10.0	1.0	0.1	0.0667	5.16b
1a	60.0	10.0	4.0	0.4	0.067	5.16c
	112.5	10.0	7.5	0.75	0.067	5.16d
	150.0	10.0	10.0	1.0	0.067	5.16e
	150.0	10.0	10.0	1.0	0.067	5.16e
	150.0	7.5	10.0	1.33	0.067	5.17a
1b	150.0	4.0	10.0	2.5	0.067	5.17b
	150.0	1.0	10.0	10.0	0.067	5.17c
	150.0**	0.0**	10.0**			5.17d
	1000.0	1.0	10.0	10.0	0.01	5.18a
	250.0	1.0	10.0	10.0	0.04	5.18b
2	150.0	1.0	10.0	10.0	0.067	5.17c
	100.0	1.0	10.0	10.0	0.1	5.18c
	150.0	1.0	1.5	1.5	0.01	5.19a
	150.0	1.0	6.0	6.0	0.04	5.19b
3	150.0	1.0	10.0	10.0	0.067	5.17c
	150.0	1.0	15.0	15.0	0.1	5.19c

* Limiting case of steady flow over a fixed body.
** Limiting case of an oscillating body in stationary fluid.

Group 2 set of results are presented in figures 5.18a to 5.18c. R_{e_1} and R_{e_2} are kept constant at 1.0 and 10.0 respectively. R_ω is changed such that β_2 varies in the range 0.01 to 0.1. At $\beta_2 = 0.01$, there are localized vortices at the front and the top of the body. At $\beta_2 = 0.04$ (Fig 5.18b), a huge vortex appears behind the body. This vortex moves to the front of the body at about $\beta_2 = 0.067$ (Fig 5.17c), just as in the case of a circular body. At $\beta_2 = 0.1$ (Fig. 5.18c), the vortex at the front of the body becomes well developed.

Group 3 set of results are presented in figures 5.19a to 5.19c. R_ω and R_{e_1} are kept

constant at 150.0 and 1.0 respectively. R_{e_2} is changed such that β_2 varies in the range 0.01 to 0.1. For the same values of β_2 as that in group 2, the flow patterns are very similar to those obtained in group 2. The phenomenon of the vortex moving from the back to the front of the body is also observed to occur at about β_2 =0.067 (Fig. 5.17c).

The minimum and maximum values of stream functions and their respective locations for different cases of R_ω , R_{e_1} and R_{e_2} are tabulated in table 5.7. In all the cases a plotting domain from -2.5 to 3.7 along the x-axis and 0.0 to 3.1 along the y-axis is used. The dot (.) in the streamline plots represents the location of the minimum value of the stream function.
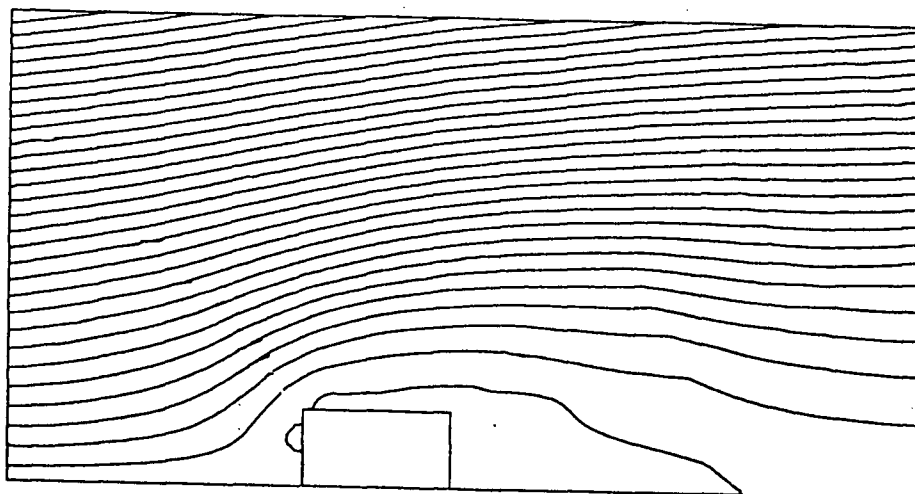
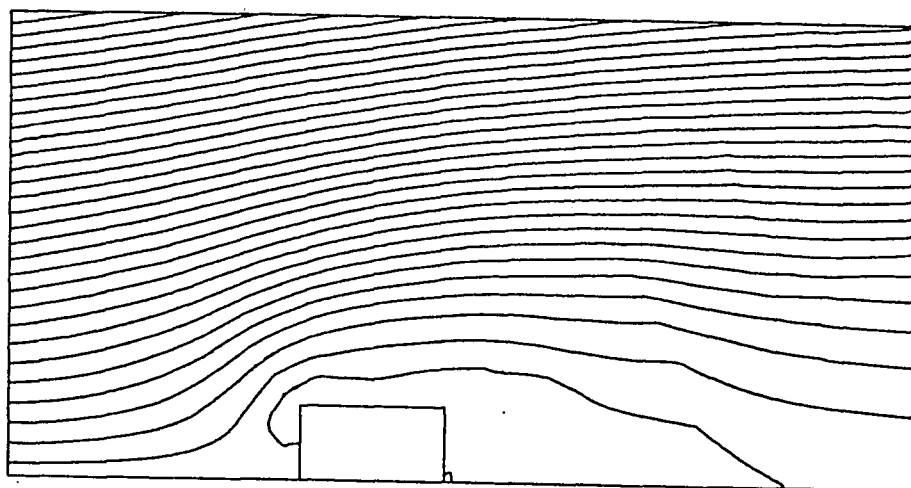Figure 5.16a Group 1.a R_ω =0.0 R_{e_1} =10.0 R_{e_2} =0.0

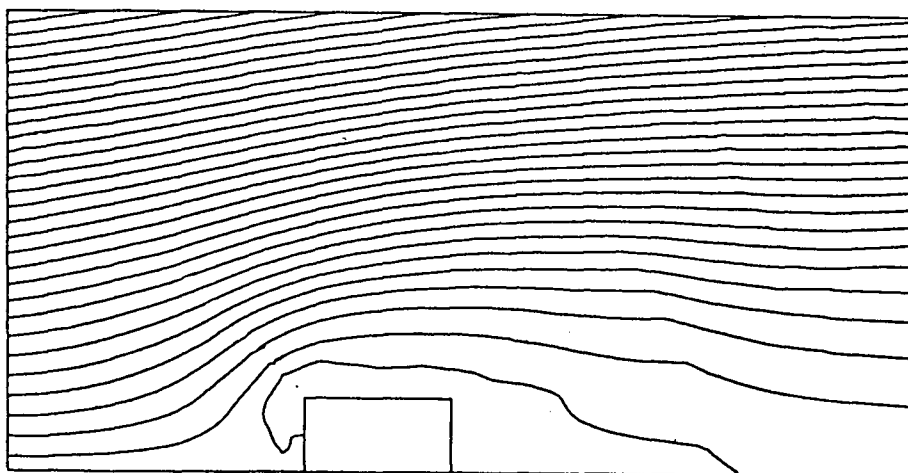Figure 5.16b Group 1.a R_ω =15.0 R_{e_1} =10.0 R_{e_2} =1.0 R_{e_2}/R_{e_1} =0.1 β_2 =0.067

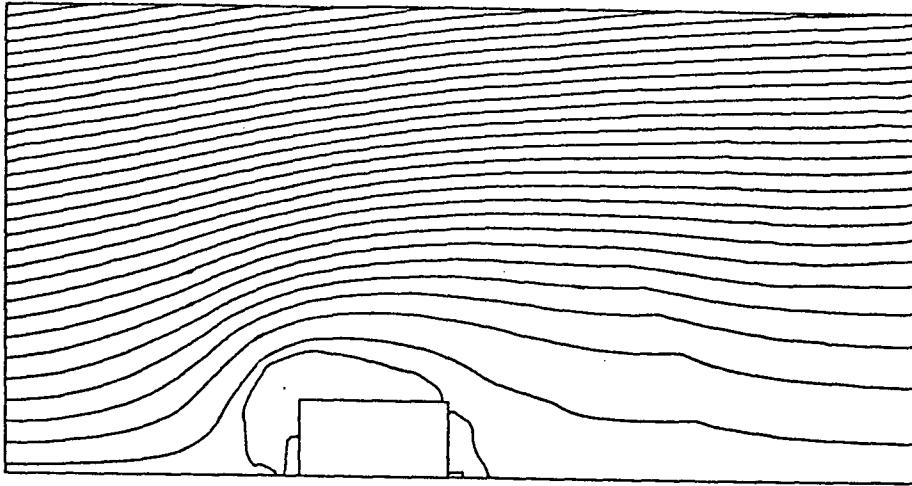Figure 5.16c Group 1.a R_ω =60.0 R_{e_1} =10.0 R_{e_2} =4.0 R_{e_2}/R_{e_1} =0.4 β_2 =0.067

Figure 5.16d Group 1.a R_ω =112.5 R_{e_1} =10.0 R_{e_2} =7.5 R_{e_2}/R_{e_1} =0.75 β_2 =0.067
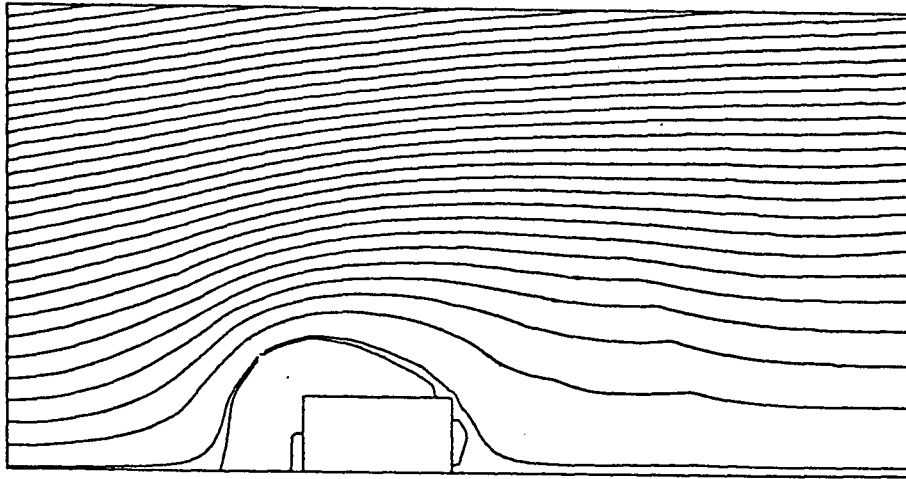

Figure 5.16e Group 1.a R_ω =150.0 R_{e_1} =10.0 R_{e_2} =10.0 R_{e_2}/R_{e_1} =1.0 β_2 =0.067

Figure 5.17a Group 1.b R_ω =150.0 R_{e_1} =7.5 R_{e_2} =10.0 R_{e_2}/R_{e_1} =1.33 β_2 =0.067

Figure 5.17b Group 1.b R_ω =150.0 R_{e_1} =4.0 R_{e_2} =10.0 R_{e_2}/R_{e_1} =2.5 β_2 =0.067

Figure 5.17c Group 1.b R_ω =150.0 R_{e_1} =1.0 R_{e_2} =10.0 R_{e_2}/R_{e_1} =10.0 β_2 =0.067

Figure 5.17d Group 1.b R_ω =150.0 R_{e_1} =0.0 R_{e_2} =10.0 β_2 =0.067

Figure 5.18a Group 2 $R_\omega = 1000.0$ $R_{e_1} = 1.0$ $R_{e_2} = 10.0$ $R_{e_2}/R_{e_1} = 10.0$ $\beta_2 = 0.01$

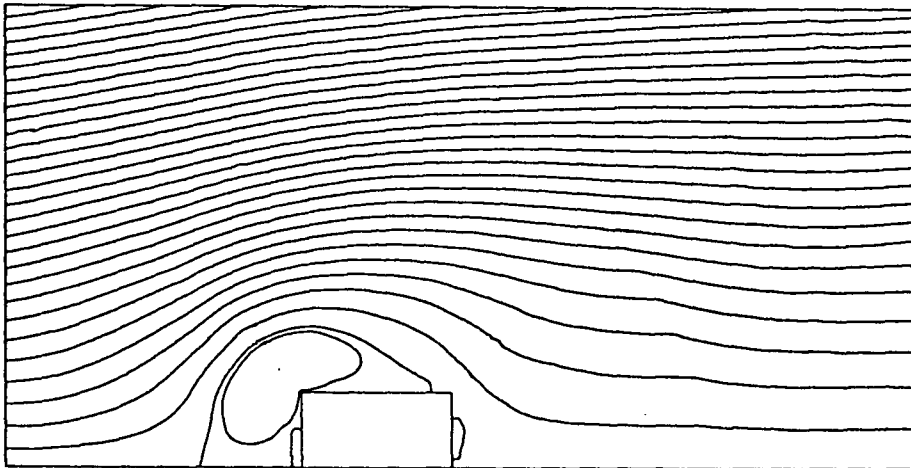Figure 5.18b Group 2 $R_\omega = 250.0$ $R_{e_1} = 1.0$ $R_{e_2} = 10.0$ $R_{e_2}/R_{e_1} = 10.0$ $\beta_2 = 0.04$

Figure 5.18c Group 2 $R_\omega = 100.0$ $R_{e_1} = 1.0$ $R_{e_2} = 10.0$ $R_{e_2}/R_{e_1} = 10.0$ $\beta_2 = 0.1$

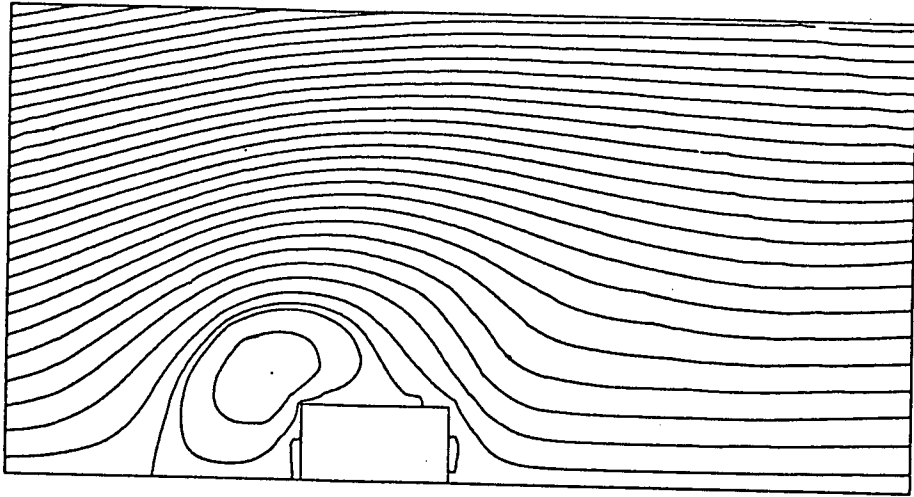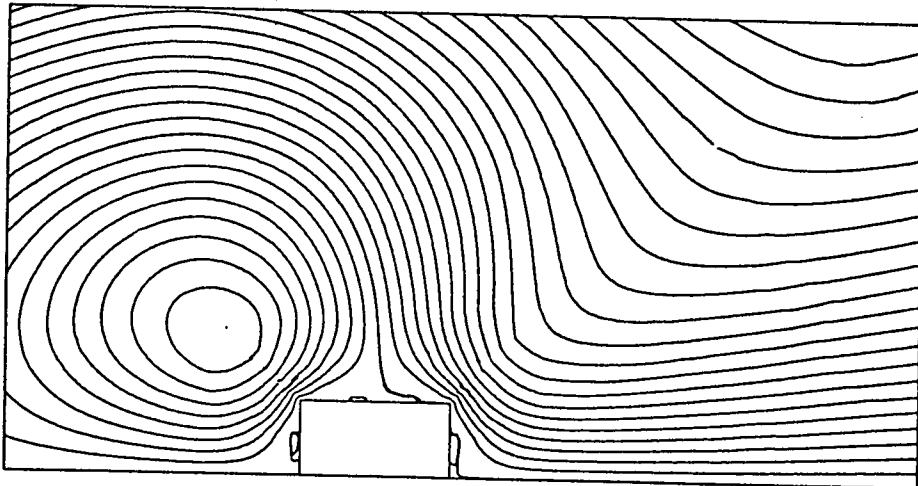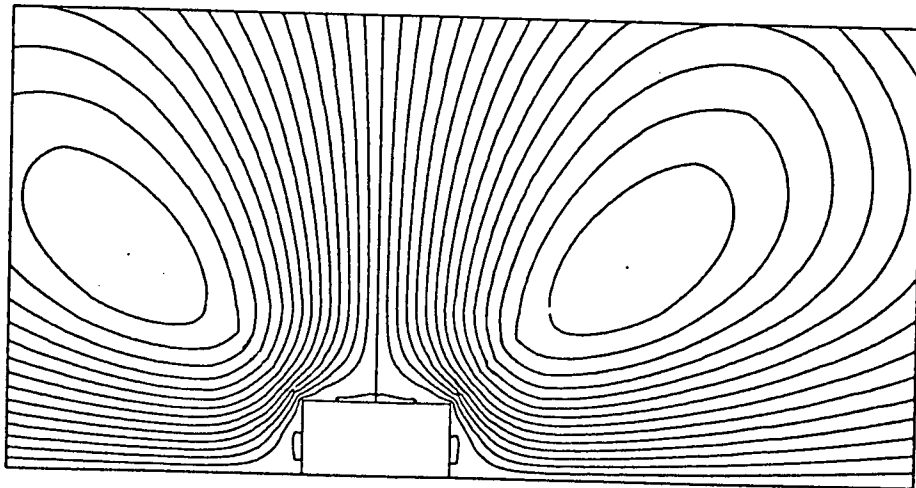**Figure 5.19a Group 3** $R_\omega =150.0$ $R_{e_1} =1.0$ $R_{e_2} =1.5$ $R_{e_2}/R_{e_1} =1.5$ $\beta_2 =0.01$

Figure 5.19b Group 3 $R_\omega =150.0$ $R_{e_1} =1.0$ $R_{e_2} =6.0$ $R_{e_2}/R_{e_1} =6.0$ $\beta_2 =0.04$

Figure 5.19c Group 3 $R_\omega =150.0$ $R_{e_1} =1.0$ $R_{e_2} =15.0$ $R_{e_2}/R_{e_1} =15.0$ $\beta_2 =0.1$
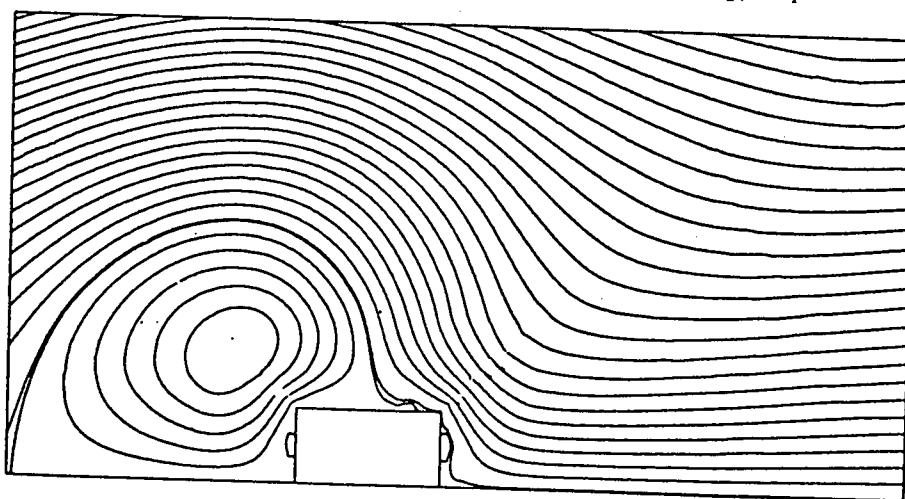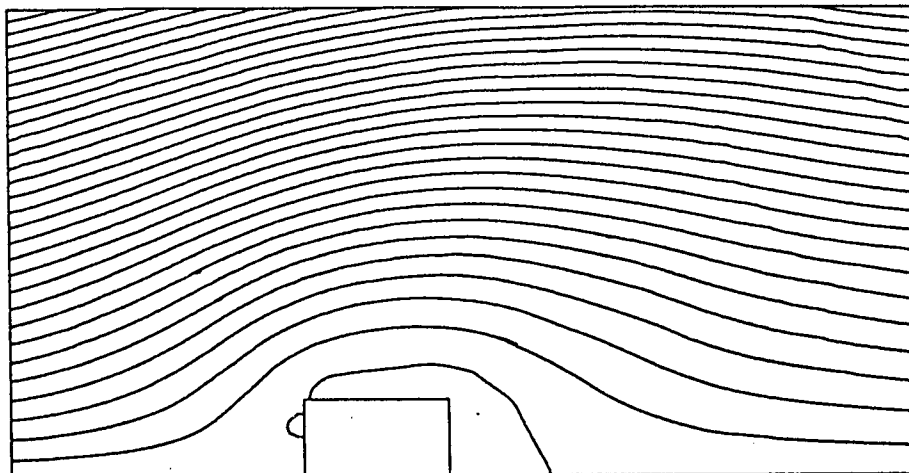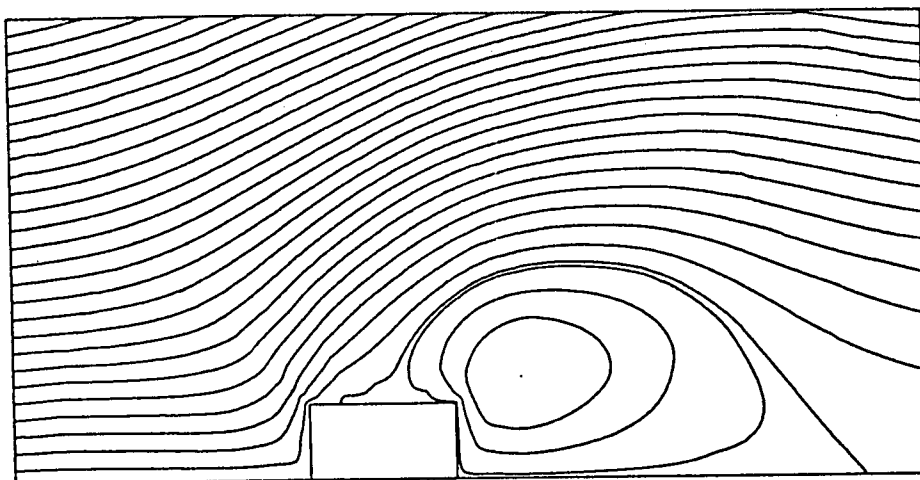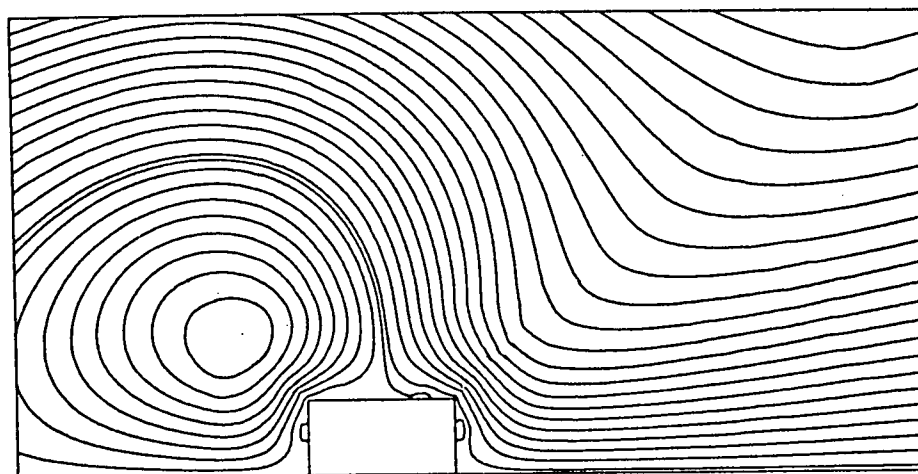
Table 5.7

Maximum and Minimum Stream Function Values of the
Steady Component of the Velocity Field

R_ω	R_{e_1}	R_{e_2}	Stream Function	location	
				x	y
0.0	10.0	0.0	min. val.=-0.0204	0.8	0.425
			max. val.=2.6710	-2.5	3.1
15.0	10.0	1.0	min. val.=-0.0267	0.90	0.475
			max. val.=2.4010	-2.5	3.1
60.0	10.0	4.0	min. val.=-0.0173	-0.55	0.575
			max. val.=1.8770	-2.5	3.1
112.5	10.0	7.5	min. val.=-0.0293	-0.6	0.575
			max. val.=1.4930	-2.5	3.1
150.0	10.0	10.0	min. val.=-0.0400	-0.6	0.625
			max. val.=1.3010	-2.5	3.1
150.0	7.5	10.0	min. val.=-0.0462	-0.65	0.65
			max. val.=1.1150	-2.5	3.1
150.0	4.0	10.0	min. val.=-0.0626	-0.7	0.7
			max. val.=0.7299	-2.5	3.1
150.0	1.0	10.0	min. val.=-0.1213	-1.0	0.975
			max. val.=0.2837	-2.5	3.1
150.0	0.0	10.0	min. val.=-0.1719	-1.7	1.45
			max. val.=0.1719	1.7	1.45
1000.0	1.0	10.0	min. val.=-0.0016	-0.3	0.625
			max. val.=0.2316	-2.5	3.1
250.0	1.0	10.0	min. val.=-0.0415	0.95	0.75
			max. val.=0.2730	-2.5	3.1
100.0	1.0	10.0	min. val.=-0.0566	-0.95	0.95
			max. val.=0.2314	3.35	3.1
150.0	1.0	1.5	min. val.=-0.0064	0.7	0.4
			max. val.=1.0240	-2.5	3.1
150.0	1.0	6.0	min. val.=-0.0493	0.95	0.675
			max. val.=0.4114	-2.5	3.1
150.0	1.0	15.0	min. val.=-0.0759	-0.95	0.95
			max. val.=0.1880	3.15	3.1

On comparing the streamline plots of the square body with those of the circular body, it is obvious that the flow patterns in both the cases are quite similar. The parametric study conducted for both the body shapes indicate similar effects and influences of the parameters R_ω , R_{e_1} , R_{e_2} , R_{e_2}/R_{e_1} and β_2 . Similar changes in the flow patterns are observed as in the case of a circular body in groups 1, 2 and 3. Thus it can be concluded that the vortex should be quite similar for any doubly-symmetric body for the same values of the governing parameters.

The streaklines of the total velocity field are plotted for $t = 0$, $\frac{\pi}{2}$, π and $\frac{3\pi}{2}$. Streakline plots for R_ω =150.0, R_{e_1} =1.0 and R_{e_2} =10.0 are presented in figure 5.20. The minimum and maximum values of the stream function and their respective locations at different time t are presented in table 5.8. Changes in vortex are observed at very localized regions near the body. At $t=\pi$, the vortex moves closer to the body and finally moves away from the body at $t=3\frac{\pi}{2}$. The streamline plot for the same values of Reynolds numbers (Fig. 5.17c) shows a dominant vortex at the top front corner of the body. In all the streakline plots this dominant vortex remains, indicating that the basic flow pattern is maintained at all time.

Table 5.8

Maximum and Minimum Stream Function Values of the Total Velocity Field at Different Times t

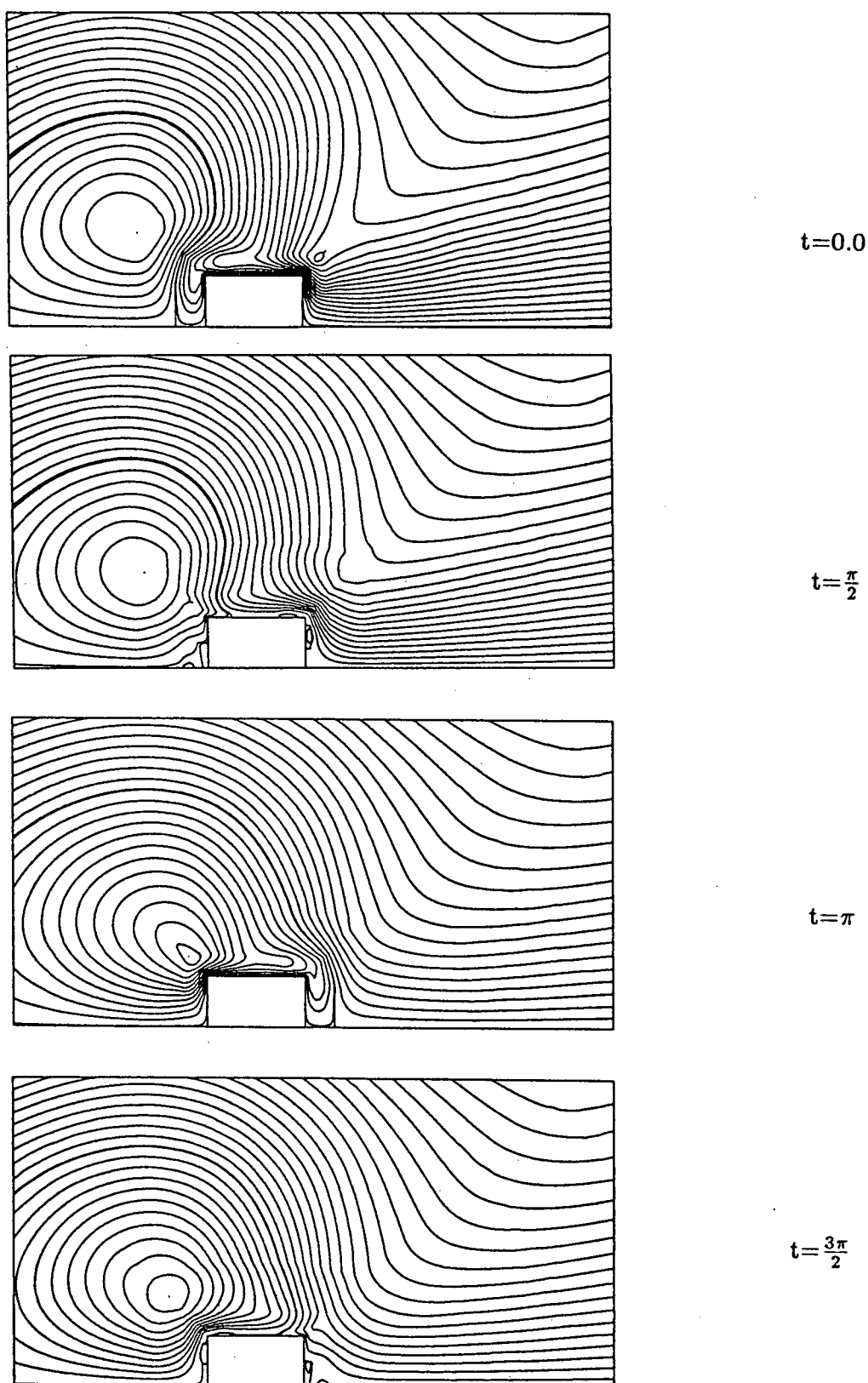| R_ω=150.0 R_{e_1}=1.0 R_{e_2}=10.0			
t	Stream Function	location	
		x	y
0	min. val.=-0.0825	-1.2	0.925
	max. val.=0.2805	3.1	3.1
$\frac{\pi}{2}$	min. val.=-0.0925	-1.15	0.95
	max. val.=0.2947	3.15	3.1
π	min. val.=-0.1942	0.7	0.7
	max. val.=0.2879	3.4	3.1
$\frac{3\pi}{2}$	min. val.=-0.1593	-0.9	0.9
	max. val.=0.2729	3.3	3.1

Figure 5.20 Streaklines for R_ω =150.0 R_{e_1} =1.0 R_{e_2} =10.0 at
t=0.0, $\frac{\pi}{2}$, π, $\frac{3\pi}{2}$ respectively

5.3.4 Added Mass, Added Damping and Added Force

The added mass, added damping and added force are tabulated for different values of R_ω , R_{e_1} and R_{e_2} in table 5.9. A parametric study described in section 5.1 is carried out for the force quantities. Figure 5.21 and 5.22 show the variation of the force quantities with change in R_{e_2}/R_{e_1} and β_2 for group 1.b and group 2 respectively. In group 1.b, as observed in figure 5.21, the added mass and added damping remain relatively constant with change in R_{e_2}/R_{e_1} while there is a significant decrease in added force. In group 2, there are drastic changes in all the force quantities in the range of $0.04 < \beta_2 < 0.07$. In this range, there is an increase in added mass while the added damping and added force decrease. In this range of β_2 , there are drastic changes in the flow patterns. The vortex moves from the back to the front of the body.

From these results, we observe that the added mass and added damping are mainly governed by the β_2 parameter while the added force is predominantly influenced by R_{e_1} . Further, the force quantities appear to be intimately related to the flow pattern. Changes in the flow pattern, cause changes in the force quantities. The variations of the force quantities for the square body is very similar to those obtained for the circular body.
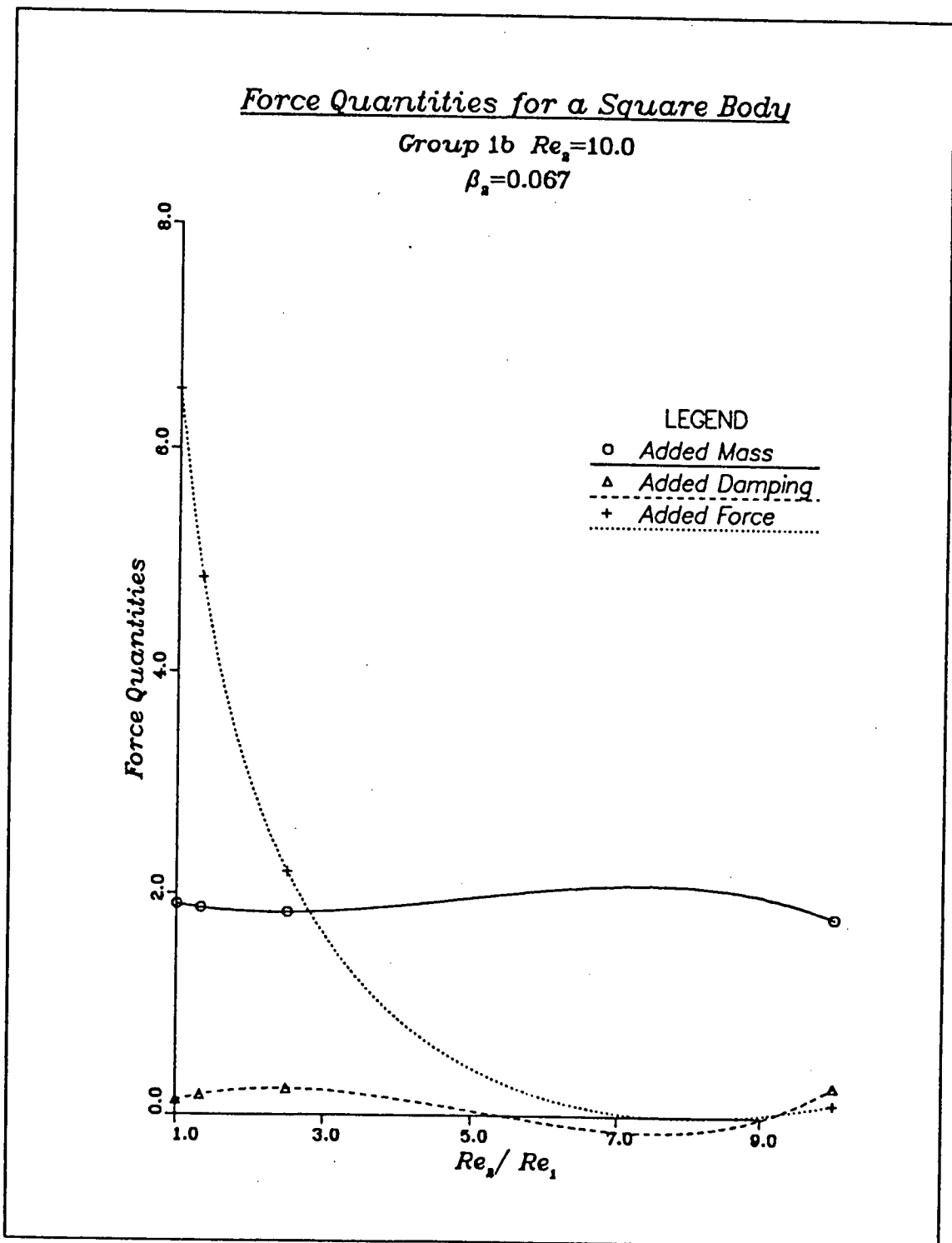
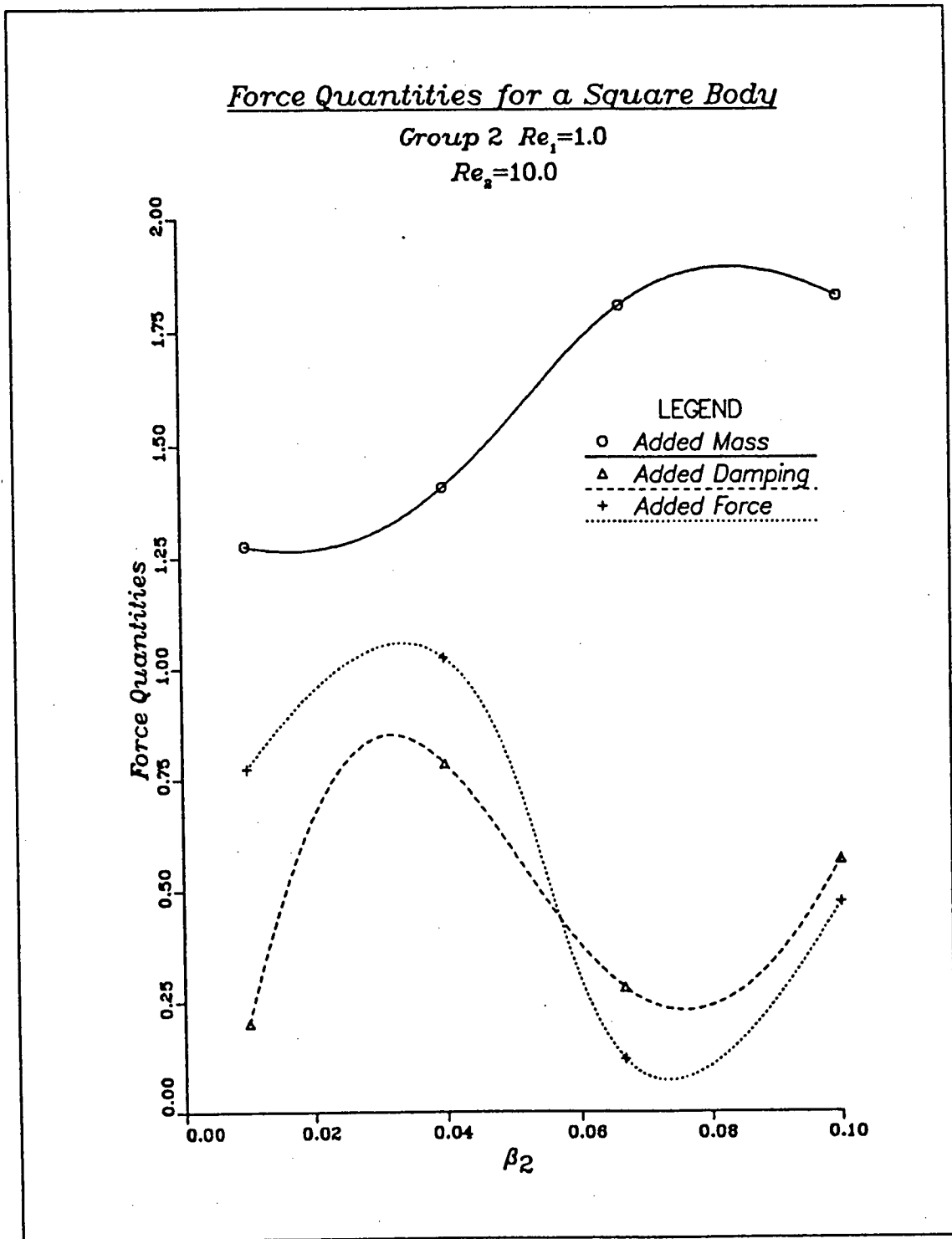Figure 5.21 Variation of Force Quantities with R_{e_2}/R_{e_1} in Group 1.b

Figure 5.22 Variation of Force Quantities with β_2 in Group 2

Table 5.9

Added Mass, Added Damping and Added Force
for a Square Body

R_ω	R_{e_1}	R_{e_2}	Added Mass	Added Damping	Added Force
0.0*	10.0*	0.0*	-	-	15.3848
150.0**	0.0**	10.0**	1.8042	0.2876	0.0000
15.0	10.0	1.0	3.8392	-0.3190	14.5020
60.0	10.0	4.0	2.3470	0.3085	11.0010
112.5	10.0	7.5	2.0088	0.1996	8.1494
150.0	10.0	10.0	1.9035	0.1346	6.5288
150.0	7.5	10.0	1.8712	0.1835	4.8415
150.0	4.0	10.0	1.8323	0.2433	2.2049
150.0	1.0	10.0	1.8074	0.2826	0.1210
1000.0	1.0	10.0	1.2753	0.2028	0.7730
250.0	1.0	10.0	1.4066	0.7852	1.0243
100.0	1.0	10.0	1.8291	0.5704	0.4751
150.0	1.0	1.5	1,6181	0.5451	3.4605
150.0	1.0	6.0	1.4831	0.9657	1.4573
150.0	1.0	15.0	1.7006	0.4622	0.1227

* Limiting case of steady flow over a fixed body.
** Limiting case of an oscillating body in stationary fluid.

5.4 Results for a Triangular Body

5.4.1 General Remarks

So far we have investigated the flow pattern around doubly-symmetric bodies. In order to investigate the streaming around asymmetrical bodies, an equilateral triangular body is chosen. Tatsuno [30] has experimentally investigated the flow pattern of steady streaming in the vicinity of an equilateral triangular body oscillating sinisoidally in an otherwise still fluid. A similar body geometry is used for this numerical investigation.

The limiting case of a triangular body oscillating in an otherwise still fluid is verified with Tatsuno [30]. No experimental or numerical results seem to be available for the limiting case of steady flow over a triangular body. Further, no results are known for the combined problem of a triangular body oscillating in steady fluid flow. Hence a parametric study is conducted as described in section 5.1.

5.4.2 Finite Element Grid and Boundary Conditions

Numerical results are obtained for an equilateral triangular body having sides of unity with the centroid of its area located at the origin of the x-y coordinate system. One side is perpendicular to the x-axis and a bisector of the triangle is parallel to the x-axis. The body is performing harmonic oscillations parallel to the x-axis. Using symmetry, only one half of the domain is modelled. The finite element grid used is shown in figure 5.23. The grid has a rectangular outer boundary and a D/b ratio of 23.7. The boundary conditions are similar to that of grid 2 for a circular body.

Boundary Conditions:-

1. $u = u_\infty$, $v = 0$ along Γ_i, the inflow boundary.

2. $u = u_\infty$, $v=?$ along Γ_u.

3. $u=?$, $v = 0$ along Γ_o, the outflow boundary.

4. $u=?$, $v = 0$ along Γ_s, the symmetry line.

5. Pressure $p = 0$ at points 1 and 2 shown in figure.

For the flow problem under consideration, there are 368 net degrees of freedom, 307 for velocities and 61 for pressure. There are three coefficients A, B, C for each degree of freedom, resulting in 1104 variables in total.
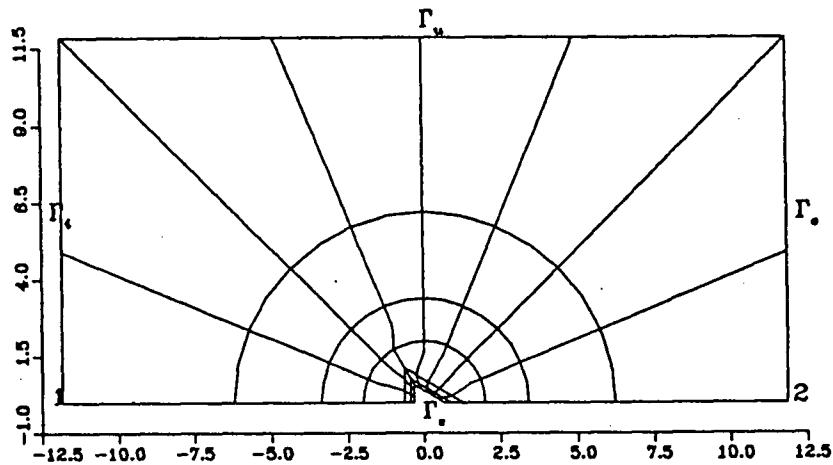

Figure 5.23 Finite Element Grid for a Triangular Body

5.4.3 Flow Results

The limiting case of a triangular bluff body oscillating in an otherwise still fluid is verified with [30]. Streamlines are plotted for R_ω =156.0, R_{e_1} =0.0 and R_{e_2} =3.712 in figure 5.24. Tatsuno obtained photographs of the steady streaming around an oscillating triangular cylinder. The experimental result shows the formation of two vortices: one at the front and one on top of the triangular body. The present numerical results also present two such vortices. Few discrepancies are apparent between the experimental and numerical result. The vortex on the top of the body in the present study appears to be much closer to the body than the experimental one. This discrepency could be attributed to the coarseness of the finite element grid near the body. On refining the grid, the numerical results are expected to converge to those obtained experimentally.

A listing of the parameters investigated and their groupings are shown in table 5.10. Streamlines of the steady component of the velocity field are plotted for each of the groups
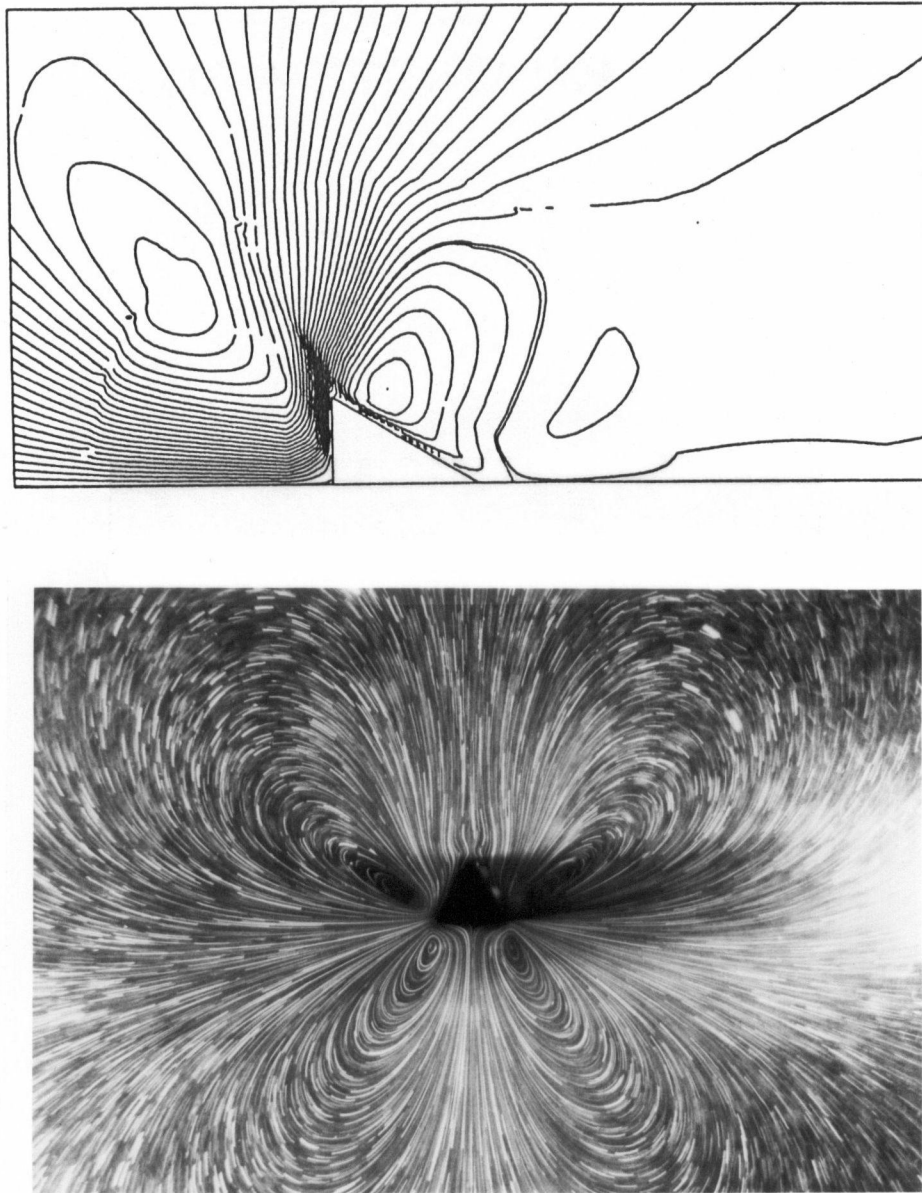
Figure 5.24 Limiting Case of an Oscillating Body in
Still Fluid. $R_\omega = 156.0$ $R_{e_1} = 0.0$ $R_{e_2} = 3.712$

Group 1.a set of results are presented in figures 5.25a to 5.25e. R_{e_1} and β_2 are kept constant at 10.0 and 0.067 respectively. R_{e_2}/R_{e_1} varies in the range 0.1 to 1.0. At R_{e_1} =10.0 (Fig. 5.25a), a small vortex is present on the top of the triangular body with the separation point slightly downstream of the corner. On introducing small oscillations to

Table 5.10

Parametric Study of the Flow Pattern For a Triangular Body

Group	R_ω	R_{e_1}	R_{e_2}	$\dfrac{R_{e_2}}{R_{e_1}}$	β_2	Figure
1a	0.0*	10.0*	0.0*			5.24a
	15.0	10.0	1.0	0.1	0.0667	5.24b
	60.0	10.0	4.0	0.4	0.067	5.24c
	112.5	10.0	7.5	0.75	0.067	5.24d
	150.0	10.0	10.0	1.0	0.067	5.24e
1b	150.0	10.0	10.0	1.0	0.067	5.24e
	150.0	7.5	10.0	1.33	0.067	5.25a
	150.0	4.0	10.0	2.5	0.067	5.25b
	150.0	1.0	10.0	10.0	0.067	5.25c
	150.0**	0.0**	10.0**			5.26d
2	1000.0	1.0	10.0	10.0	0.01	5.26a
	250.0	1.0	10.0	10.0	0.04	5.26b
	150.0	1.0	10.0	10.0	0.067	5.25c
	100.0	1.0	10.0	10.0	0.1	-
3	150.0	1.0	1.5	1.5	0.01	5.27a
	150.0	1.0	6.0	6.0	0.04	5.27b
	150.0	1.0	10.0	10.0	0.067	5.25c
	150.0	1.0	15.0	15.0	0.1	-

* Limiting case of steady flow over a fixed body.

** Limiting case of an oscillating body in stationary fluid.

the body (R_{e_2}/R_{e_1} =0.1), this vortex moves to the front of the body (Fig. 5.25b). As R_{e_2}/R_{e_1} increases, the vortex at the front of the body grows in size (Fig 5.25c to e).

Group 1.b set of results are presented in figures 5.26a to 5.26d. R_ω and R_{e_2} are kept constant at 150.0 and 10.0 respectively. R_{e_2}/R_{e_1} varies in the range 1.0 to 10.0. As R_{e_2}/R_{e_1} is increased the vortex at the front of the body grows in size and moves further away from the body. At high values of R_{e_2}/R_{e_1} (R_{e_2}/R_{e_1} =10.0), the vortex encompasses a large area around the triangular body (Fig 5.26d).

Group 2 set of results are presented in figures 5.27a to 5.27b. R_{e_1} and R_{e_2} are kept constant at 1.0 and 10.0 respectively. R_ω is changed such that β_2 varies in the range of 0.01 to 0.1. At β_2 =0.01, (Fig 5.27a) there is a small localized vortex at the front and top of the body. At β_2 =0.04 (Fig 5.27b), the vortex on the top of the body grows in size. At β_2 =0.0667 (Fig. 5.26c), the small localized vortex at the front and top of the body disappears and a huge vortex to the top left of the body is formed. The solution does not converge for β_2 =0.1.

Group 3 set of results are presented in figures 5.28a and 5.28b. R_ω and R_{e_1} are kept constant at 150.0 and 1.0 respectively. R_{e_2} is changed such that β_2 varies in the range 0.01 to 0.1. For the same values of β_2 as that in group 2, the flow patterns are very similar to those obtained in group 2. The same drastic changes occur in the flow pattern as described in group 2 set of results. This shows the significant effect the β_2 parameter has on the flow pattern. The solution does not converge for β_2 =0.1, just as in group 2.

The minimum and maximum values of the stream functions and their respective locations for different values of R_ω , R_{e_1} and R_{e_2} are tabulated in table 5.11. Two kinds of plotting domains are used:--

a. -2.5 to 3.7 along the x-axis and 0.0 to 3.1 along the y-axis.

b. -7.75 to 7.75 along the x-axis and 0.0 to 7.75 along the y-axis.

Plotting domain b. is used for the streamline plots where the vortex develops far from the body. This is indicated in table 5.11.

The streaklines of the total velocity field (Fig. 5.29) are plotted for t=0, $\frac{\pi}{2}$, π, $\frac{3\pi}{2}$ for R_ω =150.0, R_{e_1} =1.0, and R_{e_2} =10.0. It is observed that the streaklines at different time t are almost identical to the streamlines for the same values of Reynolds numbers, shown in figure 5.26c. Even the minimum and maximum values of the stream function occur at the same point.

5.4.4 Added Mass, Added Damping and Added Force

The added mass, added damping and added force for a triangular body are presented

Table 5.11

Maximum and Minimum Stream Function Values of the Steady Component of the Velocity Field

| R_ω	R_{e_1}	R_{e_2}	Stream Function	location x	location y
0.0	10.0	0.0	min. val.=-0.0030 max. val.=2.7690	-0.05 -2.5	0.475 3.1
15.0	10.0	1.0	min. val.=-0.0631 max. val.=2.5770	-0.55 -2.5	0.275 3.1
60.0	10.0	4.0	min. val.=-0.1002 max. val.=1.9240	-0.6 -2.5	0.325 3.1
112.5	10.0	7.5	min. val.=-0.1598 max. val.=1.4480	-0.65 -2.5	0.35 3.1
150.0	10.0	10.0	min. val.=-0.2081 max. val.=1.1760	-0.65 -2.5	0.35 3.1
150.0	7.5	10.0	min. val.=-0.5605 max. val.=0.2988	-2.15 3.7	1.15 3.1
150.0 *	4.0	10.0	min. val.=-1.0240 max. val.=1.8330	-3.75 7.75	2.187 7.75
150.0 *	1.0	10.0	min. val.=-1.6115 max. val.=-0.6112	-5.5 7.75	2.875 7.75
150.0 *	0.0	10.0	min. val.=-1.7160 max. val.=0.0000	-5.375 -3.25	3.125 0.0
1000.0	1.0	10.0	min. val.=-0.0017 max. val.=0.2320	-0.5 -2.5	0.275 3.1
250.0	1.0	10.0	min. val.=-0.0097 max. val.=0.2499	0.0 -2.5	0.625 3.1
100.0 *	1.0	10.0	min. val.= - max. val.= -	- -	- -
150.0	1.0	1.5	min. val.=-0.0011 max. val.=1.0110	-0.05 -2.5	0.475 3.1
150.0	1.0	6.0	min. val.=-0.0131 max. val.=0.3811	-0.05 -2.5	0.625 3.1
150.0 *	1.0	15.0	min. val.= - max. val.= -	- -	- -

* Plotting domain b is used.
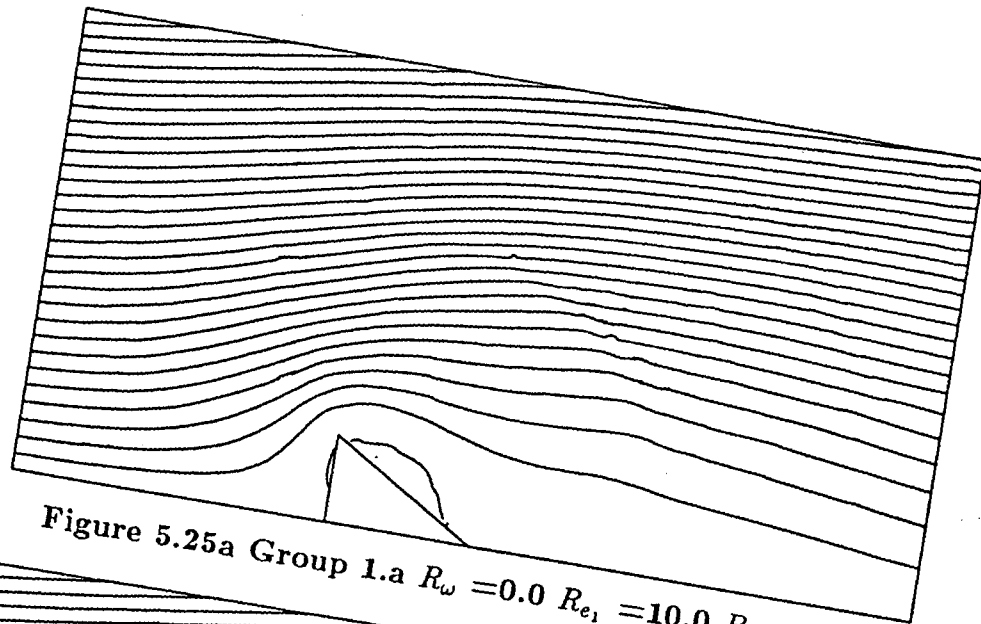
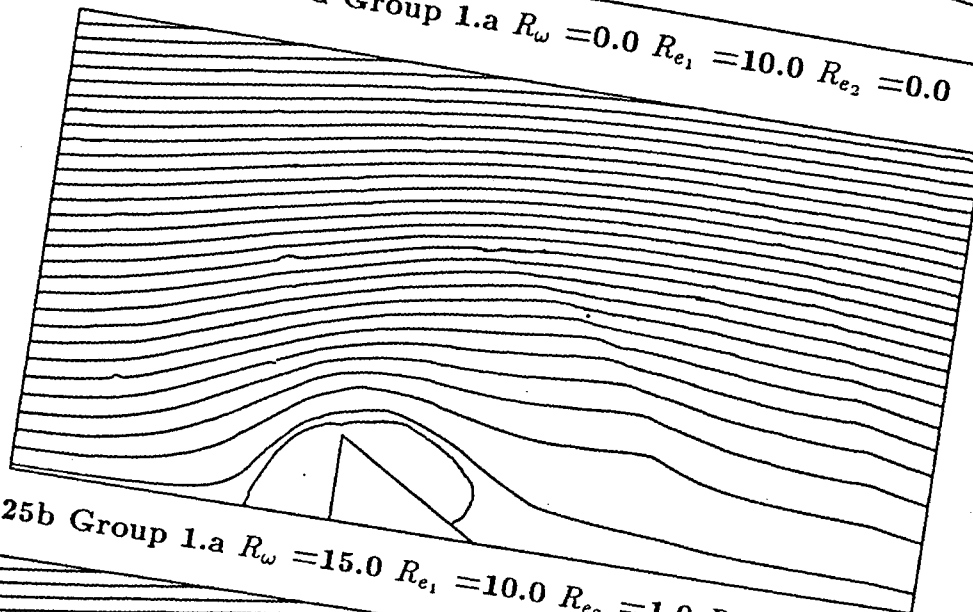Figure 5.25a Group 1.a $R_\omega = 0.0$ $R_{e_1} = 10.0$ $R_{e_2} = 0.0$

Figure 5.25b Group 1.a $R_\omega = 15.0$ $R_{e_1} = 10.0$ $R_{e_2} = 1.0$ $R_{e_2}/R_{e_1} = 0.1$ $\beta_2 = 0.067$
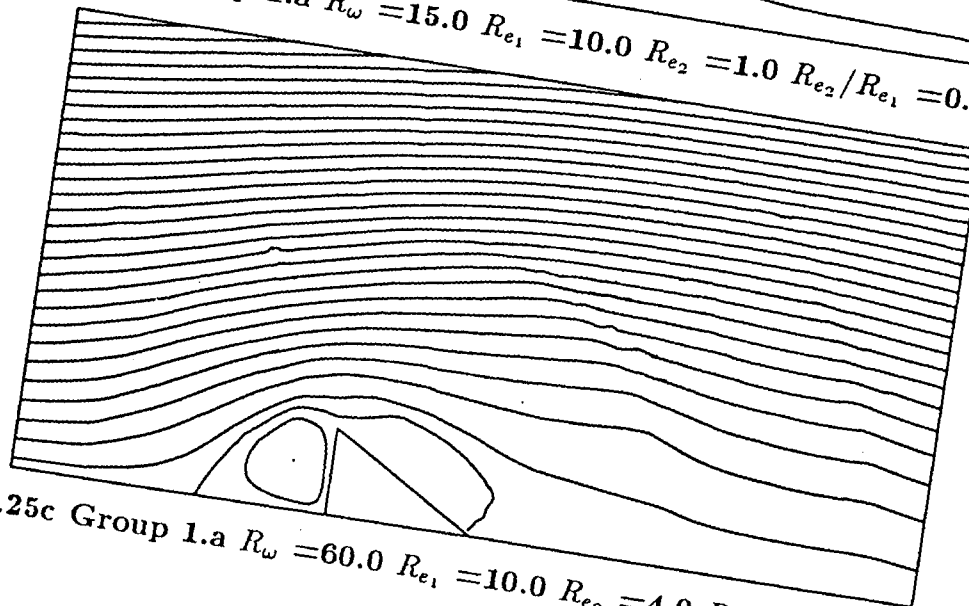
Figure 5.25c Group 1.a $R_\omega = 60.0$ $R_{e_1} = 10.0$ $R_{e_2} = 4.0$ $R_{e_2}/R_{e_1} = 0.4$ $\beta_2 = 0.067$
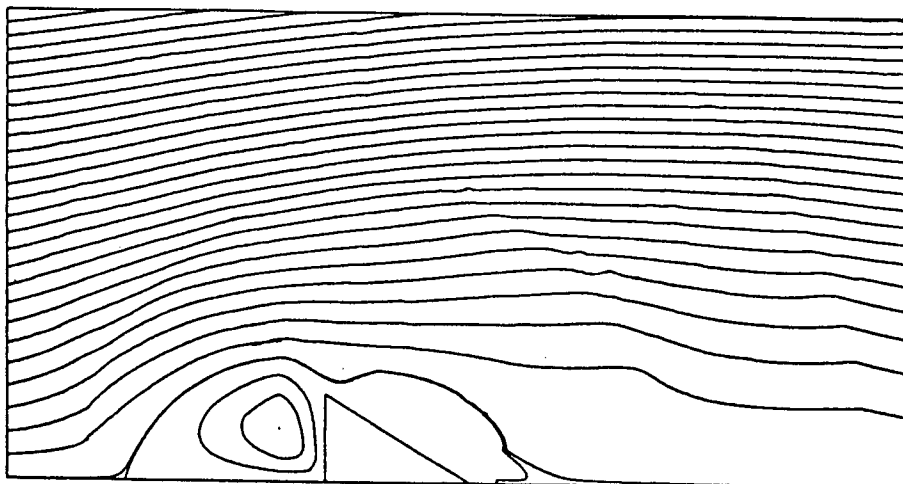
Figure 5.25d Group 1.a $R_\omega = 112.5$ $R_{e_1} = 10.0$ $R_{e_2} = 7.5$ $R_{e_2}/R_{e_1} = 0.75$ $\beta_2 = 0.067$
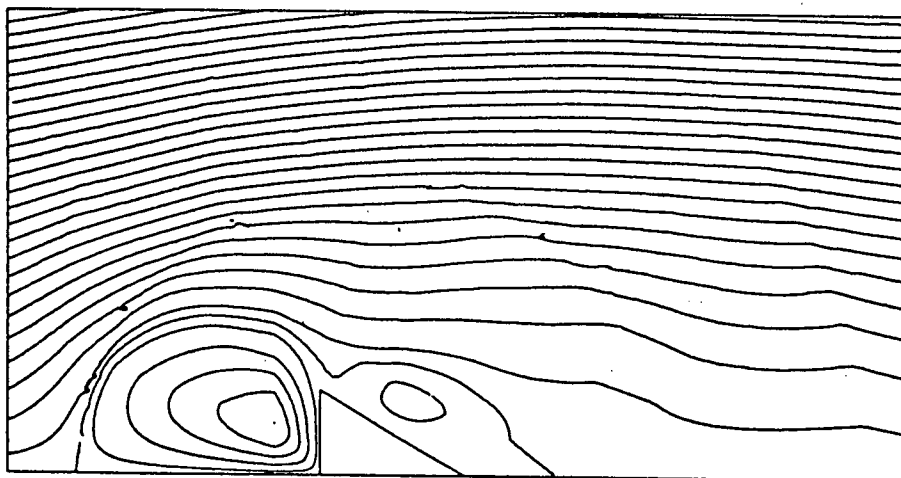

Figure 5.25e Group 1.a $R_\omega = 150.0$ $R_{e_1} = 10.0$ $R_{e_2} = 10.0$ $R_{e_2}/R_{e_1} = 1.0$ $\beta_2 = 0.067$

Figure 5.26a Group 1.b $R_\omega = 150.0$ $R_{e_1} = 7.5$ $R_{e_2} = 10.0$ $R_{e_2}/R_{e_1} = 1.33$ $\beta_2 = 0.067$

Figure 5.26b Group 1.b $R_\omega = 150.0$ $R_{e_1} = 4.0$ $R_{e_2} = 10.0$ $R_{e_2}/R_{e_1} = 2.5$ $\beta_2 = 0.067$

Figure 5.26c Group 1.b $R_\omega = 150.0$ $R_{e_1} = 1.0$ $R_{e_2} = 10.0$ $R_{e_2}/R_{e_1} = 10.0$ $\beta_2 = 0.067$
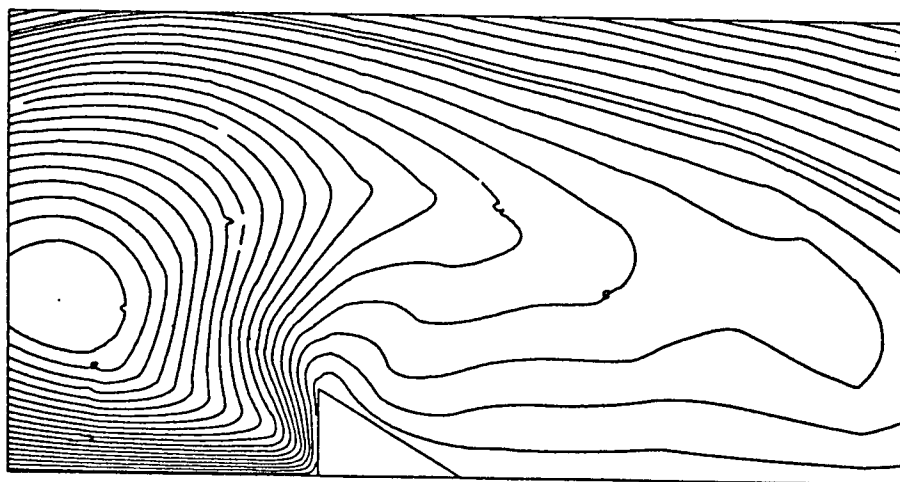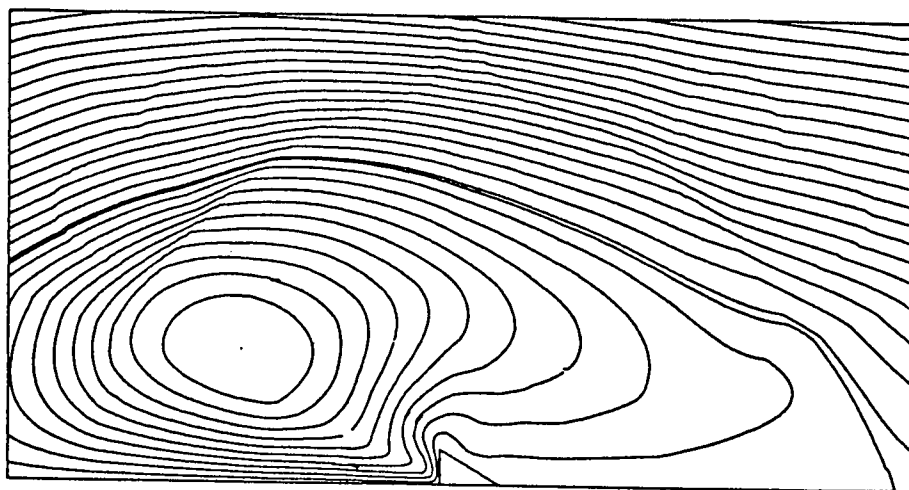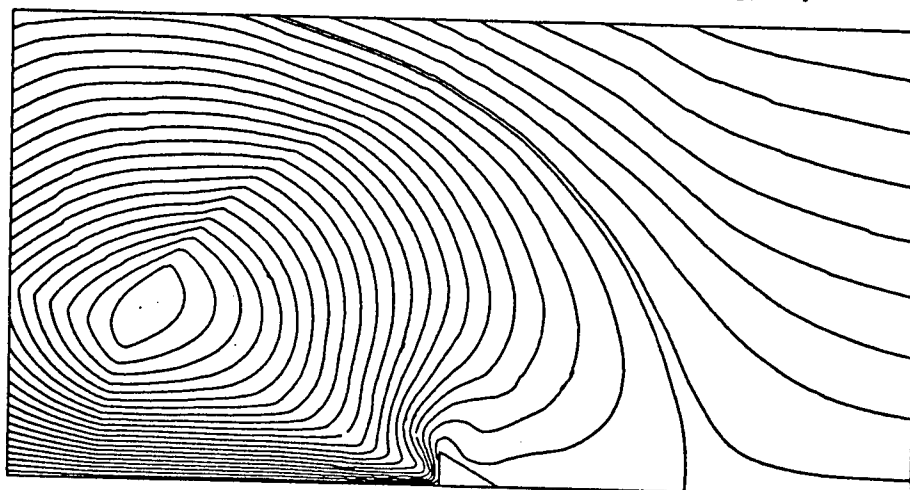

Figure 5.26d Group 1.b $R_\omega = 150.0$ $R_{e_1} = 0.0$ $R_{e_2} = 10.0$ $\beta_2 = 0.067$

Figure 5.27a Group 2 $R_\omega = 1000.0$ $R_{e_1} = 1.0$ $R_{e_2} = 10.0$ $R_{e_2}/R_{e_1} = 10.0$ $\beta_2 = 0.01$
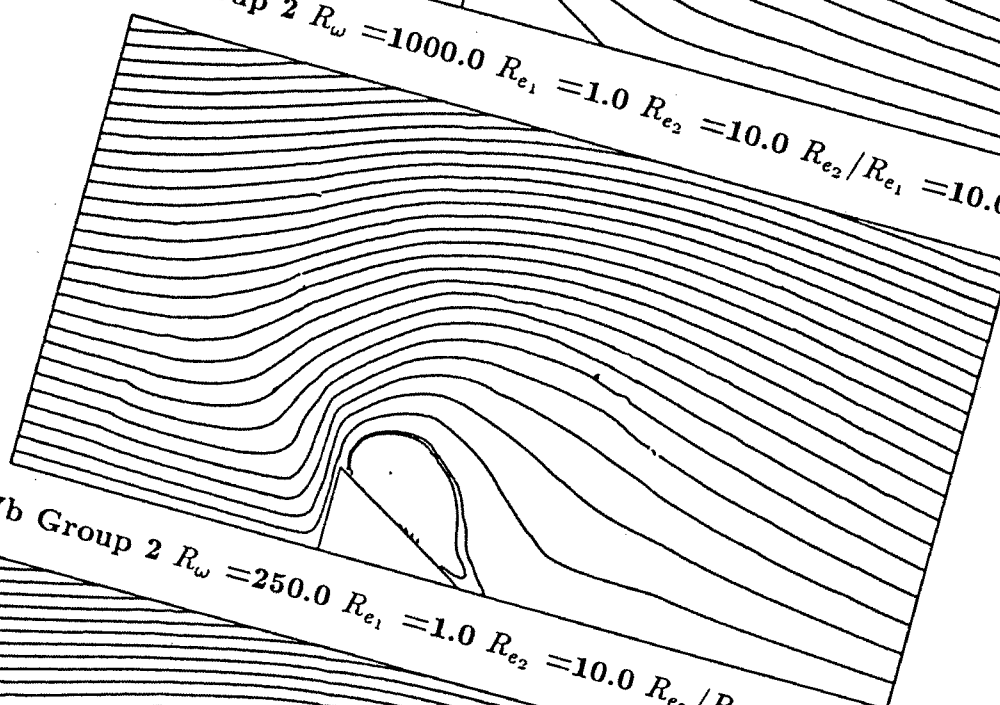
Figure 5.27b Group 2 $R_\omega = 250.0$ $R_{e_1} = 1.0$ $R_{e_2} = 10.0$ $R_{e_2}/R_{e_1} = 10.0$ $\beta_2 = 0.04$
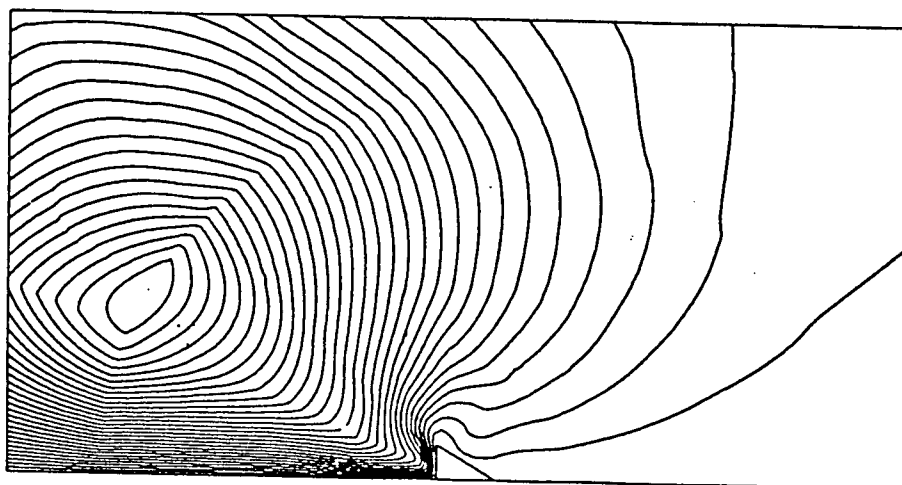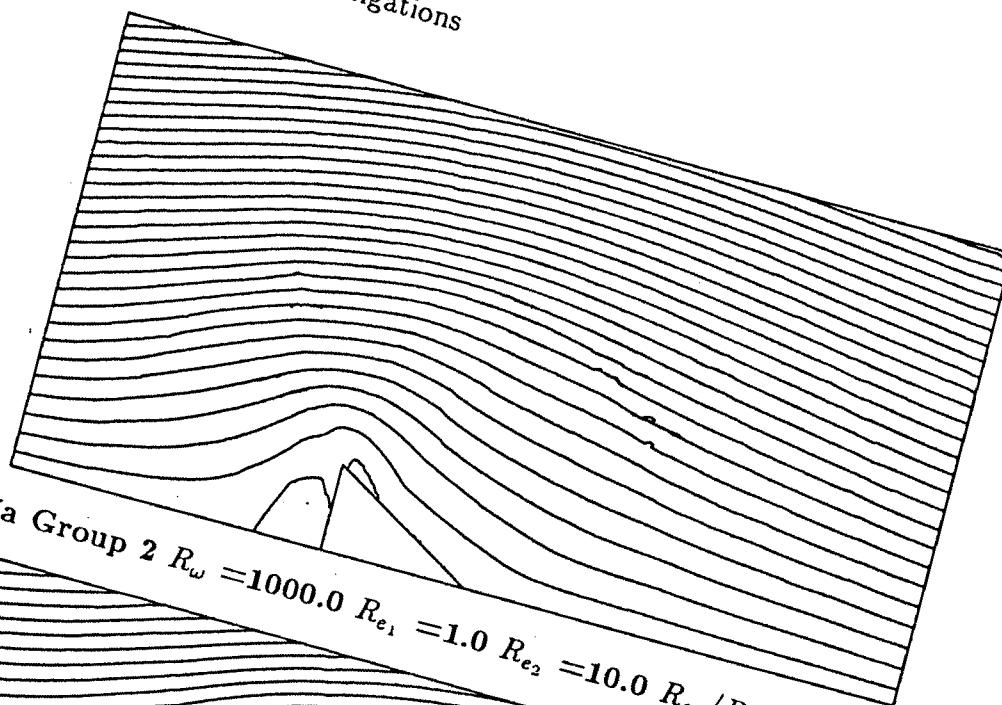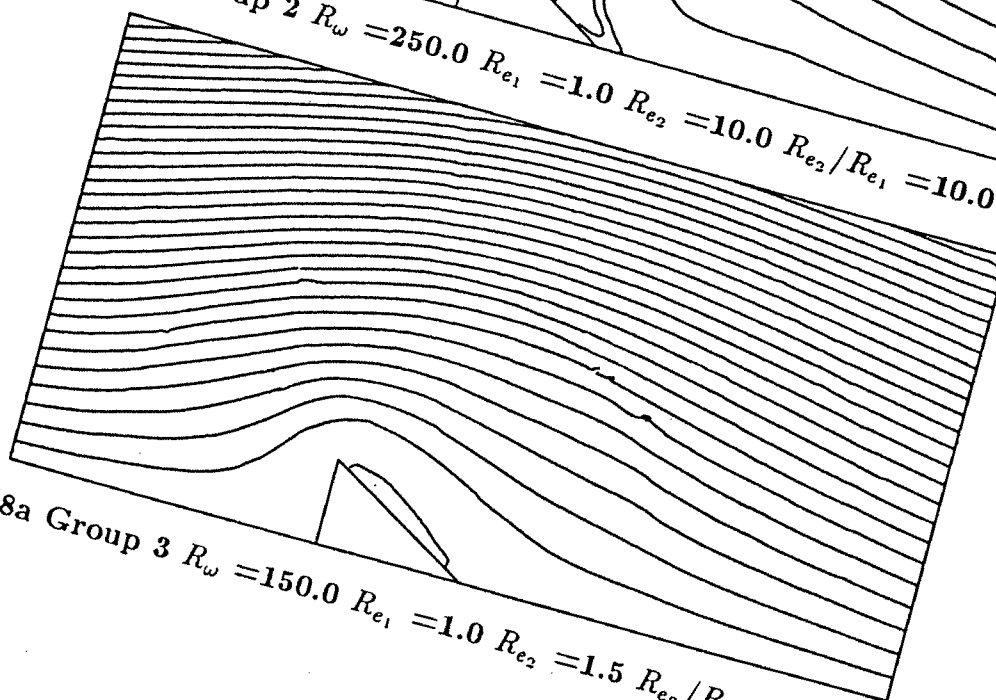
Figure 5.28a Group 3 $R_\omega = 150.0$ $R_{e_1} = 1.0$ $R_{e_2} = 1.5$ $R_{e_2}/R_{e_1} = 1.5$ $\beta_2 = 0.01$
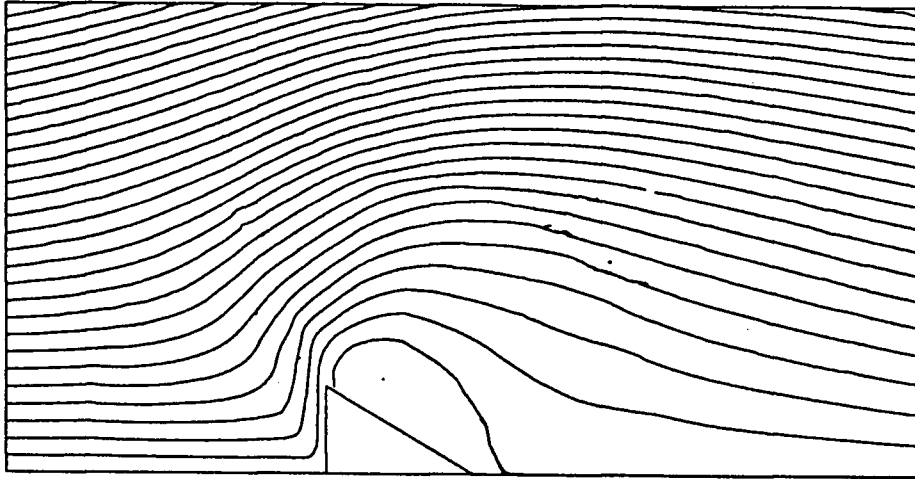
Figure 5.28b Group 3 R_ω =150.0 R_{e_1} =1.0 R_{e_2} =6.0 R_{e_2}/R_{e_1} =6.0 β_2 =0.04

in table 5.12. A similar parametric study, conducted on the circular and square bodies, is carrried out for the triangular body. The overall variation of the force quantities is similar to that observed for the circular and square body. The added mass and added damping are relatively constant for constant β_2 values while the added force decreases with increasing R_{e_2}/R_{e_1} values.

t=0.0

t=$\frac{\pi}{2}$

t=π

t=$\frac{3\pi}{2}$

Figure 5.29 Streaklines for R_ω =150.0 R_{e_1} =1.0 R_{e_2} =10.0
at t=0.0, $\frac{\pi}{2}$, π, $\frac{3\pi}{2}$ respectively

Table 5.12

Added Mass, Added Damping and Added Force for a Triangular Body

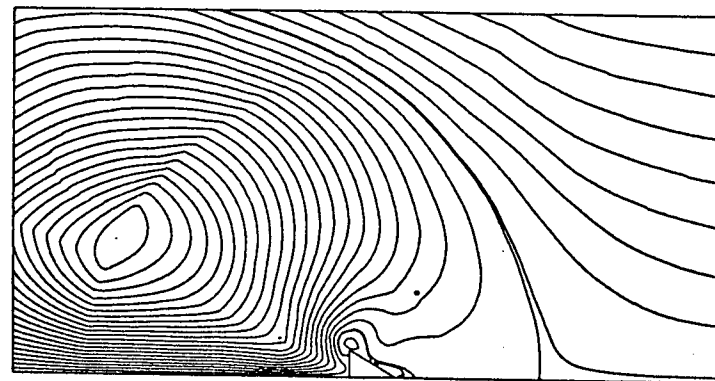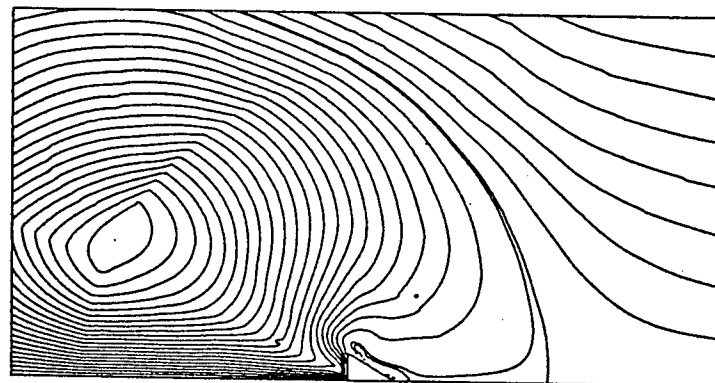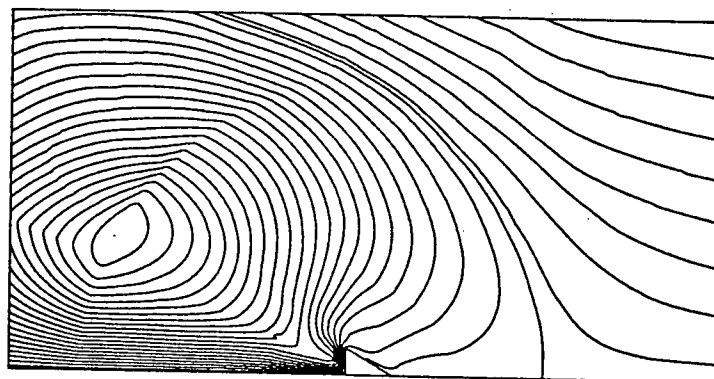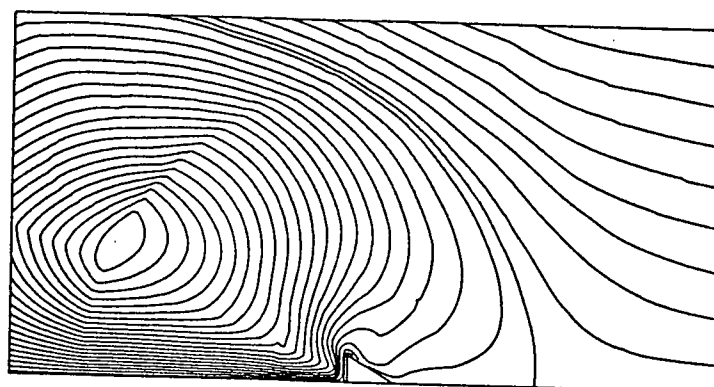| R_ω	R_{e_1}	R_{e_2}	Added Mass	Added Damping	Added Force
0.0*	10.0*	0.0*	-	-	16.2755
150.0**	0.0**	10.0**	2.6427	-0.3107	-0.9298
15.0	10.0	1.0	-6.0070	-4.7580	10.2330
60.0	10.0	4.0	2.8606	-0.8783	2.9475
112.5	10.0	7.5	2.7096	-0.3756	-1.8326
150.0	10.0	10.0	2.5700	-0.2752	-3.7253
150.0	7.5	10.0	2.6616	-0.3020	-2.7161
150.0	4.0	10.0	2.6473	-0.2899	-3.1777
150.0	1.0	10.0	2.6459	-0.3103	-1.4108
1000.0	1.0	10.0	1.6136	0.3380	-0.7303
250.0	1.0	10.0	1.9230	0.7759	-0.2386
100.0	1.0	10.0	-	-	-
150.0	1.0	1.5	2.1854	1.0430	2.8431
150.0	1.0	6.0	2.1479	1.0283	0.4604
150.0	1.0	15.0	-	-	-

*   Limiting case of steady flow over a fixed body.
** Limiting case of an oscillating body in stationary fluid.

5.5 Case a Associated Flow

5.5.1 General Remarks

So far we have considered the flow problem of a body oscillating in the direction of steady flow which corresponds to case b in figure 2.2. In this section, the results for the associated flow problem (case a), of a stationary body in a fluid flow with a steady as well as an oscillating component are presented. The investigation is carried out only for a circular body.

Goddard [7] has presented a numerical solution of the two-dimensional, time-dependent Navier-Stokes equations for the case of a fluctuating flow past a circular cylinder using a time-dependent explicit finite difference method. He obtained results for R_{e_1} =40 and 200 for different values of R_ω and R_{e_2} . The variation of the drag coefficients with time is determined and compared with [7]. Some comparisons are shown between the two associated flows.

5.5.2 Finite Element Grid and Boundary Conditions

The finite element grids used in this section are shown in figure 5.30. Grid 1 has a D/b ratio of 15.5 while that of grid 2 is 30.0. D is the total length of the fluid domain and b is the characteristic length of the body. Both the grids have circular outer boundaries.

Boundary Conditions for Grid 1 and Grid 2
Grid 1 and 2 have the same velocity and pressure boundary conditions.

1. $u = u_\infty$, $v = 0$ all along the fluid outer boundary.

2. u=0 and v=0 at the body boundary.

3. u=?, v=0 all along the symmetry line Γ_s.

4. $p = 0$ at point 2 of the grid.

For the flow problem of a stationary body in an oscillating fluid, both the finite element grids have 335 net degrees of freedom of which 273 are for the velocities and 62 are for the pressure.
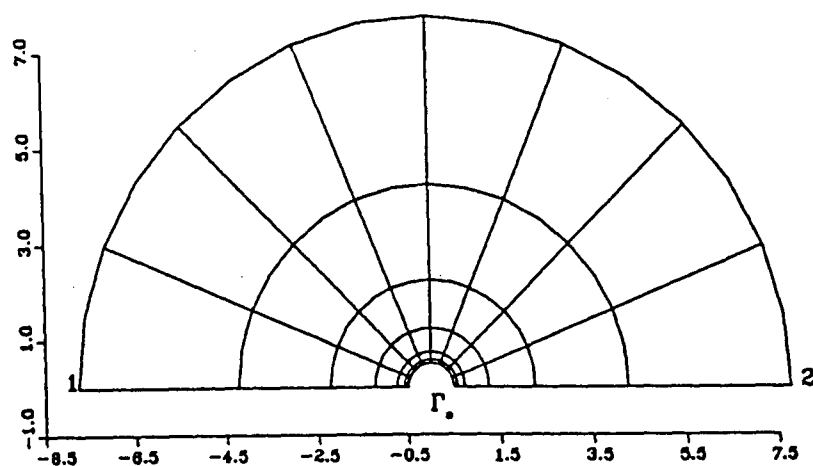
Figure 5.30a Finite Element Grid 1 for Case a Flow Problem
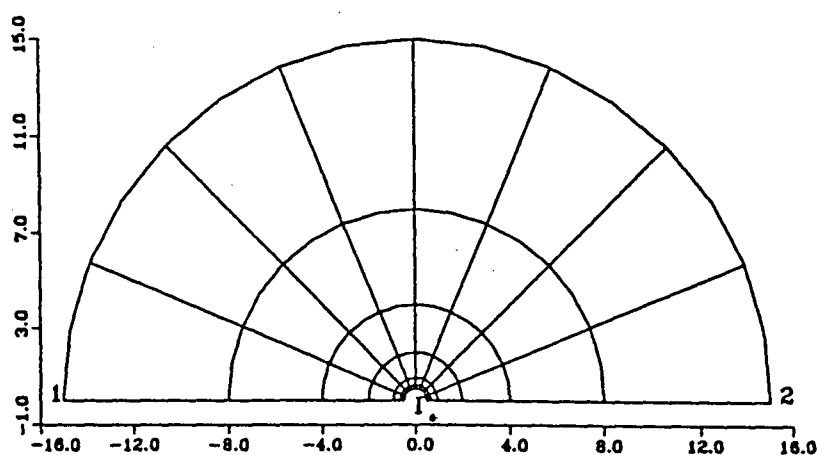
Figure 5.30b Finite Element Grid 2 for Case a Flow Problem

5.5.3 Flow Results

The limiting case of a stationary circular bluff body in an oscillating fluid is compared with the results obtained by Pattani, [18] in which he considered the same bluff body oscillating in an otherwise still fluid. The numerical solution obtained for the case b flow is transformed into that of case a using the transformation given by equation 3.15. These

transformed results are presented in terms of streamline plots of the steady component of the velocity field. Figures 5.31a and 5.31b are the streamline plots for both the associated flows for R_ω =21.34, R_{e_1} =0.0, R_{e_2} =0.6402 and β_2 =0.03. Figures 5.32a and 5.32b are the streamline plots for both the associated flows for R_ω =21.34, R_{e_1} =0.0 ,R_{e_2} =2.134 and β_2 =0.1. Grid 2 was used in both the cases. Figures 5.33a and 5.33b are the streamline plots for the two associated flows for R_ω =250.0, R_{e_1} =20.0, R_{e_2} =20.0. Grid 1 was used in this case. The general flow pattern in both case a and case b is similar. Table 5.13 presents the minimum and maximum values of the stream functions and their respective locations for case a and case b flows. In all the cases, the contour plots are obtained by plotting 31 equally spaced contours between the maximum and minimum values of the stream function in the plotted domain. The stream function values and their respective locations do not match well between the two associated flows.

The transformation between the two associated flows is valid for flows oscillating at far field. The boundary conditions simulated by the finite element grid may be such that the far field boundary is not far enough. This implies that there would be effect of the outer boundary even near the body. It is expected that by refining the grid near the outer boundary, the results in the two associated flows would match better. The transformation appears to work better in the present study for low values of the body amplitude parameter, β_2 . The steady component of the velocity field is a secondary phenomenon and is very small. Hence though the steady components of the velocity field do not match well, it is expected that the overall flow field would conform with the transformation.
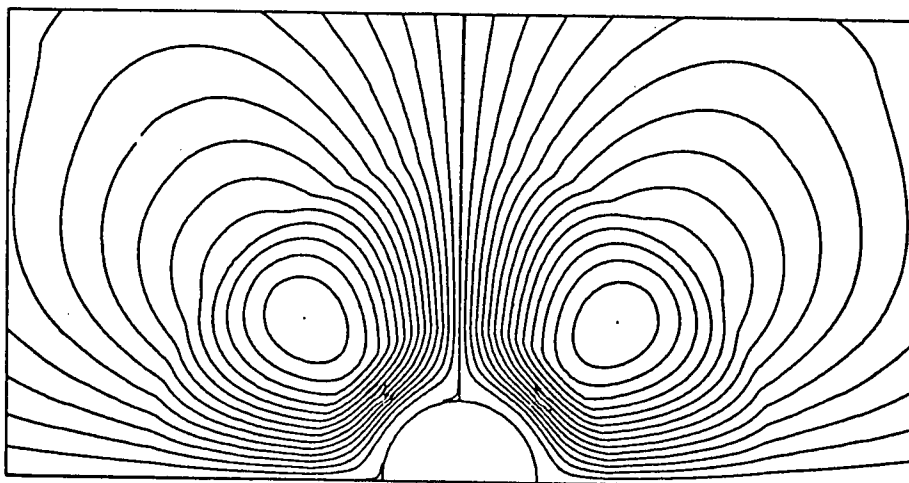
Figure 5.31a Case a $R_\omega = 21.34$, $R_{e_1} = 0.0$, $R_{e_2} = 0.6402$

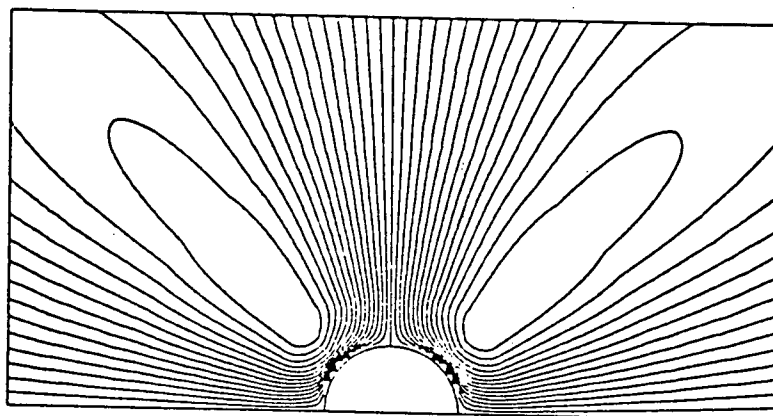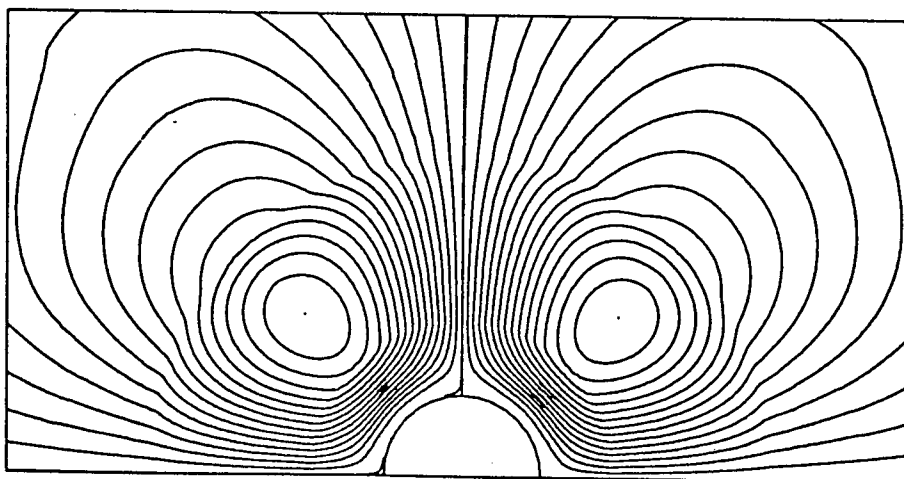**Figure 5.31b Case b** $R_\omega = 21.34$, $R_{e_1} = 0.0$, $R_{e_2} = 0.6402$

Figure 5.32a Case a $R_\omega = 21.34$ $R_{e_1} = 0.0$ $R_{e_2} = 2.134$
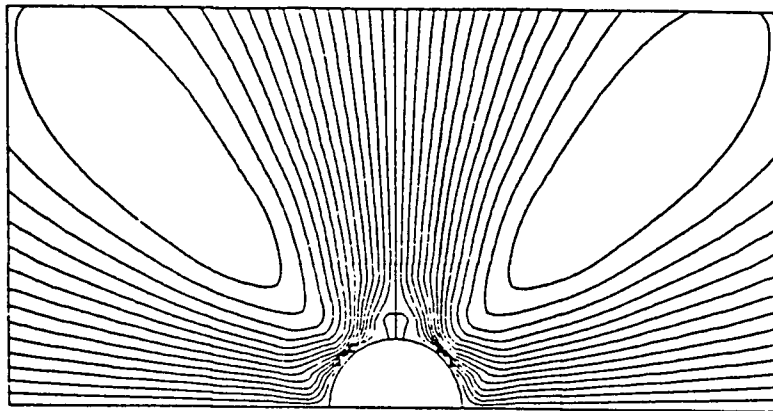
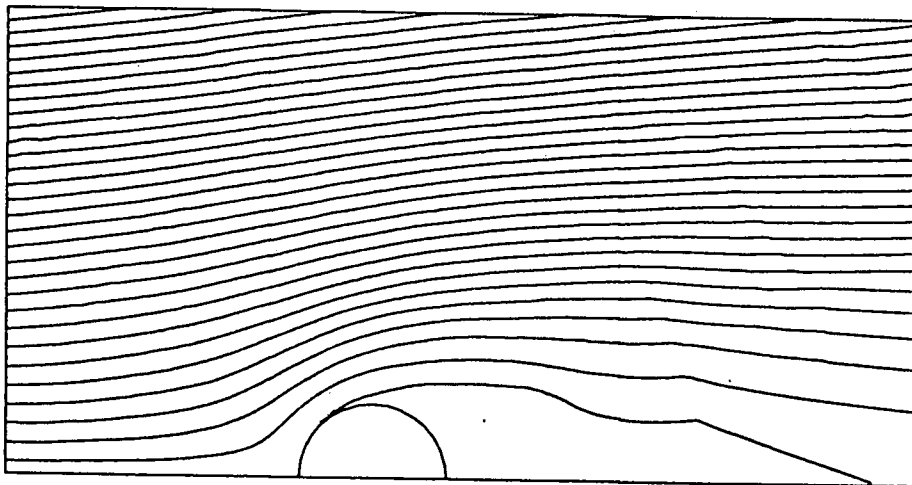Figure 5.32b Case b R_ω =21.34 R_{e_1} =0.0 R_{e_2} =2.134

Figure 5.33a Case a R_ω =250.0 R_{e_1} =20.0 R_{e_2} =20.0
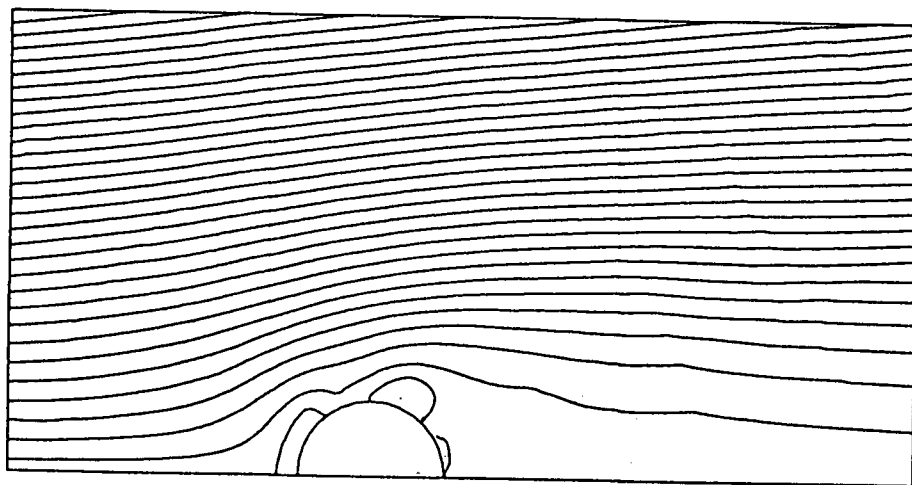
Figure 5.33b Case b R_ω =250.0 R_{e_1} =20.0 R_{e_2} =20.0

Table 5.13

Maximum and Minimum Stream Function Values of the Steady Component of the Velocity Field

R_ω	R_{e_1}	R_{e_2}	Case	Stream Function	location	
					x	y
21.34	0.0	0.640	a	min. val.=-0.0045	-1.0	1.0
			a	max. val.=0.0045	1.0	1.0
21.34	0.0	0.640	b	min. val.=-0.0088	-0.65	0.625
			b	max. val.=0.0088	0.65	0.625
21.34	0.0	2.134	a	min. val.=-0.0150	-1.0	1.0
			a	max. val.=0.0150	1.0	1.0
21.34	0.0	2.134	b	min. val.=-0.0798	-1.65	1.65
			b	max. val.=0.0798	1.65	1.65
250.0	20.0	20.0	a	min. val.=-0.0145	0.75	0.4
			a	max. val.=1.3570	-2.5	3.1
250.0	20.0	20.0	b	min. val.=-0.0189	0.2	0.525
			b	max. val.=1.3560	-2.5	3.1

Table 5.14

Added Mass/ Inertia Force, Added Damping and Added Force for the Two Associated Flows

R_ω	R_{e_1}	R_{e_2}	Case	Added Mass/ Inertial Force	Added Damping	Added Force
21.34	0.0	0.6402	a	3.1827	1.5899	0.0000
			b	2.1721	1.5899	0.0000
21.34	0.0	2.134	a	3.1803	1.5956	0.0000
			b	2.0903	1.6232	0.0000
250.0	20.0	20.0	a	2.3081	0.4117	9.3566
			b	1.2827	0.4014	7.7800

5.5.4 Inertia Force, Added Damping and Added Force

The transformation of added mass-inertia force, added damping and added force between case a and case b, presented in equation 4.27 is verified in this section. Table 5.14 presents the force quantities for case a and case b. It is observed that the results conform to the transformation of equation 4.27 quite well. Hence it can be concluded that though the steady components of the velocity field do not match well between the two associated flows, the overall flow results do conform.

Figures 5.34a to 5.34c presents the variation of the drag coefficients with time for R_ω =800.0, R_{e_1} =40.0 and R_{e_2} =4.0 for case a, case b and the results from [7] respectively. In this case R_{e_2}/R_{e_1} =0.1 and β_2 =0.005. The drag coefficients obtained for case b are transformed to those of case a using equation 4.28. The results of case b compare very well with [7] while those of case a show higher fluctuations in the pressure drag and total drag coefficients. Figure 5.35 presents the streaklines for case a and case b for R_ω =800.0, R_{e_1} =40.0 and R_{e_2} =4.0. The flow patterns in all three cases are quite similar. This is due to the high value of the steady Reynolds number (R_{e_1} =40) and the low value of the body amplitude parameter (β_2 =0.005).

Figures 5.36a to 5.36c presents the variation of the drag coefficients with time for R_ω =30.0, R_{e_1} =40.0 and R_{e_2} =4.0 for case a, case b and the results from [7] respectively. In this case, R_{e_2}/R_{e_1} =0.1 and β_2 =0.13. As in the previous case, the results of case b presented, are those after the transformation using equation 4.28. The results of case a compare quite well with those of [7]. The results of case b show smaller fluctuations in the drag coefficients than [7] or case a. Figure 5.37 presents the streaklines for case a and case b for R_ω =30.0, R_{e_1} =40.0 and R_{e_2} =4.0. The flow patterns of case a and case b do not compare well as observed from figure 5.37. These results are at a high value of β_2 and hence very accurate results are not expected by the present method.

Goddard's results show that the variation of the drag coefficients at steady state is similar to a sine wave. This shows that the assumption of a periodic solution in the method of averaging is fairly accurate. The results seem to match better for low values of β_2 . The discrepancy in the results can be attributed to the crudeness of the grid. Better agreement in results is expected with grid refinement.
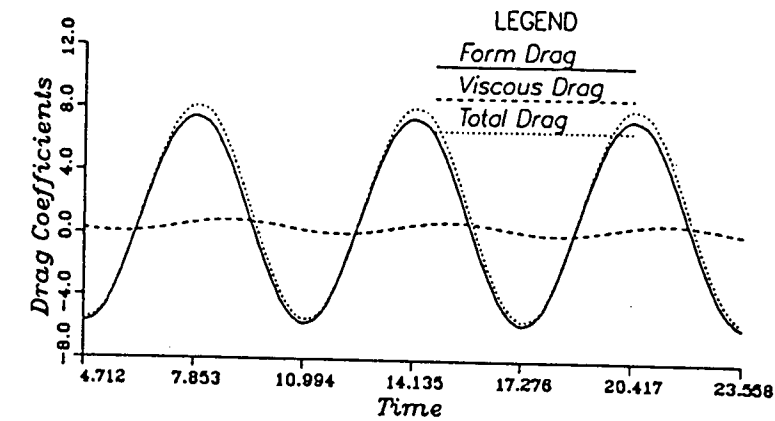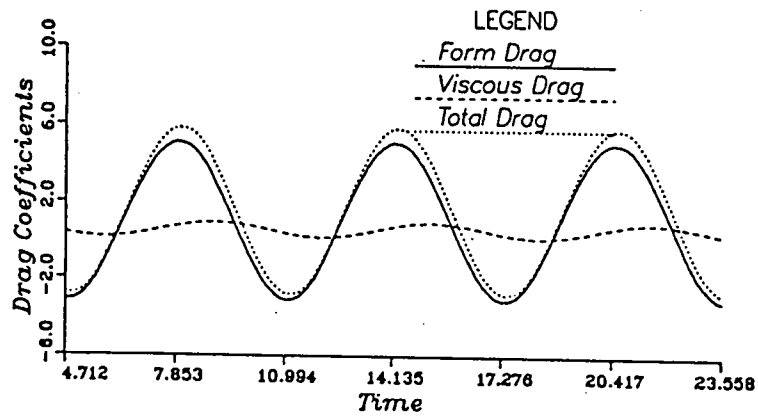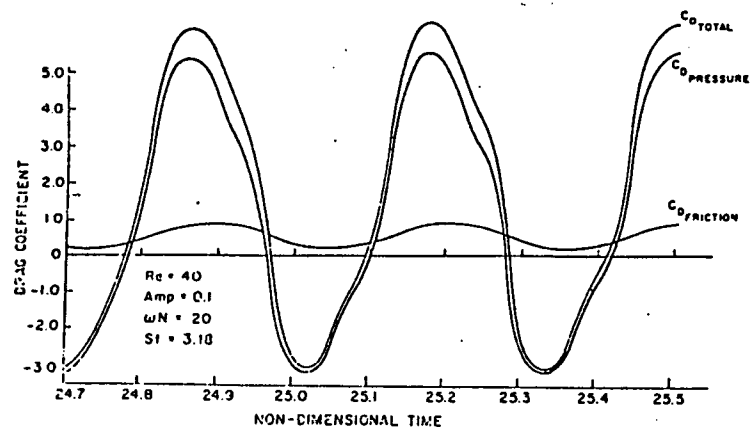
Figure 5.34 Drag Coefficients vs Time for $R_\omega = 800.0$ $R_{e_1} = 40.0$ $R_{e_2} = 4.0$ (a) case 1, (b) case b, (c) [7]
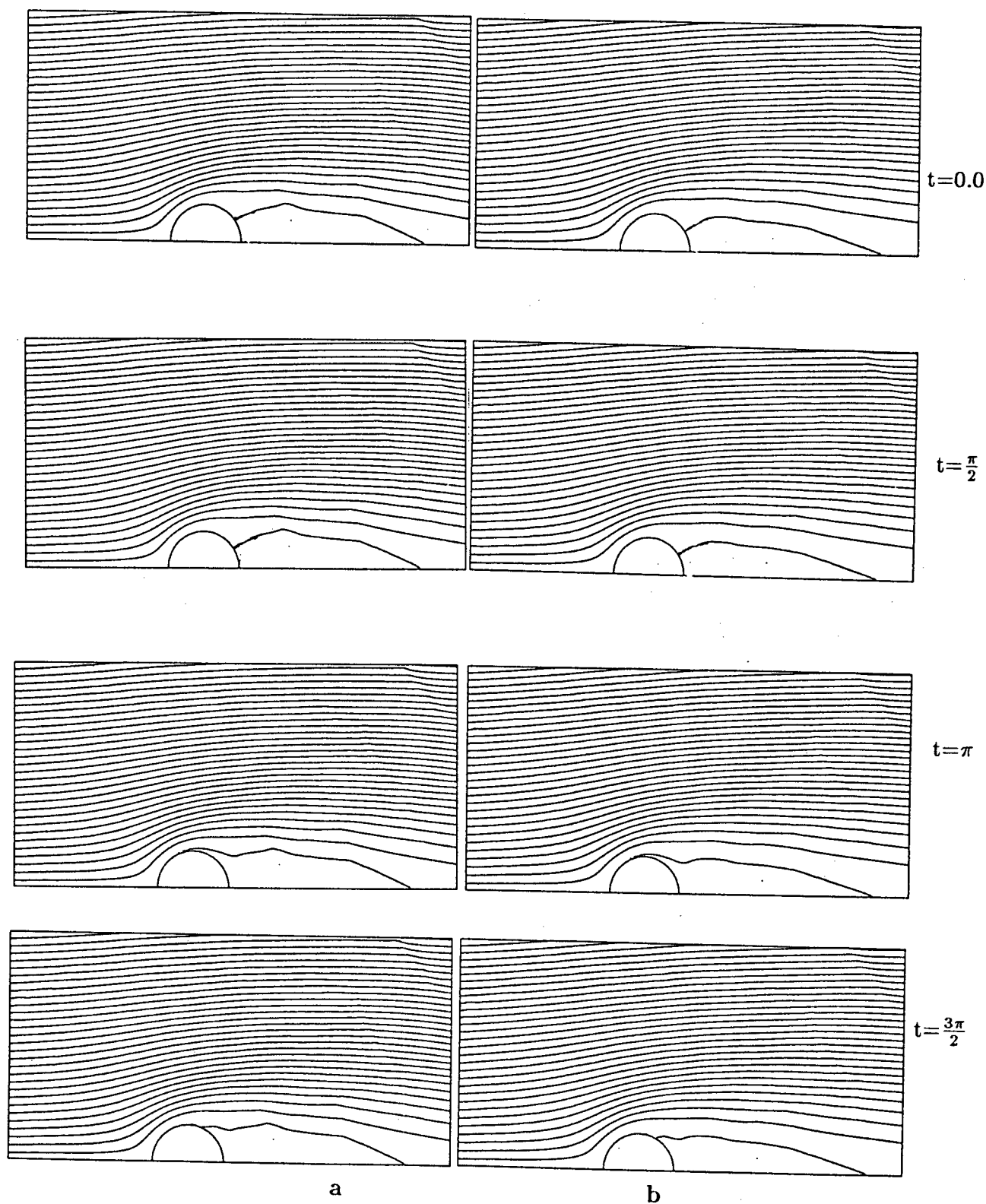
Figure 5.35 Streaklines for $R_\omega =800.0$ $R_{e_1} =40.0$ $R_{e_2} =4.0$
at t=0.0, $\frac{\pi}{2}$, π, $\frac{3\pi}{2}$ respectively
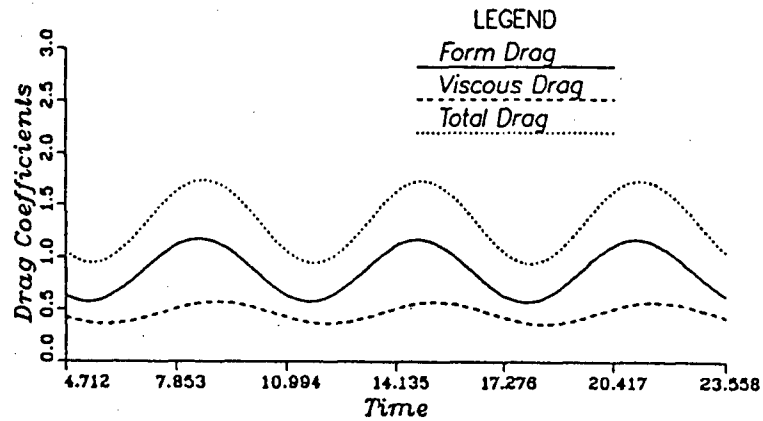
a
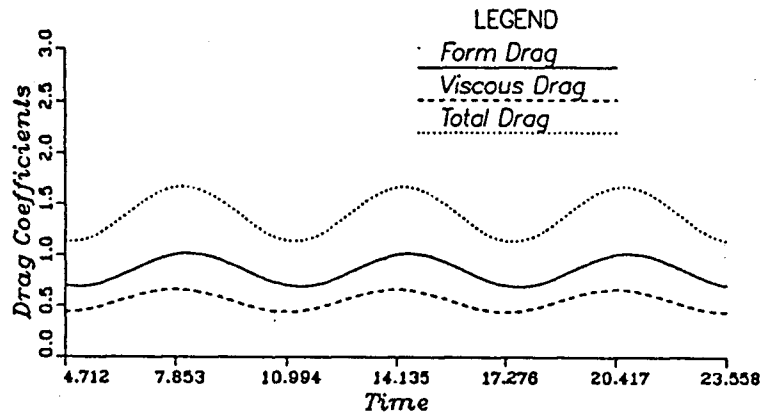
b
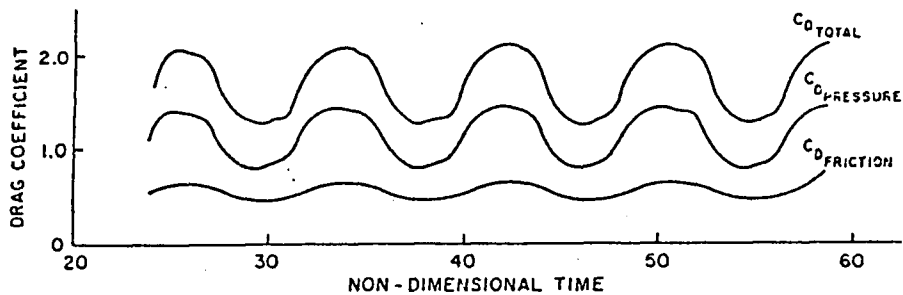
c

Figure 5.36 Drag Coefficients vs Time for $R_\omega = 30.0$

$R_{e_1} = 40.0$ $R_{e_2} = 4.0$. (a) case a, (b) case b, (c) [7]

Figure 5.37 Streaklines for $R_\omega = 30.0$ $R_{e_1} = 40.0$ $R_{e_2} = 4.0$ at $t = 0.0$, $\frac{\pi}{2}$, π, $\frac{3\pi}{2}$ respectively

5.5.5 Drag and Inertia Coefficients for the Morison Equation

The coefficients $C_d(1)$, $C_d(2)$ and C_m are determined from the added mass, added damping and the added force results presented in table 5.5 using equation 4.32. These results are presented in table 5.15. $C_d(1)$ for purely steady flow ($R_{e_1}=20.0$, $R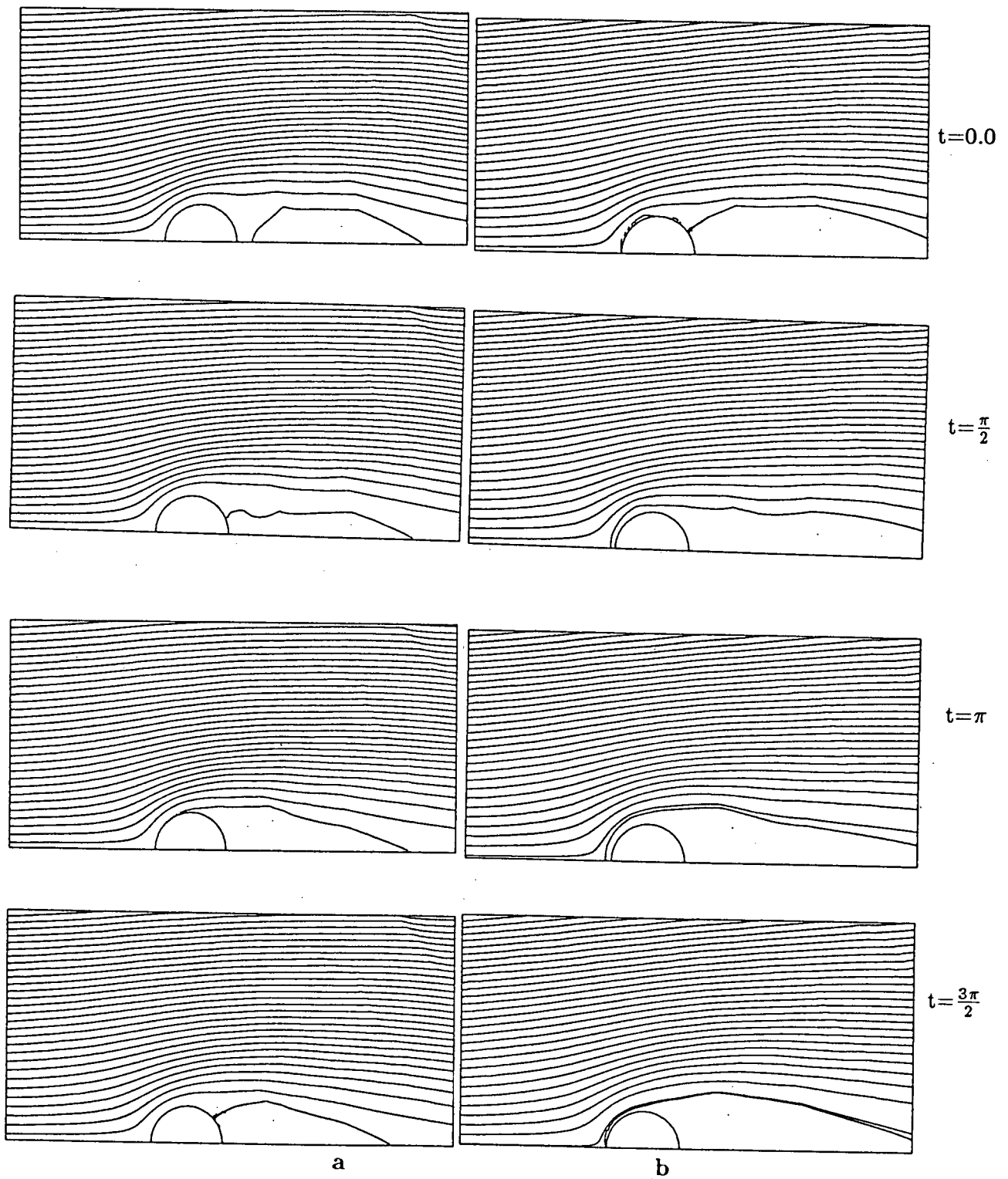_\omega=R_{e_2}=0.0$) is 2.0 and C_m for purely oscillatory flow is also 2.0. It is observed that C_m decreases with increase in R_{e_2}/R_{e_1} and increases with increase in β_2 . Overall, C_m lies in the range 2.2 to 2.5. $C_d(1)$ decreases with increase in R_{e_2}/R_{e_1} and β_2 . $C_d(2)$ increases with increase in R_{e_2}/R_{e_1} and decreases with increase in β_2 .

$C_d(1)$ and $C_d(2)$ as obtained from the results of the present investigation using equation 4.32 and those obtained by linearising the Morison equation (equation 4.30), are presented in figures 5.38 and 5.39. $C_d(1)$ and $C_d(2)$ are obtained from equation 4.30 by considering C_d to be that for purely steady flow for the given value of R_{e_1}. Figure 5.38 presents the variation of $C_d(1)$ and $C_d(2)$ with respect to R_{e_2}/R_{e_1} . It is observed that at oscillations of low amplitude ($R_{e_2}/R_{e_1} \leq 0.75$), the results of the present investigation compare quite well with the results from the linearised Morison equation. However, for higher values of R_{e_2}/R_{e_1} , the two results deviate substantially.

Figure 5.39 presents the variation of $C_d(1)$ and $C_d(2)$ with respect to β_2 . It is observed that the drag coefficients obtained from equation 4.30 are constant with changes in β_2 . This implies that the drag coefficients (obtained from equation 4.30) are independent of R_ω . Significant changes are observed in the variation of the drag coefficient $C_d(2)$ (obtained from the present study using equation 4.32) with β_2 . This variation is very similar to that observed in the variation of the added force given in figure 5.14.

Table 5.15

Inertia and Drag Coefficients for a Circular Body

R_ω	R_{e_1}	R_{e_2}	Cm	Cd(1)	Cd(2)
0.0*	2.0*	0.0*	0.0	3.588	0.0
0.0*	20.0*	0.0*	0.0	2.000	0.0
0.0*	40.0*	0.0*	0.0	1.5	0.0
250.0**	0.0**	20.0**	2.2696	0.0000	8.3723
25.0	20.0	2.0	3.1312	1.1917	0.3150
62.5	20.0	5.0	2.5815	0.9427	1.1069
187.5	20.0	15.0	2.3003	0.5332	1.7411
250.0	20.0	20.0	2.2827	0.3989	1.9703
500.0	20.0	40.0	2.2161	0.1519	2.3256
250.0	15.0	20.0	2.2776	0.3365	2.6332
250.0	5.0	20.0	2.2706	0.1290	5.3244
250.0	2.0	20.0	2.2697	0.0397	6.9112
1000.0	2.0	20.0	2.1383	0.0671	13.5854
500.0	2.0	20.0	2.1723	0.0932	12.5729
333.33	2.0	20.0	2.3306	0.0315	4.6756
200.0	2.0	20.0	2.5158	-0.0034	4.9681
250.0	2.0	10.0	2.1873	0.3213	11.6041
250.0	2.0	15.0	2.3852	0.0729	5.6928
250.0	2.0	25.0	2.4734	-0.0288	4.5734

* Limiting case of steady flow over a fixed body.
** Limiting case of an oscillating body in stationary fluid.
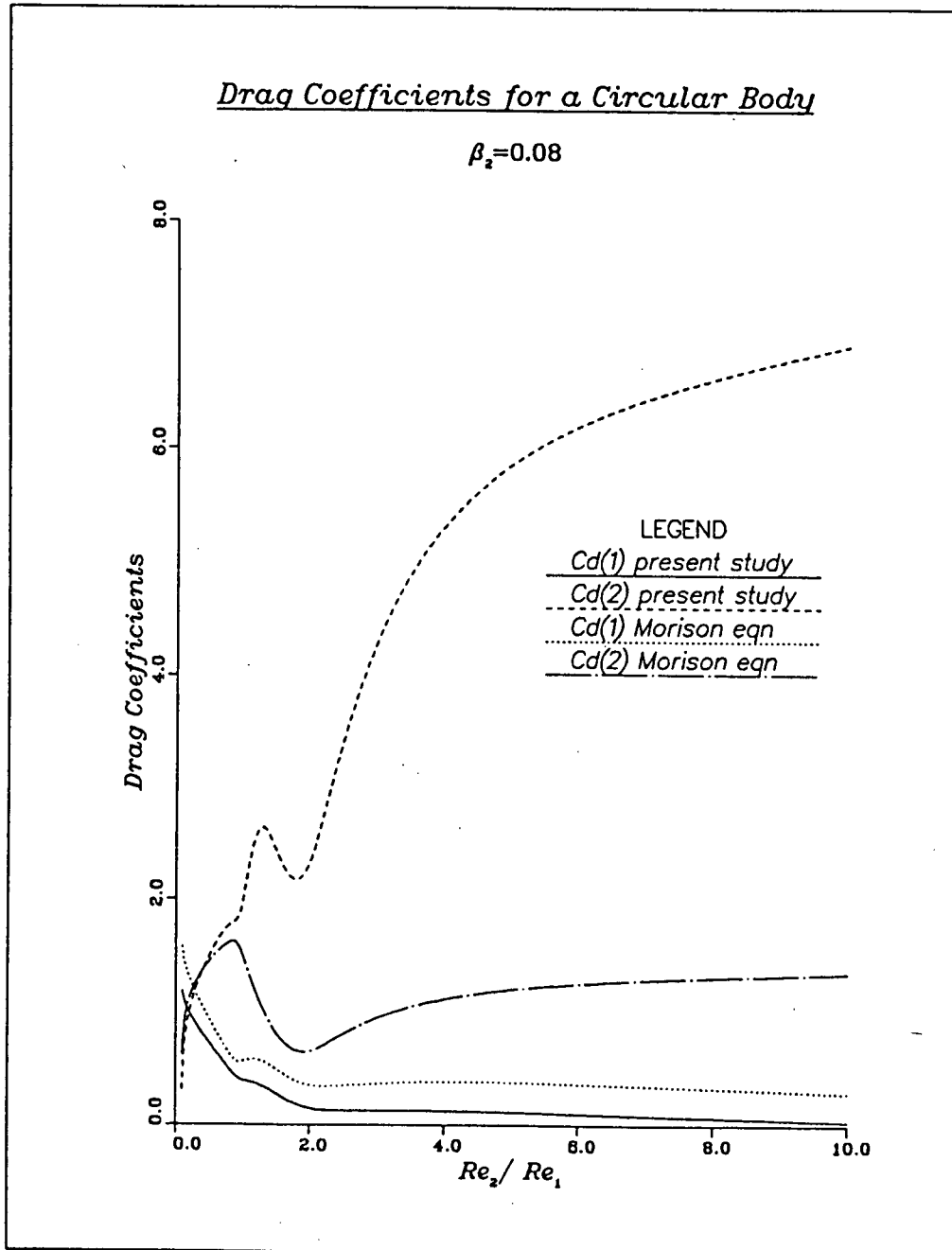
Figure 5.38 Variation of $C_d(1)$ and $C_d(2)$ with R_{e_2}/R_{e_1}
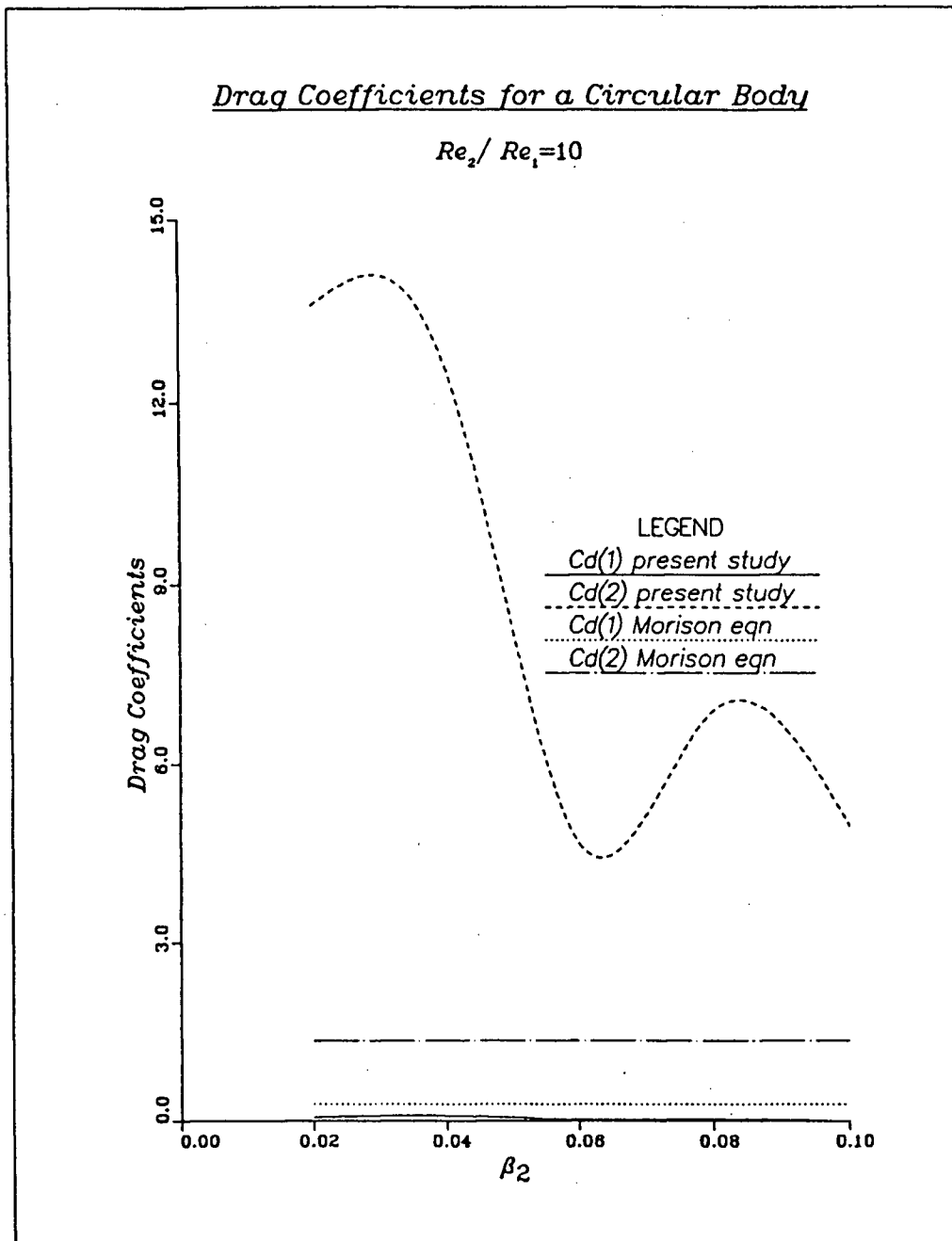
Figure 5.39 Variation of $C_d(1)$ and $C_d(2)$ with β_2

Conclusions

6.1 Concluding Remarks

The present method of representing the interaction between a solid body and viscous flow seems to work very well. The modified method of averaging used is also observed to be quite accurate. The overall agreement between the present study and other known results is very good.

Dramatic changes in the flow patterns are observed with changes in the three parameters R_ω , R_{e_1} and R_{e_2} . The body amplitude parameter β_2 is found to have the most significant effect on the flow patterns. At high values of R_{e_2}/R_{e_1} , the vortex behind the body moves to the front at a certain value of β_2 . Similar flow patterns are observed for the circular and square body for different values of Reynolds numbers. The limiting cases of steady flow over a fixed body and an oscillating body in a stationary fluid compare quite well with known results.

The added mass, added damping and the added force are intimately related to the flow pattern. Drastic changes in the flow pattern result in drastic changes in the force quantities. The added mass and added damping are influenced by R_ω and R_{e_2} , while the added force is predominately influenced by R_{e_1} . The drag coefficients obtained for the limiting case of steady flow over a fixed body compare quite well with known results. The inertia and the drag coefficients obtained from the present study results compare quite will with those obtained from the linearised Morison equation for $R_{e_2}/R_{e_1} \leq 0.75$. At higher values of R_{e_2}/R_{e_1} , the two results deviate substantially indicating the inaccuracy of the Morison equation at high values of R_{e_2}/R_{e_1} .

The numerical results for the related associate flow in which the body is at rest in a two-dimensional, time-dependent, viscous flow, compare quite well with known results. The transformations derived between the two associated flows for the velocities, pressure and the force quantities agree with numerical results. The flow patterns for the two associated flows agree better at lower values of β_2 and high values of R_{e_1} . Better agreement in results is expected with grid refinement.

6.2 Suggestions for Further Development

Some specific recommendations for further studies based on the work in this thesis are

1 Extend the analysis to include the unsymmetric vortex shedding by using the full fluid domain.

2 Incorporate turbulence modelling for the fluid to obtain results for large values of Reynolds numbers suitable for engineering applications

3 Conduct a grid refinement study to determine the effect of grid refinement on the numerical results.

References

[1] Bertelsen, A. F. *An Experimental Investigation of High Reynolds Number Steady Streaming Generated by Osicllating Cylinders*, J. Fluid Mech., 1974, vol 64, part 3, pp 589–597.

[2] Davis, R.W. and Moore, E.F., *The Numerical Solutions of Flow around Squares*, Proc. 2nd Int. Conf. on Num. Meth. in Lam. and Turb. Flow, Venice,1981, Italy, pp 279–290.

[3] Davis, R.W. and Moore, E.F., *Numerical-Experimental Study of Confined Flow around Rectangular Cylinders*, Physics of Fluids, vol 27 N1, Jan 1984, pp 1–11.

[4] Dorodnicyn, A.A., *Review of Methods for Solving the Navier-Stokes Equations*,1981, Proc. of 3rd Int. Conf. on Num. Meth. in Fluid Mech., vol 1, pp 1–11.

[5] Duck, P.W. and Smith, F.T., *Steady Streaming Induced between Oscillating Cylinders*, J. Fluid Mech., 1979, vol 91, part 1, pp 93–110.

[6] Finlayson, B. A., *The Method of Weighted Residuals and Variational Principles*, 1972, Academemic Press, New York.

[7] Goddard V.P., *Numerical Solutions of the Drag Response of a Circular Cylinder to Streamwise Velocity Fluctuations*, 1972, Ph.D. Thesis, Univ. of Notre Dame.

[8] Graham, J.M.R, Bearman P.W.,*Vortex Shedding from Bluff Bodies in Oscillatory Flow*, Report on Euromech 119, 1980, Journal of Fluid Mechanics, vol 9, pp 225–245.

[9] Hughes, T.J.R., Liu, W.K., and Zimmerman, T.K., *Langragian-Eulerian Finite Element Formulation for Incompressible Viscous Flows*, U.S.-Japan Conf. Interdisciplinary Finite Element Analysis.

[10] Isaacson, M. de St. Q., *The Force on Circular Cylinders in Waves*, Ph.D. Thesis, 1974, University of Cambridge, England.

[11] Leal, L.G., Lea, S.H., *Low Reynolds Number Flow Past Cylindrical Bodies of Arbitrary Cross-Sectional Shape*, J. Fluid Mech., (1986), vol 164, pp 401–427.

[12] Liu, W.K., *Development of Finite Element Procedures for Fluid-Structure Interaction*, Ph.D. Thesis, 1980, California Instt. of Tech., Pasadena.

[13] Nicolaides, R.A., Liu, C.H., *Algorithmic and Theoretical Results on Computation of Incompressible Viscous Flows by Finite Element Method*, Comput. Fluids,1985, v13 N3, pp 361–373.

[14] Olson, M.D., and Irani, M., *Finite Element Analysis of Viscous Flow-Solid Body Inter-action*, Proc. of 2nd Int. Conf. on Num. Meths. in Lam. and Turb. Flow, 1983,Seattle, U.S.A.

[15] Okajima, A. *Strouhal Numbers of Rectangular cylinders*, J. Fluid Mech., 1982,vol 123, pp 379–398.

[16] Olson, M.D. and Pattani, P.G., *Nonlinear Analysis of Rigid Body-Viscous Flow Inter-action*, 5th Symp. on Finite Element Meths. in Flow Probs., 1984, Austin, Texas, also in *Finite Elements in Fluids*,1985, vol 6, Eds. Gallagher,R.H., Carey, G.F., Oden, J.T., Zienkiewicz, O.C.,Wiley.

[17] Olson, M.D., *Comparison of Various Finite Element Solution Methods for the Navier-Stokes Equations*, Finite Elements in Water Resources,1977,Ed. Grey, W.G., at al, pp 4.185–4.203.

[18] Pattani, P.G., *Nonlinear Analysis of Rigid Body-Viscous Flow Interaction*, Ph.D. The-sis, 1986, The University of British Columbia, Vancouver, Canada.

[19] Pattani, P.G., *Forces on Oscillating Bodies in Viscous Fluids*,to be published

[20] Ramber, E.S., Griffin O.M., *Vortex Shedding from a Cylinder Vibrating In Line with an Incident Uniform Flow*, J. Fluid Mech., 1976, vol 75 part 2, pp 255–271.

[21] Riley, N., *The Steady Streaming Induced by a Vibrating Cylinder*, J. Fluid Mech., 1975, vol 68, part 4, pp 801–812.

[22] Roache, P.G., *Computational Fluid Dynamics*, 1972, Hermosa Publishers, Alburquerque, New Mexico.

[23] Sarpkaya, T., and Isaacson, M., *Mechanics of Wave Forces on Offshore Structures*, 1981, Van Nostrand Reinhold Company, New York.

[24] Sarpkaya, T., *In Line Force on a Cylinder Translating in Oscillatory Flow*, Storm M. Appl. Ocean Res., vol 7 N4, Oct 1985, pp 188–196.

[25] Schlichting, H., *Boundary Layer Theory*, 1968, Mcgraw-Hill, 6th Ed.

[26] Tanida, Y., Okajima, A., Watanabe, Y., *Stability of a Circular Cylinder Oscillating in Uniform Flow or in a Wake*, J. Fluid Mech., 1973,vol 61, pt. 4, pp 769–784.

[27] Tatsuno M., *Vortex Wakes Behind a Circular Cylinder Oscillating in the Flow Direc-tion*, Bulletin Research Instt. Applied Mech., 1972, Kyushu University, No. 36.

[28] Tatsuno M., *Circulatory Streaming around an Oscillating Circular Cylinder at Low Reynolds Numbers*, 1973, J. Physical Society of Japan, Vol. 35, No. 3, pp 915–920.

[29] Tatsuno M., *Circulatory Streaming in the Viscinity of an Oscillating Square Cylinder*, J. of Physical Society of Japan,1974, vol. 36, No. 4, pp 1185–1191.

[30] Tatsuno M., *Circulatory Streaming in the Viscinity of an Oscillating Triangular Cylinder*, J. Physical Soc. Japan,Jan 1975,vol. 38, No. 1, pp 257–264.

[31] Tuann, S.Y., and Olson, M.D., *Numerical Studies of the Flow around a Circular Cylinder by a Finite Element Method*,1978, Computers in Fluids, vol 6, pp 219–240.

[32] Zienkiewicz, O.C., *The Finite Element Method*, Ed. 3,Mcgraw Hill Book Company, U.K.

Appendix A

Verification of the Restricted Variational Principle

Take the first variation of Π (equation 3.1) keeping u^0 and v^0 constant.

$$\delta\Pi = \iint_\Omega \left\{ \left[R_\omega \frac{\partial u}{\partial t} + R_e \left(u^0 \frac{\partial u^0}{\partial x} + v^0 \frac{\partial u^0}{\partial y} \right) \right] \delta u \right.$$

$$+ \left[R_\omega \frac{\partial v}{\partial t} + R_e \left(u^0 \frac{\partial v^0}{\partial x} + v^0 \frac{\partial v^0}{\partial y} \right) \right] \delta v$$

$$+ [2\frac{\partial u}{\partial x}\frac{\partial \delta u}{\partial x} + 2\frac{\partial v}{\partial y}\frac{\partial \delta v}{\partial y} + (\frac{\partial u}{\partial y} + \frac{\partial v}{\partial x})\frac{\partial \delta u}{\partial y} + (\frac{\partial u}{\partial y} + \frac{\partial v}{\partial x})\frac{\partial \delta v}{\partial x}]$$

$$\left. - [p(\frac{\partial \delta u}{\partial x} + \frac{\partial \delta v}{\partial y}) + (\frac{\partial u}{\partial x} + \frac{\partial v}{\partial y})\delta p] \right\} dA - \int_{\Gamma_*} \overline{X}\delta u + \overline{Y}\delta v \, ds = 0$$

Integrate the appropriate terms by parts

$$\iint_{\Omega_e} \left\{ \left[R_\omega \frac{\partial u}{\partial t} + R_e \left(u^0 \frac{\partial u^0}{\partial x} + v^0 \frac{\partial u^0}{\partial y} \right) \right] \delta u \right.$$

$$+ \left[R_\omega \frac{\partial v}{\partial t} + R_e \left(u^0 \frac{\partial v^0}{\partial x} + v^0 \frac{\partial v^0}{\partial y} \right) \right] \delta v - [2\frac{\partial^2 u}{\partial x^2} + \frac{\partial^2 u}{\partial y^2} + \frac{\partial^2 v}{\partial x \partial y} - \frac{\partial p}{\partial x}]\delta u$$

$$\left. - [\frac{\partial^2 v}{\partial x^2} + 2\frac{\partial^2 v}{\partial y^2} + \frac{\partial^2 u}{\partial x \partial y} - \frac{\partial p}{\partial y}]\delta v - [\frac{\partial u}{\partial x} + \frac{\partial v}{\partial y}]\delta p \right\} dA$$

$$+ \int_{\Gamma_*} \left\{ (2\frac{\partial u}{\partial x} - p)n_1 + (\frac{\partial u}{\partial y} + \frac{\partial v}{\partial x})n_2 - \overline{X} \right\} \delta u \, dS$$

$$+ \int_{\Gamma_*} \left\{ (\frac{\partial u}{\partial y} + \frac{\partial v}{\partial x})n_1 + (2\frac{\partial v}{\partial y} - p)n_2 - \overline{Y} \right\} \delta v \, dS = 0$$

n_1 and n_2 are the direction cosines of the outward pointing normal to the boundary.

But δu and δv are arbitrary variations. Hence by virtue of Lagrange's Lemma, we

get:-

$$\left[R_\omega \frac{\partial u}{\partial t} + R_e\left(u^0\frac{\partial u^0}{\partial x} + v^0\frac{\partial u^0}{\partial y}\right)\right] - \left[2\frac{\partial^2 u}{\partial x^2} + \frac{\partial^2 u}{\partial y^2} + \frac{\partial^2 v}{\partial x\partial y} - \frac{\partial p}{\partial x}\right] = 0$$

$$\left[R_\omega \frac{\partial v}{\partial t} + R_e\left(u^0\frac{\partial v^0}{\partial x} + v^0\frac{\partial v^0}{\partial y}\right)\right] - \left[\frac{\partial^2 v}{\partial x^2} + 2\frac{\partial^2 v}{\partial y^2} + \frac{\partial^2 u}{\partial x\partial y} - \frac{\partial p}{\partial y}\right] = 0$$

$$-\left(\frac{\partial u}{\partial y} + \frac{\partial v}{\partial x}\right) = 0$$

Boundary terms:-

$$\left(2\frac{\partial u}{\partial x} - p\right)n_1 + \left(\frac{\partial u}{\partial y} + \frac{\partial v}{\partial x}\right)n_2 - \overline{X} = 0$$

$$\left(\frac{\partial u}{\partial y} + \frac{\partial v}{\partial x}\right)n_1 + \left(2\frac{\partial v}{\partial y} - p\right)n_2 - \overline{Y} = 0$$

Equating u^0 to u and v^0 to v, we obtain the governing equations (2.17) and (2.18).

Appendix B

Derivation of the Discretised Form of the Navier-Stokes Equations

Substitute the interpolating functions (eqn 3.2) into the functional Π^e (eqn 3.1) and take the first variation of Π^e with respect each variable u, v and p.

$$\Pi^e = \iint_{\Omega_e} \left\{ \left[R_\omega N_iN_ju_iu^0_{j,t} + R_e\left(N_iN_jN_{k,x}u_iu^0_ju^0_k + N_iN_jN_{k,y}u_iv^0_ju^0_k\right)\right] \right.$$
$$+ \left[R_\omega N_iN_jv_iv^0_{j,t} + R_e\left(N_iN_jN_{k,x}v_iu^0_jv^0_k + N_iN_jN_{k,y}v_iv^0_jv^0_k\right)\right]$$
$$+ N_{i,x}N_{j,x}u_iu_j + N_{i,y}N_{j,y}v_iv_j + \frac{1}{2}\left(N_{i,y}N_{j,y}u_iu_j + N_{i,x}N_{j,y}v_iv_j + 2N_{i,x}N_{j,y}v_iu_j\right)$$
$$\left. - \left(M_jN_{i,x}p_ju_i + M_jN_{i,y}p_jv_i\right)\right\} dA - \int_{\Gamma_e}\left(\overline{X}N_iu_i + \overline{Y}N_iv_i\right) dS$$

where

$$N_{i,x} = \frac{\partial N_i}{\partial x} \qquad N_{i,y} = \frac{\partial N_i}{\partial y}$$

$$N_{j,x} = \frac{\partial N_j}{\partial x} \qquad N_{j,y} = \frac{\partial N_j}{\partial y}$$

$$N_{k,x} = \frac{\partial N_k}{\partial x} \qquad N_{k,y} = \frac{\partial N_k}{\partial y}$$

$$u_{j,t} = \frac{\partial u_j}{\partial t} \qquad v_{j,t} = \frac{\partial v_j}{\partial t}$$

$$\frac{\partial \Pi^e}{\partial u_i} = \iint_{\Omega_e} \left\{ R_\omega N_i N_j u_{j,t}^0 + R_e \left(N_i N_j N_{k,x} u_j^0 u_k^0 + N_i N_j N_{k,y} v_j^0 u_k^0 \right) \right.$$

$$\left. + \left(2N_{i,x}N_{j,x} + N_{i,y}N_{j,y} \right)u_j + N_{i,x}N_{j,y}v_j - N_{i,x}M_j p_j \right\} dA$$

$$- \int_{\Gamma_e} \overline{X} N_i \, dS = 0$$

$$\frac{\partial \Pi^e}{\partial v_i} = \iint_{\Omega_e} \left\{ R_\omega N_i N_j v_{j,t}^0 + R_e \left(N_i N_j N_{k,x} u_j^0 v_k^0 + N_i N_j N_{k,y} v_j^0 v_k^0 \right) \right.$$

$$\left. + \left(N_{i,x}N_{j,x} + 2N_{i,y}N_{j,y} \right)v_j + N_{i,y}N_{j,x}u_j - N_{i,y}M_j p_j \right\} dA$$

$$- \int_{\Gamma_e} \overline{Y} N_i \, dS = 0$$

$$\frac{\partial \Pi^e}{\partial p_i} = - \iint_{\Omega_e} \left(M_j N_{i,x} u_i + M_j N_{i,y} v_i \right) dA = 0$$

Representing the above three equations in matrix format, equation (3.3) is obtained. For elements not on the boundary, the line integral vanishes, but for the elements on the boundary, the line integral becomes the consistant load vector.

Appendix C

Details of Matrices used in Newton-Raphson Iteration Procedure

Equation (3.11) can be written as

$$
\begin{bmatrix} \mathcal{A} & \mathcal{B} & \mathcal{C} \\ \mathcal{D} & \mathcal{E} & \mathcal{F} \\ \mathcal{G} & \mathcal{H} & \mathcal{I} \end{bmatrix} \begin{Bmatrix} \Delta A \\ \Delta B \\ \Delta C \end{Bmatrix} = \begin{Bmatrix} Z_1 \\ Z_2 \\ Z_3 \end{Bmatrix}
$$

where

$$
\begin{Bmatrix} Z_1 \\ Z_2 \\ Z_3 \end{Bmatrix} = \begin{Bmatrix} \frac{R_e u_b^2}{2}\mathbf{H}_2 \\ u_b\mathbf{G} \\ u_b\mathbf{F} \end{Bmatrix} - \begin{bmatrix} \mathbf{K} & \frac{R_e u_b}{2}\mathbf{Q} & \frac{\beta_2}{2}\mathbf{R} \\ \beta_2\mathbf{P} + R_e u_b\mathbf{Q} & \mathbf{K} & \mathbf{M} \\ \beta_2\mathbf{R} & -\mathbf{M} & \mathbf{K} \end{bmatrix} \begin{Bmatrix} \mathbf{A} \\ \mathbf{B} \\ \mathbf{C} \end{Bmatrix}
$$

$$
- R_e \begin{Bmatrix} \delta_{ijk}^x(A_j^u A_k^u + B_j^u B_k^u/2 + C_j^u C_k^u/2) + \delta_{ijk}^y(A_j^v A_k^u + B_j^v B_k^u/2 + C_j^v C_k^u/2) \\ \delta_{ijk}^x(A_j^u A_k^v + B_j^u B_k^v/2 + C_j^u C_k^v/2) + \delta_{ijk}^y(A_j^v A_k^v + B_j^v B_k^v/2 + C_j^v C_k^v/2) \\ 0 \\ \delta_{ijk}^x(A_j^u B_k^u + A_k^u B_j^u) + \delta_{ijk}^y(A_j^v B_k^u + A_k^u B_j^v) \\ \delta_{ijk}^x(A_j^u B_k^v + A_k^v B_j^u) + \delta_{ijk}^y(A_j^v B_k^v + A_k^v B_j^v) \\ 0 \\ \delta_{ijk}^x(A_j^u C_k^u + A_k^u C_j^u) + \delta_{ijk}^y(A_j^v C_k^u + A_k^u C_j^v) \\ \delta_{ijk}^x(A_j^u C_k^v + A_k^v C_j^u) + \delta_{ijk}^y(A_j^v C_k^v + A_k^v C_j^v) \\ 0 \end{Bmatrix}
$$

$$
\mathcal{A} = \mathbf{K} + R_e \begin{bmatrix} \delta_{ijm}^x A_m^u + \delta_{imj}^x A_m^u & & \\ \quad + \delta_{imj}^y A_m^v & \delta_{ijm}^y A_m^u & 0 \\[2ex] \delta_{ijm}^x A_m^v & \delta_{imj}^x A_m^u + \delta_{imj}^y A_m^v & \\ & \quad + \delta_{ijm}^y A^v & 0 \\[2ex] 0 & 0 & 0 \end{bmatrix}
$$

$$
\mathcal{B} = \frac{R_e u_b}{2}\mathbf{Q} + \frac{R_e}{2} \begin{bmatrix} \delta_{ijm}^x B_m^u + \delta_{imj}^x B_m^u & & \\ \quad + \delta_{imj}^y B_m^v & \delta_{ijm}^y B_m^u & 0 \\[2ex] \delta_{ijm}^x B_m^v & \delta_{imj}^x B_m^u + \delta_{imj}^y B_m^v & \\ & \quad + \delta_{ijm}^y B^v & 0 \\[2ex] 0 & 0 & 0 \end{bmatrix}
$$

$$C = \frac{\beta_2}{2}\mathbf{R} + \frac{R_e}{2}\begin{bmatrix} \delta^x_{ijm}C^u_m + \delta^x_{imj}C^u_m \\ + \delta^y_{imj}C^v_m & \delta^y_{ijm}C^u_m & 0 \\ \\ \delta^x_{ijm}C^v_m & \delta^x_{imj}C^u_m + \delta^y_{imj}C^v_m \\ & + \delta^y_{ijm}C^v & 0 \\ \\ 0 & 0 & 0 \end{bmatrix}$$

$$\mathcal{D} = \beta_2\mathbf{P} + R_e u_b\mathbf{Q} + R_e\begin{bmatrix} \delta^x_{ijm}B^u_m + \delta^x_{imj}B^u_m \\ + \delta^y_{imj}B^v_m & \delta^y_{ijm}B^u_m & 0 \\ \\ \delta^x_{ijm}B^v_m & \delta^x_{imj}B^u_m + \delta^y_{imj}B^v_m \\ & + \delta^y_{ijm}B^v & 0 \\ \\ 0 & 0 & 0 \end{bmatrix}$$

$$\mathcal{E} = \mathcal{A} \qquad \mathcal{F} = \mathbf{M}$$

$$\mathcal{G} = \beta_2\mathbf{R} + R_e\begin{bmatrix} \delta^x_{ijm}C^u_m + \delta^x_{imj}C^u_m \\ + \delta^y_{imj}C^v_m & \delta^y_{ijm}C^u_m & 0 \\ \\ \delta^x_{ijm}C^v_m & \delta^x_{imj}C^u_m + \delta^y_{imj}C^v_m \\ & + \delta^y_{ijm}C^v & 0 \\ \\ 0 & 0 & 0 \end{bmatrix}$$

$$\mathcal{H} = -\mathbf{M} \qquad I = \mathcal{A}$$

Appendix D

Determination of the Nodal Values of the Stream Functions
for the Plotting Grid from those of the Finite Element Grid

Consider and eight noded isoparametric element as shown in the figure 3.1. The shape functions N_i and M_i for the element are presented in section 3.4. The value of the stream function Ψ and the coordinates (x, y) at a point can be obtained in terms of the nodal

values Ψ_i and nodal coordinates (x_i, y_i).

$$\Psi = N_i \Psi_i$$

$$x = N_i x_i \qquad\qquad i = 1, 2, \cdots, 8$$

$$y = N_i y_i$$

The following procedure is adopted to obtain the value of Ψ accurately at each node of the the plotting grid which lie within the finite element.

Step 1:

Determination of the s,t interpolation within the finite element

Assume a quadratic interpolation for s and t of the form

$$s = A_1 + A_2 x + A_3 y + A_4 x^2 + A_5 xy + A_6 y^2 + A_7 x^2 y + A_8 y^2 x$$
$$t = B_1 + B_2 x + B_3 y + B_4 x^2 + B_5 xy + B_6 y^2 + B_7 x^2 y + B_8 y^2 x$$

$$1$$

The (x, y) and (s, t) values at each of the eight nodes on the element are known. Hence eight equations each in $A_1, A_2, \cdots, A_8$ and $B_1, B_2, \cdots, B_8$ are obtained. Thus for any point (x_o, y_o) in the finite element, it is possible to calculate the corresponding (s_o, t_o) coordinates using equation 1.

Step 2:

Determination of the approximate plotting grid area occupied by each element

Determine the maximum and minimum value of x and y coordinates of the finite element. The approximate area occupied by this element is a rectangle of length x_{max} to x_{min} along the $x-$axis and height y_{max} to y_{min} along $y-$axis. For an element which is not too skewed from a rectangular shape, this approximate method works reasonably well.

Step 3:

Determination of the (s, t) value of each point of the plotting grid with coordinates (x_p, y_p) within the finite element

a. Take the initial guess value of (s_p, t_p) to be that obtained from equation 1.

$$s_p = A_1 + A_2 x_p + A_3 y_p + A_4 x_p^2 + \cdots + A_8 y_p^2 x_p$$
$$t_p = B_1 + B_2 x_p + B_3 y_p + B_4 x_p^2 + \cdots + B_8 y_p^2 x_p$$

b. Calculate the shape functions N_i for $i = 1, 2, \cdots, 8$ for these values of s_p, t_p using the equations given in section 3.4.

c. Calculate the jacobian J.

$$J = \begin{bmatrix} \frac{\partial N_j}{\partial s} x_j & \frac{\partial N_j}{\partial t} x_j \\ \frac{\partial N_j}{\partial s} y_j & \frac{\partial N_j}{\partial t} y_j \end{bmatrix}$$

d. Determine the (x^*, y^*) coordinates of the point using the calculated value of shape functions.

$$x^* = N_j x_j$$
$$y^* = N_j y_j$$
$$j = 1, 2, \cdots, 8$$

e. Determine the error in the (x, y) coordinates

$$\Delta x = x_p - x^*$$
$$\Delta y = y_p - y^*$$

f. Determine the error in the (s, t) coordinates.

$$[J] \begin{Bmatrix} \Delta s \\ \Delta t \end{Bmatrix} = \begin{Bmatrix} \Delta x \\ \Delta y \end{Bmatrix}$$

g. The new value of (s, t) is given as

$$s^* = s_p + \Delta s$$
$$t^* = t_p + \Delta t$$

With these new values of (s, t), repeat steps b to f until convergence occurs.

Step 4:

Determination of Ψ at the nodal points of the plotting grid

Once convergence has occured in step 3, the stream function value can be obtained using the calculated shape functions.

$$\Psi = N_i \Psi_i$$

Appendix E

Solving the Equation of Motion in Case b Flow Configuration

The case b flow configuration is presented in figures 2.1 and 2.2. The body is oscillating in the direction of steady fluid flow of velocity u_s. $F_e(t)$ is the external force and F_f is the fluid force acting on the body. The equation of motion is

$$M\ddot{s} + Ks = F_e + F_f \tag{1}$$

The fluid force F_f can be represented in terms of the added mass, added damping, and the added force given in equation 4.16. They are represented in their respective dimensional form as

$$M_a = \rho A_b M_a'$$

$$C_a = \rho A_b \omega C_a'$$

$$F_a = \mu u_o l F_a'$$

The primes represent the non-dimensional quantities. Thus the equation of motion becomes

$$(M + M_a)\ddot{s} + C_a\dot{s} + Ks = F_e + F_a \tag{2}$$

Solution procedure to solve equation (2):

1. Let the external force $F_e = F_o \sin \omega t$, then we would expect the response of the body to be of form $s = s_o \sin(\omega t - \delta)$.

2. Assume a displacement s_o of the body. A good initial value is the solution of the equation $M\ddot{s} + Ks = F_e$. Hence, knowing the steady fluid velocity u_s, the frequency of oscillations ω, and the amplitude of oscillations s_o, determine R_ω, R_{e_1} and R_{e_2}.

3. The flow problem is completely defined by R_ω, R_{e_1} and R_{e_2}. Obtain the added mass M_a, the added damping C_a and the added force F_a for these values of R_{e_1} , R_{e_2} and R_ω using the tables and graphs presented in chapter 5.

4. Solve the equation of motion (2) using the values of M_a, C_a and F_a obtained in step 3 and determine a new value of s_o.

5. Repeat steps 2, 3 and 4 using the new value of s_o until convergence occurs.